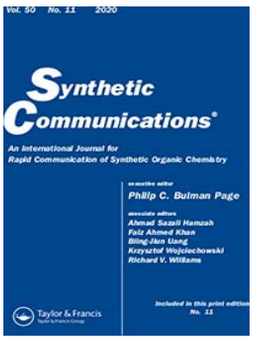

Taylor & Francis
Taylor & Francis Group

Synthetic Communications

An International Journal for Rapid Communication of Synthetic Organic Chemistry

ISSN: 0039-7911 (Print) 1532-2432 (Online) Journal homepage: https://www.tandfonline.com/loi/lsyc20

Synthesis and characterization of Mannich bases of lawsone and their anticancer activity

Pratik Nariya, Falguni Shukla, Hitarthi Vyas, Ranjitsinh Devkar & Sonal Thakore

To cite this article: Pratik Nariya, Falguni Shukla, Hitarthi Vyas, Ranjitsinh Devkar & Sonal Thakore (2020) Synthesis and characterization of Mannich bases of lawsone and their anticancer activity, Synthetic Communications, 50:11, 1724-1735, DOI: 10.1080/00397911.2020.1755440

To link to this article: https://doi.org/10.1080/00397911.2020.1755440

SYNTHETIC COMMUNICATIONS®
2020, VOL. 50, NO. 11, 1724–1735
https://doi.org/10.1080/00397911.2020.1755440

Taylor & Francis
Taylor & Francis Group

Synthesis and characterization of Mannich bases of lawsone and their anticancer activity

Pratik Nariya[a], Falguni Shukla[a], Hitarthi Vyas[b], Ranjitsinh Devkar[b], and Sonal Thakore[a]

[a]Department of Chemistry, Faculty of Science, The Maharaja Sayajirao University of Baroda, Vadodara, India; [b]Department of Zoology, Faculty of Science, The Maharaja Sayajirao University of Baroda, Vadodara, India

ABSTRACT

Natural and synthetic naphthoquinones are known for a large number of biological activities. Lawsone (2-hydroxy-1, 4-naphthoquinone) is a simplest naturally occurring compound obtained from dried henna (*Lawsonia inermis*) leaves. In literature, some lawsone derivatives have been reported to exhibit anticancer activity. Hence, a clean and facile one-pot protocol was developed for the synthesis of new aminonaphthoquinones derived from lawsone by three-component Mannich reaction, at room temperature for potential anti-cancer application. Herein we present a small library of Mannich bases with different amines and aromatic aldehydes with moderate to high yield. Synthesized compounds were characterized using various spectroscopic techniques. The anticancer activity (3-(4,5-dimethylthiazol-2-yl)-2,5-diphenyl tetrazolium bromide (MTT) assay) along with nuclear morphology assessment (4′,6-diamidino-2-phenylindole or DAPI staining), apoptosis assessment (acridine orange/ ethidium bromide staining), hemolysis and DNA ladder assay evaluated on human liver carcinoma cell line HepG2 are presented.

GRAPHICAL ABSTRACT

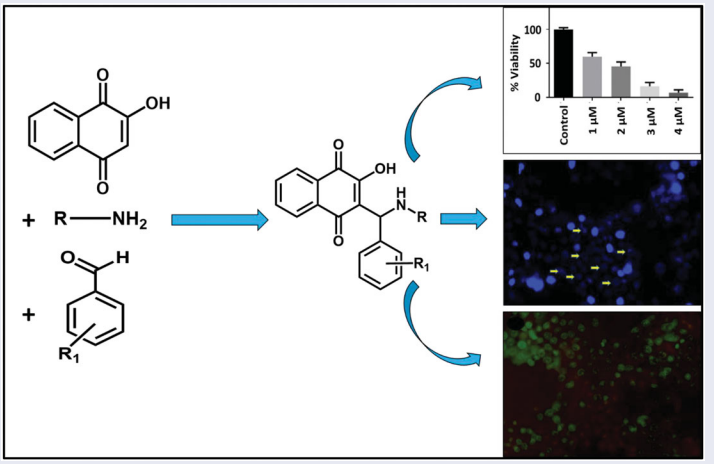

ARTICLE HISTORY

Received 11 March 2020

KEYWORDS

Lawsone; Mannich bases; anticancer activity; aminonaphthoquinones; HepG2 cells

CONTACT Sonal Thakore chemistry2797@yahoo.com Department of Chemistry, Faculty of Science, The Maharaja Sayajirao University of Baroda Faculty of Science, Vadodara, 390002 India.

Supplemental data for this article is available online at https://doi.org/10.1080/00397911.2020.1755440.

Introduction

Cancer is a major health problem worldwide and the second most common cause of death.[1] The strategies used for combating cancer generally include specialized surgical operations, radiation therapy, and chemotherapy. Despite continued research efforts toward the development of anticancer (chemotherapeutic) drugs, cancer remains a primary cause of death.[2] However, due to toxicity and drug resistance problems encountered with many currently available treatments, a great deal of effort has been devoted to the exploration and screening of new drugs for combating cancer which is one of the paramount goals in medicinal chemistry.

Quinone containing natural products has a notable pharmacophoric element as reported by the National Cancer Institute. It exhibits an array of pharmacological properties and it is one of the important subunits found in many drugs such as doxorubicin, daunorubicin, mitoxantrone, and mitomycin-C which have been used for clinical trials for cancer therapy.[3] Due to the intimate relationship between quinones and the biochemical processes of cells, these compounds have been extensively explored in the synthesis of several bioactive compounds with antitumor activities.[4]

Naphthoquinones belong to the family of quinones. Natural and synthetic derivatives of naphthoquinone have been reported to show a wide range of biological activity such as anticancer, antibacterial, antiparasitic, antioxidant, etc.[5] Lawsone, plumbagin, juglone, menadione, thymoquinone, lapachol and parvaquone are known naturally occurring naphthoquinone derivatives.[6] Among all these naphthoquinones, lawsone (2-hydroxy-1, 4-naphthoquinone) is one of the simplest naturally occurring naphthoquinones which is obtained from dry powdered leaves of the henna plant (*Lawsonia inermis*) and showed weak toxicity both to hepatocytes and various tumor cell lines.[7] However, introducing nitrogen atom in lawsone or naphthoquinone enhances its anticancer activities.[8] Nitrogen-containing derivatives and metal complexes are known to have enhanced biological activity. 2-hydroxy (3-aminomethyl)-1,4- naphthoquinone and its Pt^{2+}complexes derived from lawsone were reported to have cellular accumulation and topoisomerase against cancer cells.[9] Similarly, ruthenium (II) complexes of lawsone are known for inhibiting tumor cell lines by apoptosis.[10] Quinonoid compounds derived from lawsone are known to have cytotoxic evolution against cancer cells.[5] One of the strategies for introducing nitrogen atom in lawsone is the formation of its Mannich base via Mannich reaction. Al Nasr et al.[11] recently reported lawsone Mannich bases derived from salicylaldehyde or nitro furfural for antiparasitic activity. Similarly, series of anticancer active Mannich bases derived from lawsone were also reported recently.[12,13] Cytotoxicity of Mannich bases has been attributed partially to the α,β-unsaturated ketones liberated by deamination of the hydrogen atom of the amine group.[14] These α,β-unsaturated ketones have a markedly greater affinity for thiols over amino and hydroxynucleophiles. This preferential affinity may result in a lack of mutagenicity and carcinogenicity which are associated with certain alkylating agents due to presumed interaction with nucleic acids.[15]

In this study, we have successfully explored a series of anticancer active 3-aminomethyl-1,4-naphthoquinone synthesized from lawsone via one pot Mannich

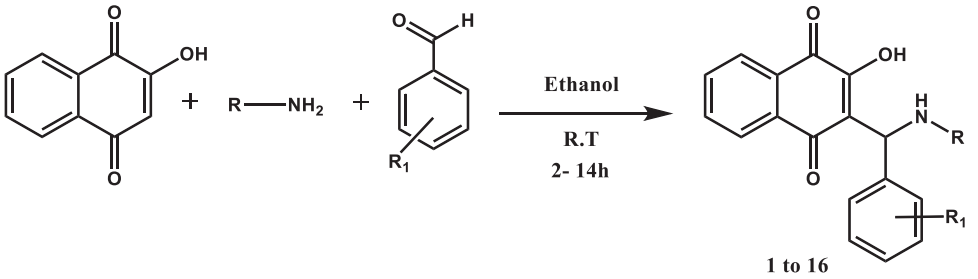

Scheme 1. Schematic for synthesis of Mannich bases of lawsone.

reaction to investigate their cytotoxicity/anticancer activity effects on human liver carcinoma cell line HepG2.

Results and discussion

Synthesis of Mannich bases of lawsone

Mannich bases were synthesized from the reaction of lawsone with various amine and aldehydes using ethanol as a solvent on stirring at room temperature (Scheme 1). Reaction was monitored by thin layer chromatography (TLC), pet ether and ethyl acetate (5:5) was used as a mobile phase for TLC. Products were recrystallized in hot ethanol. The yield of the compounds is in 54 to 85% range and the formation of compounds was confirmed by ^{1}H NMR, ^{13}C NMR, Fourier-transform infrared spectroscopy (FT-IR) and mass spectrometry as discussed in the upcoming sections. Since we have used the classical method to synthesize Mannich base from lawsone without catalyst and ethanol as solvent, it follows the classical route of mechanism. It primarily forms the iminium ion by condensation of amine and aldehyde. Subsequently, the nucleophile lawsonate attacks iminium ion (analogous to the enolate) to give a Mannich base.[16] All synthesized compounds are stable in solid state but have a tendency to undergo decomposition in solution (dimethyl sulfoxide (DMSO), ethanol, methanol, and chloroform) after a long period of time as reported in the literature.[13]

^{1}H NMR spectroscopy

In ^{1}H NMR spectra of the compounds, four hydrogens of naphthoquinone appear in the δ 7–8 ppm region as double doublet (dd), doublet of double doublet (ddd), and triplet of doublet (td). The protons of aromatic aldehyde also appear in the expected region (δ 7–8.5 ppm). The values of the coupling constant (*J*) are in well agreement with a literature report.[17] The aliphatic hydrogens appear in δ 0.8–2.8 ppm as multiplet or triplets. A singlet is observed in the range of δ 5.4–6.1 ppm due to the formation of a new bond between aldehyde, amine and lawsone. The broad peak between δ 9–10 ppm also observed due to hydrogen bonding between hydroxy group (–OH) and secondary amine (–NH) of Mannich Base. The ^{13}C NMR spectra also show all expected peaks at their corresponding δ value (Supplementary information).

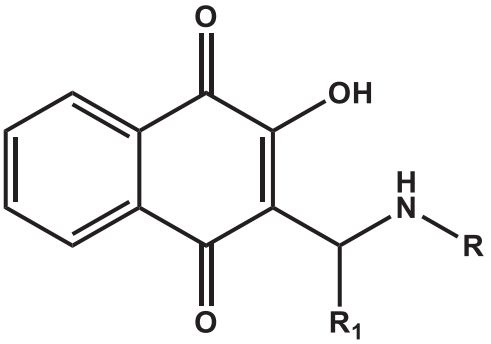

Figure 1. General structure of the compound.

FT-IR spectroscopy

The FT-IR spectra of the compounds show a broad band from 3450 to 3300 cm^{-1} corresponding to hydroxy group and secondary amine (-NH) of lawsone Mannich base. The band in the range of 3050–3180 cm^{-1} is assigned to the = C-H stretching of the aromatic ring. Several weak bands observed in the range of 2400–2900 cm^{-1} attributed to aromatic and aliphatic C–H groups. The strong band of carbonyl group observed around 1680–1695 cm^{-1}. The bending frequency of $\delta_{N\text{-}H}$ was observed at 1530 cm^{-1}. The strong ν_{c-o} band 1280 cm^{-1} was attributed to the naphthoquinone group. In the case of the Mannich base containing nitro group, symmetric and asymmetric stretching frequency for NO_2 was also observed at 1593and 1349 cm^{-1}, respectively.

Mass spectra of all synthesized compounds were recorded and the [M + 1] values of all compounds match with theoretical values. All spectroscopic data confirm the structure of compounds. Further, the structure of compound **2** was also confirmed by single crystal X-Ray analysis. Oak Ridge Thermal Ellipsoid Plot (ORTEP) diagram of compound **2** with 50% probability is given in Supplementary information along with crystal data and refinement (Fig. S66 and Table S1).

Structure activity relationship (SAR) and biological assay

The synthesized compounds were screened for 3-(4,5-dimethylthiazol-2-yl)-2,5-diphenyl tetrazolium bromide (MTT) assay[18] and half inhibitory concentration (IC_{50}) values for the compounds were determined. The general structure of compounds is shown in Figure 1. All compounds were screened at 1, 2, 3, 4, 5, and 10 µM concentrations, respectively. The IC_{50} values in µM concentration were determined from MTT assay and are presented in Table 1. The results obtained in a cytotoxicity assay for Mannich bases of lawsone analogs accounted for decreased cell viability in a dose dependent manner. The parent compound Lawsone did not exhibit significant cytotoxic activity at the concentrations used for the studies. The anticancer drug doxorubicin hydrochloride was taken as positive control. As shown in Table 1, all synthesized compounds showed promising activity except compound **9** (IC_{50} 389.40 µM). MTT graph of most active compounds are shown in Figure 2.

Table 1. List of compounds with IC_{50} values and structures.

Compound	R	R_1	IC_{50} (μM)
1	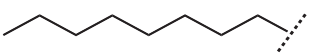	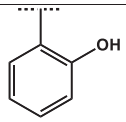	1.68
2	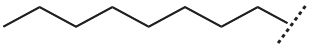	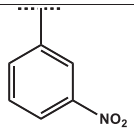	8.41
3	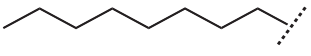	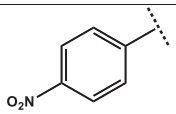	12.43
4	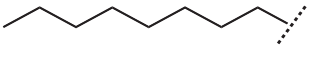	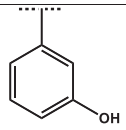	14.43
5	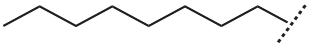	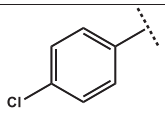	56.82
6	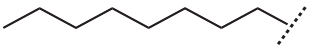	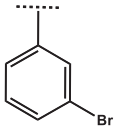	37.19
7	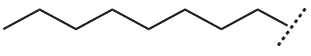	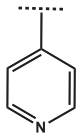	4.56
8	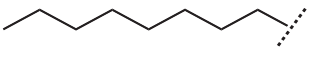	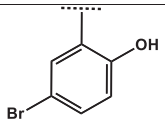	1.64
9	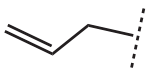	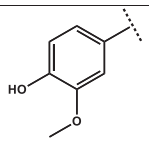	389.40
10	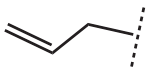	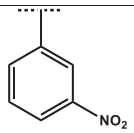	11.01

(*continued*)

11	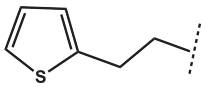	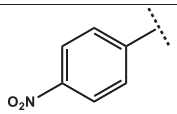	7.29
12	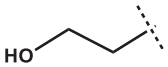	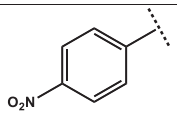	4.98
13	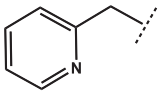	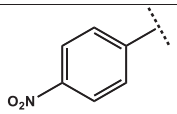	4.65
14	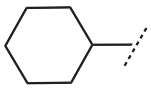	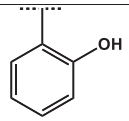	3.38
15	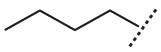	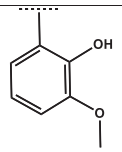	3.86
16	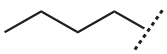	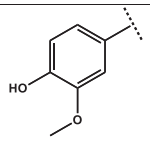	4.98
Doxorubicin hydrochloride			1.30

The results of the MTT assay showed that the activity of Mannich bases is mostly dependent on the nature of the substituent at R and R1 position. Compounds **1** (1.68 μM, derived from salicylaldehyde) and **8** (1.64 μM, derived from 5-Bromo salicylaldehyde) are the most active compounds with octyl chain substitution at R and hydroxyl group in the phenyl ring at R1. Substitution of cyclic (cyclohexyl, compound **14**) or heterocyclic ring such as pyridine (compound **13**) and thiophene (compound **11**) at R position does not show any significant changes in the activity. However, compounds **11**, **13**, and **14** have a IC_{50} lower than 5 μM.

Substitution on the aromatic ring of the R1 position is also important for anticancer potential. Aryl ring substituted with electron withdrawing groups like nitro, chloro and bromo (compounds **2, 3, 5,** and **6**) along with octyl chain leads to a decrease in activity. The compound with a shorter chain (compound **9**) is found to be the most inactive compound with IC_{50} 389.40 μM among all the Mannich base derivatives.

Overall, the compounds with aliphatic substituent at R position and hydroxyl substituted phenyl ring at R1 position are associated with the highest activities. The effective IC_{50} concentration for compounds **1, 7, 8, 13** and **14** are 1.68, 4.56, 1.63, 4.64, and

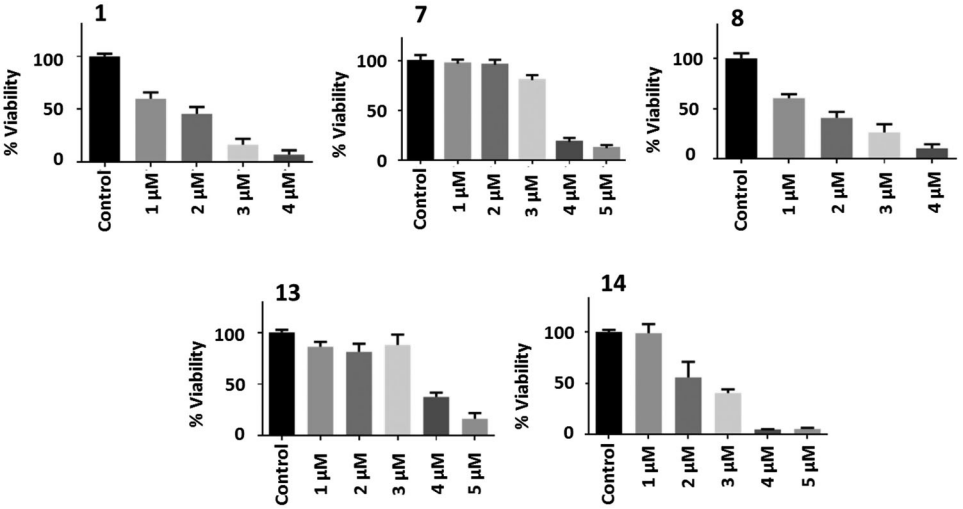

Figure 2. Graph of percentage viability against concentration for MTT assay of compounds **1**, **7**, **8**, **13**, and **14**.

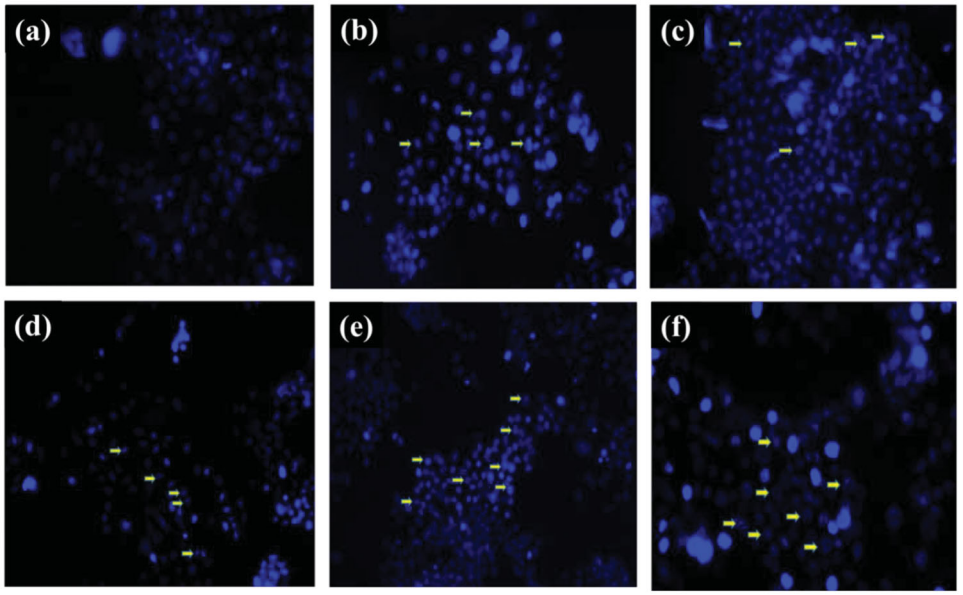

Figure 3. DAPI staining for analysis of nuclear condensation and morphology for compounds control (a), **1** (b), **7**, (c) **8**, (d) **13** (e), and **14** (f) at their IC_{50} values for 24 h (arrows indicate condensation/fragmentation/distortion of nuclei as compared to the control).

3.68 µM, respectively. These compounds showed higher anticancer potential against HepG2 cells among screened compounds and were used for further experimentations.

Detection for nuclear condensation was done using 4′,6-diamidino-2-phenylindole or DAPI staining.[19] Nuclear condensation was evident in all the compounds at different intensities. Compounds **1** and **13** showed a higher amount of nuclear condensation

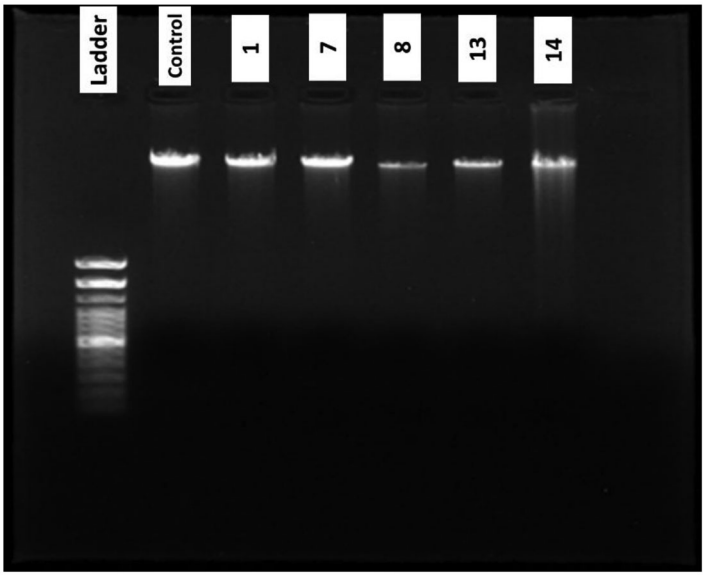

Figure 4. DNA ladder assay. Gel electrophoresis was done for DNA isolated from HepG2 cells treated with the mentioned compounds.

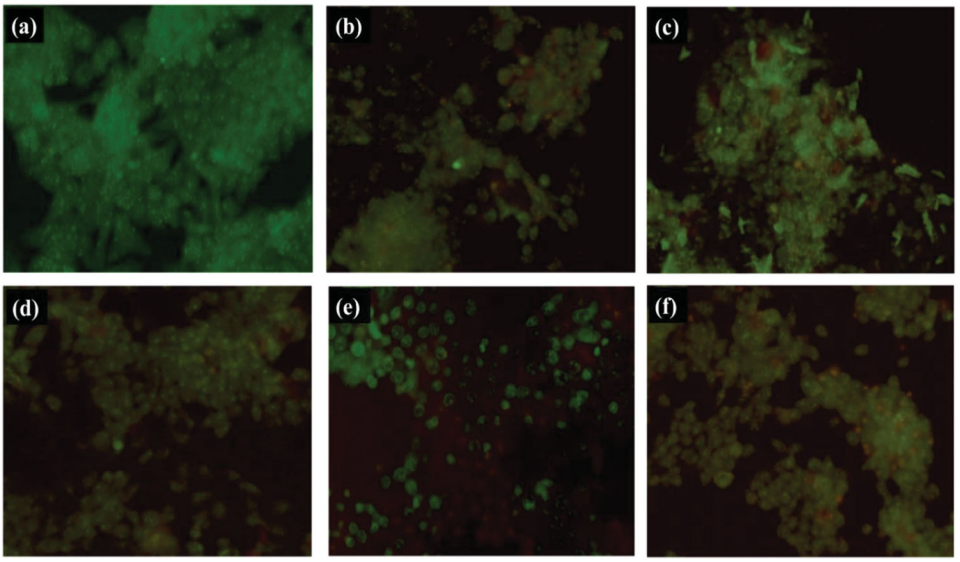

Figure 5. AO/EB staining for the compounds control (a), **1** (b), **7** (c), **8** (d), **13** (e), and **14** (f) at their IC_{50} values for 24 h. (The green cells indicate live cells whereas red ones shows apoptotic ones).

amongst all. The same is shown in Figure 3 and are marked with yellow arrows. We performed a DNA ladder assay to observe apoptosis induced DNA damage. However, not much shearing was observed in any of the compounds except for compound **14,** as shown in Figure 4.

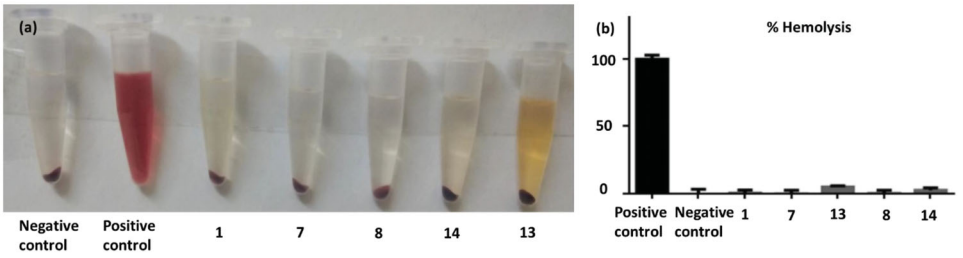

Figure 6. Hemolysis assay performed with each compound (a). Graphical representation of calculated percentage hemolysis (b).

The results of acridine orange (AO)/ ethidium bromide (EB) staining for compounds are shown in Figure 5. An interesting observation drawn from the AO/EB staining was a morphological change in cellular structures observed in compound **13**. The cells were rounded up in comparison to their natural morphology suggesting a higher number of cells progressing toward apoptosis. The same was evidenced by more red stained cells in the image Figure 5d. All the compounds showed apoptosis but compounds **1, 13,** and **14** showed higher levels of apoptotic cells.

Another important aspect of the biological study is the hemolysis assay.[20] A therapeutant when administered into the body, first encounters the circulatory system and then reaches the target organ. This makes it inevitable to test the compound for its effect on red blood cells (RBCs) of the body. Here we performed hemolysis assay, where RBCs were exposed to the synthesized compounds for 3 h at physiological body temperature (37 °C). It can be concluded from the results that none of the compounds led to significant damage to the RBCs as shown in Figure 6.

Conclusion

A small library of lawsone derived Mannich bases was synthesized and the structure of the compounds were confirmed by ^{1}H NMR, ^{13}C NMR, FT-IR, mass spectrometry and elemental analysis. The IC_{50} values were determined by MTT assay in HepG2 cell line and SAR was established. The compounds exhibited good to moderate activity and were found to be hemocompatible. The most potent compounds (**1**, **7**, **8**, **13**, and **14**) were subjected to DAPI and AO/EB staining. The cytotoxicity was mediated through the induction of apoptosis. Additional experiments are required for a better understanding of the mechanism of action.

Experimental

Material and methods

Lawsone was purchased from Sigma-Aldrich, India. All other reagents (aldehydes and amines) were purchased from Sigma-Aldrich, Spectrochem and SRL chemicals, Mumbai, India. All the reagents were used without further purification. All melting points were recorded by a scientific open capillary method and are uncorrected. IR spectra (potassium bromide (KBr) pellets) were recorded using Bruker Alpha FT-IR

Spectrometer. Elemental analysis was recorded on a Thermo Finnigan Flash 11–12 series. ^{1}H and ^{13}C NMR spectra were recorded in DMSO-d_6 solvent using Bruker Avance (400 MHz) spectrometer. Chemical shift is reported in parts per million (ppm) downfield from tetramethylsilane and coupling constants (*J*) are reported in hertz (Hz). Proton count multiplicities are reported as singlet (s), doublet (d), triplet (t), multiplet (m), dd, and td. Mass spectra were determined by Water Acquity Ultra performance LC with SQ detector. The reaction progress was monitored by TLC in ultraviolet light. Solvents have been purified as per the literature process. Merck TLC plates were used to monitor the reaction progress.

General procedure for the synthesis of Mannich bases (MB) of lawsone

The compounds from **1–16** were synthesized according to the procedure reported in the literature.[17] Briefly, to a suspension of lawsone (2 mmol) in ethanol (6 mL), respective amine (2.4 mmol) was added and allowed to stir for 15 min. After the formation of lawsonate in the solution the aldehyde (2.4 mmol) was added to the reaction mixture and the resulting reaction mixture was left on stirring at room temperature. In less than an hour, the reactants get dissolved and the product started to separate from the reaction mixture as a solid. The reaction time depends on the substrate. The progress of the reaction was monitored by TLC. The obtained solid product was filtered and washed with water, ethanol followed by diethyl ether. The crude product was recrystallized in ethanol and dried in a vacuum oven. General schematic for synthesis is shown in Scheme 1.

2-Hydroxy-3-((2-hydroxyphenyl)(octylamino)methyl)naphthalene-1,4-dione (1)

Orange solid; yield: 74%; M.P.: 152 –155 °C. ^{1}H NMR (DMSO-d_6, 400 MHz) δ (ppm): 7.87 (dd, $J = 8.2$ Hz, $J = 1.2$ Hz, 2H), 7.71 (td, $J = 8.2$ Hz, $J = 1.2$ Hz 1H), 7.62 (td, $J = 8.2$ Hz, $J = 1.2$ Hz, 1H), 7.31 (dd, $J = 6.0$ Hz, $J = 1.6$ Hz, 1H), 7.14 (td, $J = 8.8$ Hz, $J = 0.8$ Hz, 1H), 6.87 (dd, $J = 6.8$ Hz, $J = 0.8$ Hz,1H), 6.74 (td, $J = 8$ Hz, $J = 0.8$ Hz,1H), 5.72 (s, 1H), 2.89 (t, $J = 7.4$ Hz,2H), 1.59 (q, 2H), 1.19 (m, 10H), 0.81 (m, 3H).^{13}C NMR (DMSO-d_6, 100 MHz) δ (ppm):14.37, 22.48, 26.04, 26.30, 28.83, 28.87, 31.58, 46.30, 54.42, 110.29, 116.27, 119.46, 123.96, 125.56, 125.91, 129.03, 129.90, 131.52, 131.98, 134.24, 155.82, 171.93, 179.88, 184.42. IR (KBr) cm^{-1}: 3254 (N–H), 3068 (=C–H), 2955 (C–H), 2928 (C–H), 1680 (C=O), 1592 (C=C), 1516 (δ N–H), 1276 (C–O), 1099 (C–N). ESI/MS 408.7$[M+1]^{+}$ calculated for $C_{25}H_{29}NO_4$. Anal. calculated for: C, 73.69; H, 7.17; N, 3.44; O, 15.70; Found C, 73.80; H, 7.10; N, 3.39.

Spectral and analytical data of remaining compounds are given in Supplementary information. Experimental information for *in vitro* studies are provided in the Supplementary information.

Acknowledgments

The authors acknowledge DST-FIST for ^{1}H NMR facility and DST-PURSE, The Maharaja Sayajirao University of Baroda for Single Crystal X-Ray facility. The authors also acknowledge SAIF Chandigarh for ^{13}C NMR analysis.

Disclosure statement

No potential conflict of interest was reported by the authors.

Funding

PN received financial assistance from Gujarat State Biotechnology Mission (GSBTM), Gandhinagar. FS and HV received financial assistance from Sudeep pharma AACD Research fellowship and Lady Tata junior research fellowship, respectively.

ORCID

Sonal Thakore http://orcid.org/0000-0002-3893-0604

References

[1] Wellington, K. W. Understanding Cancer and the Anticancer Activities of Naphthoquinones-a Review. *RSC Adv.* **2015**, *5*, 20309–20338. DOI: 10.1039/C4RA13547D.

[2] Kumar, B. S.; Ravi, K.; Verma, A. K.; Fatima, K.; Hasanain, M.; Singh, A.; Sarkar, J.; Luqman, S.; Chanda, D.; Negi, A. S. Synthesis of Pharmacologically Important Naphthoquinones and Anticancer Activity of 2-Benzyllawsone through DNA Topoisomerase-II Inhibition. *Bioorganic Med. Chem.* **2017**, *25*, 1364–1373. DOI: 10.1016/j.bmc.2016.12.043.

[3] Sreelatha, T.; Kandhasamy, S.; Dinesh, R.; Shruthy, S.; Shweta, S.; Mukesh, D.; Karunagaran, D.; Balaji, R.; Mathivanan, N.; Perumal, P. T. Synthesis and SAR Study of Novel Anticancer and Antimicrobial Naphthoquinone Amide Derivatives. *Bioorganic Med. Chem. Lett.* **2014**, *24*, 3647–3651. DOI: 10.1016/j.bmcl.2014.04.080.

[4] Jordão, A. K.; Vargas, M. D.; Pinto, A. C.; da Silva, F. d C.; Ferreira, V. F. Lawsone in Organic Synthesis. *RSC Adv.* **2015**, *5*, 67909–67943. DOI: 10.1039/C5RA12785H.

[5] Baiju, T. V.; Almeida, R. G.; Sivanandan, S. T.; de Simone, C. A.; Brito, L. M.; Cavalcanti, B. C.; Pessoa, C.; Namboothiri, I. N. N.; da Silva Júnior, E. N. Quinonoid Compounds via Reactions of Lawsone and 2-Aminonaphthoquinone with α-Bromonitroalkenes and Nitroallylic Acetates: Structural Diversity by C-Ring Modification and Cytotoxic Evaluation against Cancer Cells. *Eur. J. Med. Chem.* **2018**, *151*, 686–704. DOI: 10.1016/j.ejmech.2018.03.079.

[6] Anaissi-Afonso, L.; Oramas-Royo, S.; Ayra-Plasencia, J.; Martín-Rodríguez, P.; García-Luis, J.; Lorenzo-Castrillejo, I.; Fernández-Pérez, L.; Estévez-Braun, A.; Machín, F. Lawsone, Juglone, and β-Lapachone Derivatives with Enhanced Mitochondrial-Based Toxicity. *ACS Chem. Biol.* **2018**, *13*, 1950–1957. DOI: 10.1021/acschembio.8b00306.

[7] Ahmad, A.; Mahal, K.; Padhye, S.; Sarkar, F. H.; Schobert, R.; Biersack, B. New Ferrocene Modified Lawsone Mannich Bases with anti-Proliferative Activity against Tumor Cells. *J. Saudi Chem. Soc.* **2017**, *21*, 105–110. DOI: 10.1016/j.jscs.2016.03.005.

[8] Tandon, V. K.; Yadav, D. B.; Chaturvedi, A. K.; Shukla, P. K. Synthesis of (1,4)-Naphthoquinono-[3,2-c]-1H-Pyrazoles and Their (1,4)-Naphthohydroquinone Derivatives as Antifungal, Antibacterial, and Anticancer Agents. *Bioorganic Med. Chem. Lett.* **2005**, *15*, 3288–3291. DOI: 10.1016/j.bmcl.2005.04.066.

[9] Neves, A. P.; Pereira, M. X. G.; Peterson, E. J.; Kipping, R.; Vargas, M. D.; Silva, F. P.Jr; Carneiro, J. W. M.; Farrell, N. P. Exploring the DNA Binding/Cleavage, Cellular Accumulation and Topoisomerase Inhibition of 2-Hydroxy-3-(Aminomethyl)-1,4-Naphthoquinone Mannich Bases and Their Platinum(II) Complexes. *J. Inorg. Biochem.* **2013**, *119*, 54–64. DOI: 10.1016/j.jinorgbio.2012.10.007.

[10] Oliveira, K. M.; Liany, L. D.; Corrêa, R. S.; Deflon, V. M.; Cominetti, M. R.; Batista, A. A. Selective Ru(II)/Lawsone Complexes Inhibiting Tumor Cell Growth by Apoptosis. *J. Inorg. Biochem.* **2017**, *176*, 66–76. DOI: 10.1016/j.jinorgbio.2017.08.019.

[11] Al Nasr, I.; Jentzsch, J.; Winter, I.; Schobert, R.; Ersfeld, K.; Koko, W. S.; Mujawah, A. A. H.; Khan, T. A.; Biersack, B. Antiparasitic Activities of New Lawsone Mannich Bases. *Arch. Pharm. Chem. Life. Sci.* **2019**, *352*, 1900128–1900129. DOI: 10.1002/ardp.201900128.

[12] Mahal, K.; Ahmad, A.; Schmitt, F.; Lockhauserbäumer, J.; Starz, K.; Pradhan, R.; Padhye, S.; Sarkar, F. H.; Koko, W. S.; Schobert, R.; Ersfeld, K.; et al. Improved Anticancer and Antiparasitic Activity of New Lawsone Mannich Bases. *Eur. J. Med. Chem.* **2017**, *126*, 421–431. DOI: 10.1016/j.ejmech.2016.11.043.

[13] da Silva, G. B.; Neves, A. P.; Vargas, M. D.; Marinho-Filho, J. D. B.; Costa-Lotufo, L. V. New Insights into 3-(Aminomethyl)Naphthoquinones: Evaluation of Cytotoxicity, Electrochemical Behavior and Search for Structure-Activity Correlation. *Bioorganic Med. Chem. Lett.* **2016**, *26*, 3537–3542. DOI: 10.1016/j.bmcl.2016.06.027.

[14] Bala, S.; Sharma, N.; Kajal, A.; Kamboj, S.; Saini, V. Mannich Bases: An Important Pharmacophore in Present Scenario. *Int. J. Med. Chem.* **2014**, *2014*, 1–15. DOI: 10.1155/2014/191072.

[15] Hossain, M.; Das, U.; Dimmock, J. R. Recent Advances in α,β-Unsaturated Carbonyl Compounds as Mitochondrial Toxins. *Eur. J. Med. Chem.* **2019**, *183*, 111687. DOI: 10.1016/j.ejmech.2019.111687.

[16] Filho, J. F. A.; Lemos, B. C.; de Souza, A. S.; Pinheiro, S.; Greco, S. J. Multicomponent Mannich Reactions: General Aspects, Methodologies and Applications. *Tetrahedron* **2017**, *73*, 6977–7004. DOI: 10.1016/j.tet.2017.10.063.

[17] Neves, A. P.; Barbosa, C. C.; Greco, S. J.; Vargas, M. D.; Visentin, L. C.; Pinheiro, C. B.; Mangrich, A. S.; Barbosa, J. P.; da Costa, G. L. Novel Aminonaphthoquinone Mannich Bases Derived from Lawsone and Their Copper(II) Complexes: Synthesis, Characterization and Antibacterial Activity. *J. Braz. Chem. Soc.* **2009**, *20*, 712–727. DOI: 10.1590/S0103-50532009000400015.

[18] Oramas-Royo, S.; Torrejón, C.; Cuadrado, I.; Hernández-Molina, R.; Hortelano, S.; Estévez-Braun, A.; De Las Heras, B. Synthesis and Cytotoxic Activity of Metallic Complexes of Lawsone. *Bioorganic Med. Chem.* **2013**, *21*, 2471–2477. DOI: 10.1016/j.bmc.2013.03.002.

[19] Soni, J. Y.; Sanghvi, S.; Devkar, R. V.; Thakore, S. Synthesis and Evaluation of Novel Quinuclidinone Derivatives as Potential anti-Proliferative Agents. *RSC Adv.* **2015**, *5*, 82112–82120. DOI: 10.1039/C5RA15127A.

[20] Das, M.; Solanki, A.; Joshi, A.; Devkar, R.; Seshadri, S.; Thakore, S. Dual-Responsive Multifunctional Nanotheranostics for Cancer Cell Targeting and Dual Drug Delivery. *Carbohydr. Polym.* **2019**, *206*, 694–705. DOI: 10.1016/j.carbpol.2018.11.049.

Journal of Molecular Structure 1248 (2022) 131508

Contents lists available at ScienceDirect

Journal of Molecular Structure

journal homepage: www.elsevier.com/locate/molstr

Synthesis, characterization, DNA/BSA binding and cytotoxicity studies of Mononuclear Cu(II) and V(IV) complexes of Mannich bases derived from Lawsone

Pratik Nariya[a], Falguni Shukla[a], Hitarthi Vyas[c], Ranjitsinh Devkar[c], Sonal Thakore[a,b,*]

[a] Department of Chemistry, Faculty of Science, The Maharaja Sayajirao University of Baroda, Vadodara 390002, India
[b] Institute of Interdisciplinary Studies, The Maharaja Sayajirao University of Baroda, Vadodara, 390002, India
[c] Department of Zoology, Faculty of Science, The Maharaja Sayajirao University of Baroda, Vadodara 390002, India

ARTICLE INFO

Article history:
Received 17 July 2021
Revised 13 September 2021
Accepted 14 September 2021
Available online 16 September 2021

Keywords:
Mannich base
Lawsone
Copper complex
Anticancer activity
Dna binding
BSA binding

ABSTRACT

A series of new mononuclear copper complexes (1–5) and a vanadium complex (6) were synthesized using bidentate Mannich base ligands derived from bioactive molecule Lawsone. The structure of these new molecules/complexes (1–6) were characterized by various spectroscopic techniques such as UV-Vis, FT-IR, EPR, and ESI-MS. The structure of complex 1 was also confirmed by single crystal X-ray diffraction analysis, which revealed that complexes containing copper atom has slightly distorted square planar geometry. Computational studies were carried out for the synthesized compounds (1–6) using the DFT method with B3LYP/6–311 G (d, p) and LanL2DZ basis sets to assess the bond length, bond angle, HOMO, and LUMO energy gap (ΔE). The CT-DNA and BSA binding (protein binding affinity) studies revealed that complex 4 exhibited the highest DNA binding affinity and complexes 5 and 6 exhibited the highest protein binding affinity. The cytotoxic activity of complexes 3–6 was evaluated using MTT assay along with the apoptosis assessment (AO/EB staining) against HepG2 (human liver carcinoma cell line). Furthermore, the data revealed that all the complexes 3–6 displayed very good anticancer activity with IC_{50} values in the range of 5.46–2.71 μM which is comparable with that of standard anticancer drug.

1. Introduction

Quinone containing compounds exhibits an array of pharmacological properties. A wide range of biological activity such as anticancer, antibacterial, antiparasitic, antimalarial, and antioxidant have been reported by natural and synthetic naphthoquinone in the literature [1,2]. Lawsone is the simplest naturally occurring naphthoquinone among Juglone, Parvaquone, Plumbagin, Lapachol, Thymoquinone, and Menadione [3,4].

Lawsone can bind potentially to metal ions in different oxidations states coordinating metals in a bidentate way which allows them to play an essential role in biological systems. It has been revealed from the literature reports that some metal complexes comprising of lawsone ligands exhibited higher biological activity than free lawsone. The introduction of a nitrogen atom in naphthoquinone can enhance its biological activity [5]. Mannich reaction is the simplest way to introduce nitrogen atom in lawsone, which is also known as a Mannich base [6]. We have recently reported a new series of Mannich bases derived from lawsone with improved anticancer activity [7]. Metal complexes derived from Lawsone derivatives are known for their cytotoxic activities. Platinum (II)/Pt^{2+} complexes of 2–hydroxy (3-aminomethyl)−1,4-naphthoquinone, Ruthenium (II)-arene complexes of naphthoquinone and lawsone are known to have cytotoxic evolution against cancer cells [8–10]. Ferrocene modified lawsone mannich bases with anti-proliferative activity against cancer cells have also been reported [11].

The presence of transition metals in our body in form of mettalo-enzyme motivated researchers to find out its potential in the pharmaceutical industry. Copper is one of the essential trace element in the human body and plays crucial roles in many biological processes, enzyme regulations, structural and functional enhancement of proteins. Copper complexes have been investigated under the assumption that endogenous metals may be less toxic to normal cells than to cancer cells. Anti-cancer active copper complexes may act in various ways, e.g. by DNA binding, apoptosis induction via reactive oxygen species (ROS) generation, and by inhibition of topoisomerase I. Some of the copper complexes are used as a model molecule for the biological oxygen carrier system. There are many copper complexes derived from the schiff

* Corresponding author at: Department of Chemistry, Faculty of Science, The Maharaja Sayajirao University of Baroda, Vadodara 390 002, India.
E-mail address: chemistry2797@yahoo.com (S. Thakore).

https://doi.org/10.1016/j.molstruc.2021.131508
0022-2860/

base are known for their enhanced biological activity [12–14]. Similarly, vanadium complexes are under research for their probable use as therapeutics due to their insulin like behavior [15]. It was also reported that vanadium complex causes reduction of hyperlipidemia and hypertension to suppress tumor cell growth [16,17]. Copper complexes of aminonaphthoquinone have been reported for antibacterial activity but it is less explored for anticancer activity while vanadium complexes of aminonaphthoquinones are not reported and explored [18].

In this study, we have successfully synthesized a series of anticancer active Cu(II) complexes and a vanadium complex of 3-aminomethyl-1,4-naphthoquinone derived from lawsone Mannich bases. The structures of these synthesized complexes were established on the basis of FTIR, ESI-MS, UV–vis and elemental analysis. The redox properties of the complexes were studied by cyclic voltammetry (CV). EPR analysis was carried out for all the complexes to understand the chemical environment and binding pattern around the metal center.The geometry optimization and FMO analysis of the complexes were analyzed by means of DFT calculations. In order to get an insight into the charge distribution over the complexes MEP surfaces computational tool was also scrutinized. The interactions of complexes towards biomolecules (CT-DNA and BSA) was investigated in detail with the aid of UV–vis and florescence techniques to demonstrate their biological potential. Further, *in vitro* anticancer activity of complexes 3–6 was successfully evaluated against HepG2 (Human liver carcinoma cell lines) using MTT assay along with apoptosis assessment (AO/EB staining).

2. Experimental

2.1. Material and methods

Lawsone, vanadyl sulfate, aldehydes, and amines were purchased from Sigma-Aldrich, Mumbai, India and used as received. Copper acetate was purchased from Loba Chemie, India. Calf thymus DNA (CT-DNA), Trisodium citrate ($Na_3C_6H_5O_7$), Ethidium Bromide (EB), and bovine serum albumin (BSA) were procured from Sisco Research Laboratory (SRL) Mumbai, India. HepG2 cell line was procured from National Center for Cell Science (NCCS) Pune, India. The buffer solution was prepared by mixing 5 mM trisodium citrate and 50 mM NaCl in doubly distilled water and NaOH solution was used to adjust pH to 7.4.

All melting points were recorded by the scientific open capillary method and are uncorrected. FTIR spectra of ligands and complexes were recorded on Bruker Alpha FT-IR Spectrometer using KBr pellets. Thermo Finnigan Flash 11–12 series instrument was used to record elemental analysis. ^{1}H &^{13}C NMR spectra of ligands were recorded in DMSO–d6 solvent using Bruker Avance (400 MHz) spectrometer. Chemical shift is reported in parts per million (ppm) downfield from TMS and coupling constants (J) are reported in Hertz (Hz). Proton count multiplicities are reported as singlet (s), doublet (d), triplet (t), multiplet (m), doublet of doublet (dd), triplet of doublet (td). Mass spectra were determined by water acquity ultra-performance LC with SQ detector. ESR spectra were recorded using JOEL JES-FA-200 ESR spectrometer operating with X-band (9.6 GHz) microwave at liquid nitrogen temperature in a suitable solvent. Thermogravimetric Analysis (TGA) of ligands and complexes were performed TG–DTA 6300 INCARP EXSTAR 6000 at a heating rate of 10 °C/min in the temperature range of 30–500 °C, nitrogen atmosphere was maintained throughout the measurement. UV-Visible spectra were recorded on Perkin Elmer Lambda-35 dual-beam spectrophotometer and Fluorescence spectra were recorded in solution on JASCOFP-6300 fluorescence spectrophotometer. Powder XRD was recorded on Bruker D2-Phased instrument with Lynux-eye detector.

2.2. General procedure for the synthesis of Ligands derived from Mannich bases of Lawsone

The ligands L1-L5 were synthesized according to our previously reported procedure [7]. The crude product was recrystallized in ethanol. The general schematic for the synthesis of ligands is shown in Scheme 1(a). Spectral and analytical data of synthesized ligands L1-L5 are provided in our previous report [7].

2.3. General procedure for the synthesis of complexes $[Cu(L)_2]$ 1–6 from ligands L1-L5 respectively

Copper acetate (0.5 mmol) dissolved in methanol (15 mL) was added dropwise to the solution of ligand L1-L5 (1 mmol) in methanol (20 mL). The resulting brownish reaction mixture was then refluxed for 5 h at 65 °C, with continuous stirring, after which the solution was allowed to cool to room temperature. The light green to brownish crystalline product was filtered and given washing with hot water and dried under vacuum. The general schematic for synthesis is shown in Scheme 1(b).

2.3.1. $[Cu(L1)_2]$ (1)

Green crystalline solid; Yield: 81%; M.P: 182–184 °C

For $C_{50}H_{54}CuN_4O_{10}$: Anal. Calculated%: C, 64.26; H, 5.82; N, 6.0. Found%: C, 64.52; H, 5.45; N, 5.87 IR (KBr) cm^{-1}: 3434 (N–H), 3065 (=C-H), 2926 (C-H), 1676 (C=O), 1590 (N=O), 1549 (δ N-H), 1376 (N=O), 1273 (C-O), 523 (Cu-N), 431 (Cu-O). UV-Vis ($CHCl_3$) λ/nm, (log ε): 266 (4.58), 422 (3.42), 590 (2.08).Molar conductance: 6.67 S cm^2 mol^{-1}.

2.3.2. $[Cu(L2)_2]$ (2)

Brown crystalline solid; Yield: 76%; M.P: 190–192 °C

For $C_{52}H_{60}CuN_2O_6$: Anal. Calculated%: C, 66.68; H, 6.46; N, 2.99. Found%: C, 66.67; H, 6.42; N, 3.05 IR (KBr) cm^{-1}: 3462 (N-H), 3138 (=C-H), 2928(C-H), 1678 (C=O), 1544 (δ N-H), 1275 (C-O), 1089 (C-N), 522 (Cu-N), 429 (Cu-O). UV-Vis ($CHCl_3$) λ/nm, (log ε): 268 (4.51), 424 (3.48), 594 (2.16). Molar conductance: 18.74 S cm^2 mol^{-1}

2.3.3. $[Cu(L3)_2]$ (3)

Brown crystalline solid; Yield: 76%; M.P: 190–192 °C

For $C_{50}H_{54}Br_2CuN_2O_6$: Anal. Calculated %: C, 59.91; H, 5.43; N, 2.79. Found %: C, 60.02; H, 5.51; N, 2.75.IR (KBr) cm^{-1}: 3462 (N-H), 3176 (=C-H), 2958 (C-H), 2926 (C-H), 1673 (C=O), 1620 (C=C), 1545 (δ N-H), 1273 (C-O), 703 (C-Br), 519 (Cu-N), 431 (Cu-O). UV-Vis ($CHCl_3$) λ/nm, (log ε): 428 (3.52), 586 (2.05). Molar conductance: 6.26 S cm^2 mol^{-1}.

2.3.4. $[Cu(L4)_2]$ (4)

Green crystalline solid; Yield: 81%; M.P: 178–182 °C

For $C_{48}H_{54}CuN_4O_6$: Anal. Calculated %: C, 68.11; H, 6.43; N, 6.62. Found %: C,68.15;H,6.45;N,2.75.IR (KBr) cm^{-1}: 3443 (N-H), 3070 (=C-H), 2960(C-H), 2853(C-H), 1678 (C=O), 1591 (C=N), 1547 (δ N-H), 1272 (C-O), 1064 (C-N), 566 (Cu-N), 430 (Cu-O). UV-Vis ($CHCl_3$) λ/nm, (log ε): 278 (4.22), 435 (3.78), 681 (2.17).Molar conductance: 17.95 S cm^2 mol^{-1}.

2.3.5. $[Cu(L5)_2]$ (5)

Brown crystalline solid; Yield: 70%; M.P: 188–190 °C

For $C_{42}H_{36}CuN_2O_{10}$: Anal. Calculated %: C, 63.67; H, 4.58; N, 3.54. Found %: C, 63.70; H, 4.52; N, 6.62 IR (KBr) cm^{-1}: 3491 (N-H), 2924 (C-H), 2854 (C-H), 1675 (C=O), 1547 (δ N-H), 1280 (C-O), 1064 (C-N), 523 (Cu-N), 434 (Cu-O). UV-Vis ($CHCl_3$) λ/nm, (log ε): 264 (4.67), 436 (3.85), 680 (2.32). Molar conductance: 15.44 S cm^2 mol^{-1}.

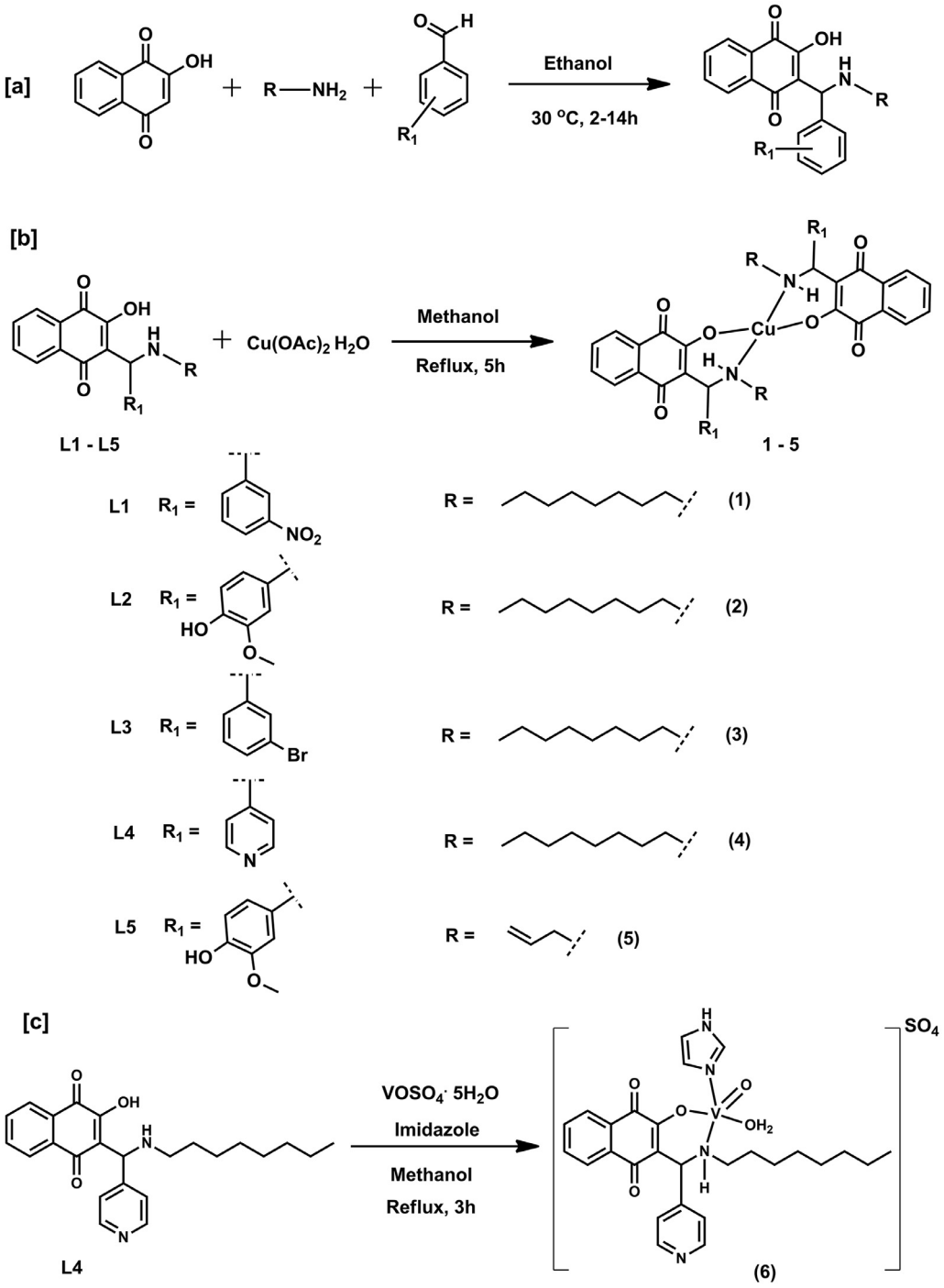

Scheme 1. General schematic for synthesis of (a) Ligands L1-L5, (b) complexes 1–5 and (c) complex 6.

2.3.6. [VO(L4)ImH(OH_2)]SO_4 (6)

Vanadyl sulfate pentahydrate (1 mmol) dissolved in aqueous methanol (10 mL) was added dropwise to a suspension of ligand L4 (1 mmol) in methanol (15 mL) and refluxed for 2 h. Then imidazole (1 mmol) dissolved in methanol (5 mL) was added and continued reflux further 1 h. The color of the solution changed to brown color. The resulting brown solid was filtered, washed with methanol and dried under vacuum. The schematic for the synthesis of complex 6 is shown in Scheme 1(c).

Brown powder; Yield: 65%; M.P: >300 °C.

For $C_{27}H_{33}VN_4O_9S$: Anal. Calculated %: C, 50.62; H, 5.19; N, 8.75. Found %: C,51.08; H,5.10; N, 8.79 IR (KBr) cm^{-1}: 3472 (N-H), 3147 (C-H), 2932 (C-H), 1636 (C=O), 1591 (C=N), 1564 (δ N-H), 1360 (C-N), 1286 (C-O),974 (V=O), 552 (V-N), 447 (V-O). UV-Vis ($CHCl_3$) λ/nm, (log ε): 436 (0.535), 838 (0.22). Molar conductance: 114 S cm^2 mol^{-1}.

2.4. X-Ray structure determination

The crystals suitable for single crystal X-ray analysis were grown by slow evaporation of complex solution in methanol at room temperature. The single crystal determination of complex 1 was carried out on Bruker CCD area diffractometer with graphite monochromatized MoKα radiation (λ = 0.071073 nm) at 293 K.

The mercury software package was used for ORTEP view of complex 1. The structure was solved by the direct method using Olex2 [19]. The structure was refined on F2 with a ShelXL refinement package using least square minimization [20]. All hydrogen atoms were included at the geometrically calculated position and all non-hydrogen atoms were refined anisotropically [CCDC No: 2,092,471].

2.5. Computational studies

Theoretical calculations were carried out using Gaussian 16 software program. Density functional theory (DFT) calculation was assigned to optimize the geometry of the complexes using B3LYP/6–311 G (d,p) and LanL2DZ basis sets. Frontier molecular orbitals(FMO), the HOMO-LUMO energy gap of the complexes (1–6), theoretical IR frequencies and Molecular electrostatic potential(MEP) were visualized with the aid of the Gauss View visualization program.

2.6. DNA binding experiments

DNA is considered as the primary biological target on numerous antitumor drugs, a series of spectroscopic tools have been employed for the determination of *in vitro* binding modes and binding strength of the complexes towards DNA. All the experiments were performed in buffer solution (5 mM trisodium citrate and 50 mM NaCl at pH 7.4) at room temperature (rt).

2.6.1. UV absorption studies

UV-visible spectroscopy is one of the popular method for evaluating the interaction of compounds with CT-DNA and to investigate possible binding modes of metal complexes towards DNA. The stock solution of CT-DNA was prepared in a buffer and stored at 4 °C while the stock solutions of complexes were prepared in DMSO. The concentration of CT DNA solution was determined from its absorption intensity at 260 nm by the use of the molar extinction coefficient (e) = 6600 M^{-1} cm^{-1} [21]. The absorbance ratio at 260 nm and 280 nm was found to be 1.8–1.9 which suggests a negligible protein-contamination of CT DNA. The absorption studies were performed with a fixed concentration of complexes (20 µL/10µL) while varying the concentration of CT-DNA (0–60µL) in 5 mM Tri sodium citrate/ 50 mM NaCl buffer, pH 7.4. The solution of CT-DNA was at different ratios to both the compound and reference solution during absorption measurement to eliminate the absorbance of CT-DNA itself in spectra [22].

2.6.2. Competitive binding studies with CT-DNA in presence of EB using fluorescence spectroscopy

Fluorescence spectroscopy is an important tool as well as the most reliable technique to examine the competitive binding study of complexes with DNA and to determine whether the compound can replace EB from DNA-EB complex.

The DNA-EB complex was prepared by adding 100 µL of each EB (1 mM) and DNA in 2.8 mL tris buffer in the cuvette. The binding mode of complexes with CT-DNA was studied by adding 2.5 or 5 µL of a complex solution (prepared in DMSO) step by step into the solution of the DNA-EB complex. The influence of the addition of complex in DNA-EB complex was recorded by fluorescence emission spectra. The fluorescence intensities of EB bound to CT-DNA were measured at 618 nm (580 nm excitation) after the addition of different complexes at different ratios.

2.7. BSA binding experiments

A protein binding study was carried out by quenching the tryptophan fluorescence residue of BSA. The fluorescence spectra were recorded at room temperature from 300 nm to 600 nm at the excitation wavelength of 296 nm. The quenching of the fluorescence intensity of the tryptophan residues of BSA was observed in the presence of increasing concentrations of complexes 1–6 (5 mM Tri sodium citrate/ 50 mM NaCl buffer, pH 7.4) at 346 nm. The Stern Volmer equation and graphs were plotted and used to study the interaction of quencher with BSA [23,24].

2.8. Biological assay

2.8.1. Cell line and culture

HepG2 Cells were procured from National Center for Cell Science (NCCS) Pune. Cells were cultured in Dulbecco's Modified Eagle's Medium (DMEM) supplemented with 10% Fetal Bovine Serum (FBS) (Gibco) and 1% antimycotic-antibiotic solution (HiMedia). Cells were maintained at 37 °C temperature in the incubator with 5% CO_2. Cells were sub-cultured at about 80% confluency using 0.25% Trypsin Phosphate Versene Glucose (TPVG) Solution (Himedia). Cell lines were utilized to examine the antitumor activity of the testing compound at varying concentrations.

2.8.2. Cell viability assay (MTT assay)

IC_{50} values of cell proliferation for synthesized compounds were determined using MTT assay. HepG2 cells (10^4 cells per well) were seeded in 96-well culture plates in 10% DMEM. Dilutions of the compounds were prepared in incomplete DMEM media. Dosing was done at about 70% confluency. After 48 h incubation 3-(4, 5-dimethylthiazol-2-yl)−2,5-diphenyl tetrazolium bromide (MTT; 5 mg/ml) was added for 4 h. At the end of incubation, MTT was removed from the wells and 150 µL/well of DMSO was added and incubated till formazan crystals dissolved completely. Absorbance was measured on Synergy HTX multimode reader at 570 nm. Statistical analysis was carried out using one way ANOVA test. IC_{50} values for the compounds were determined using MTT assay

2.8.3. Assessment of apoptosis (Acridine orange ethidium bromide (AO/EB) staining)

HepG2 cells were seeded in 96 well plate. At about 70% confluency the cells were dosed with compounds at their IC_{50} concentration in an incomplete DMEM media and incubated for 48 h. Cells were washed with 1x PBS and 5 µM of AO/EB stain was added for about 10 min. The stain was removed and cells were washed with 1x PBS twice and imaging was done on Floid Imaging Station using red and green fluorescent filters.

3. Result and discussion

3.1. Synthesis of ligands and Cu(II) complexes

The ligands were synthesized in good yield from the reaction of lawsone with various amine and aldehydes using ethanol as a solvent under stirring at 30 °C (Scheme 1a). The structures of the ligands were confirmed by various spectroscopic and analytical techniques [7]. All synthesized ligands were stable in the solid state. However they tend to undergo decomposition in solution after a long period of time as reported in the literature [6].

Cu(II) complexes 1–5 were obtained in good yield (70 to 81%) by refluxing ligands and copper acetate monohydrate in methanol (Scheme 1b). Ligands are yellow to red in color while Cu(II) complexes are greenish to brown in color. Similarly, the oxovanadium complex was prepared by a typical synthetic procedure. The methanolic aqueous solution of vanadyl sulfate was reacted with ligand (L4) and imidazole under reflux for 3 h to give a brown color complex 6as shown in Scheme 1c [25]. All complexes were stable in air at room temperature. The results of the elemental analysis (EA) was in good agreement with the proposed structure.

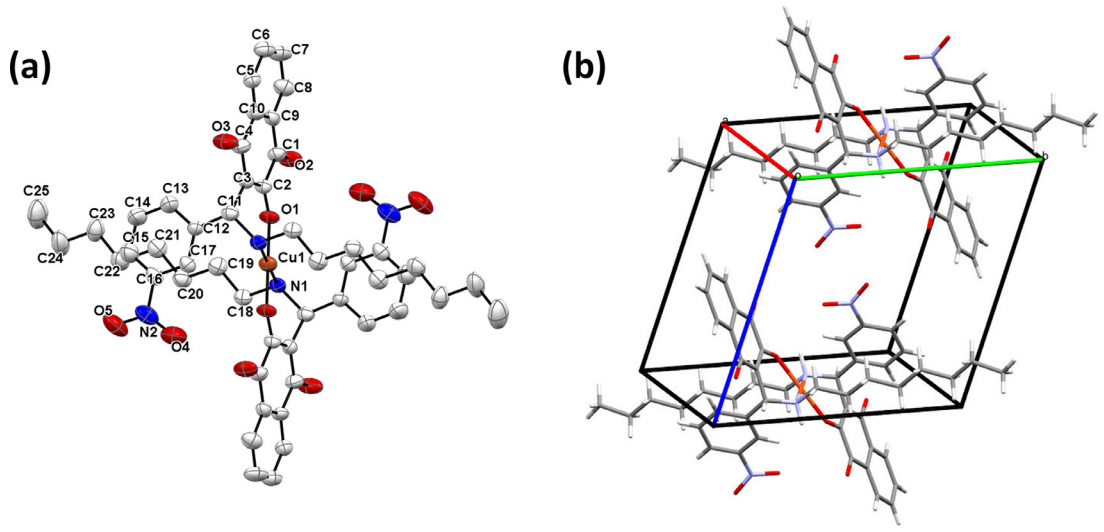

Fig. 1. (a) ORTEP view of complex 1 with 50% probability (hydrogen atoms and solvent were omitted for clarity) and (b) crystal packing along a crystallographic axis of complex 1.

Table 1
Selected bond length (Å) and bond angle (°) for complex 1.

Bond length (Å)	XRD	DFT
Cu1-O1	1.923(3)	1.9272
Cu1-O1^1	1.923(3)	1.9279
Cu1-N1	2.004(4)	2.0492
Cu1-N1^1	2.004(4)	2.0503
Bond angle (°)		
O1-Cu1-N1	87.94 (16)	87.619
O1^1-Cu1-N1^1	87.94 (16)	87.961
O1-Cu1-N1^1	92.06 (16)	92.1804
O1^1-Cu1-N1	92.06 (16)	92.2414
O1-Cu1-O1^1	180.0(2)	179.86
N1-Cu1-N1^1	180.0(2)	180.20

Table 2
Crystallographic data and structure refinement for complex 1.

Identification code	exp_1807
Empirical formula	$C_{52}H_{62}CuN_4O_{12}$
Formula weight	998.59
Temperature/K	293(2)
Crystal system	Triclinic
Space group	P-1
a/Å	10.0341(19)
b/Å	12.048(3)
c/Å	12.4074(19)
α/°	115.657(18)
β/°	111.087(15)
γ/°	90.500(16)
Volume/Å^3	1237.2(4)
Z	1
ρ_{calc}g/cm^3	1.340
μ/mm−1	0.508
F(000)	527.0
Crystal size/mm3	0.3 × 0.2 × 0.2
Radiation	MoKα (λ = 0.71073)
2Θ range for data collection/°	6.688 to 57.658
Index ranges	$-13 \le h \le 6$, $-15 \le k \le 14$, $-14 \le l \le 16$
Reflections collected	5755
Independent reflections	4912 [R_{int} = 0.0507, R_{sigma} = 0.1430]
Data/restraints/parameters	4912/0/316
Goodness-of-fit on F2	0.973
Final R indexes [$I>=2\sigma$ (I)]	R_1 = 0.0810, wR_2 = 0.1653
Final R indexes [all data]	R_1 = 0.1543, wR_2 = 0.2280
Largest diff. peak/hole / $e_{Å-3}$	0.87/−0.66

3.2. Crystal structure description

The molecular structure of complex 1 was confirmed by single crystal X-ray diffraction analysis. The ORTEP view of complex 1 with atom numbering is presented in Fig. 1(a) and crystal packing along a crystallographic axis is shown in Fig. 1(b). The selected bond angle and bond length are given in Table 1. The crystallographic data and molecular structure refinement data are presented in Table 2.

The central Cu(II) atom is in a trans N_2O_2 environment of two chelating ligands. Two deprotonated ligands ($L1^-$) coordinates through the naphthalene-2-olate oxygen and secondary amine nitrogen atoms. It forms two six-membered chelate ring around the centrosymmetric copper atom. The complex crystallizes in the triclinic space group (P-1). The bond angles between O1-Cu1-N1 and O1-Cu1-N1^1 were found to be 87.94 (16) and 92.06 (16) respectively, which indicated slightly distorted square planar geometry of complex [26]. The bond lengths between Cu-O (1.923(3) Å) and Cu-N (2.004(4) Å) were in the normal range compared to those Cu(II) complexes with a similar coordination environment [18,27]. The coordinating atoms lying on the same plane as the center atom with N1-Cu1-N1^1 and O1-Cu1-O1^1 angles equal to 180° proves complex has square planar geometry. The bond angles and bond lengths obtained by the DFT study further proved the square planar geometry of complexes.

The intermolecular hydrogen bonding interaction is shown in Fig.S1 (a). The C6-H6—O4 hydrogen bonds are formed between hydrogen atoms of naphthoquinone ring and oxygen of nitro group with a distance d (H—O) 2.660 Å. The layered structure of complex 1 along b crystallographic axis in a crystal lattice is shown in Fig. S1 (b).

3.3. Fourier transform-infrared (FTIR) analysis

The FT-IR spectra showed a broad band near 3450 to 3300 cm^{-1}for stretching frequencies of hydroxyl and secondary amine for ligands, while complexes showed a sharp band near 3450 to 3350 cm^{-1} (Fig. 2). The new bands in the region of 3200 to 3300 cm^{-1} can be attributed to ν (N–H) [28,29]. These bands were not observed in free ligands.

The ~20 cm^{-1} shift in bending frequency of N–H around 1500 cm^{-1} was observed in complexes as compared to ligands. The carbonyl stretching (C=O) frequency was observed around

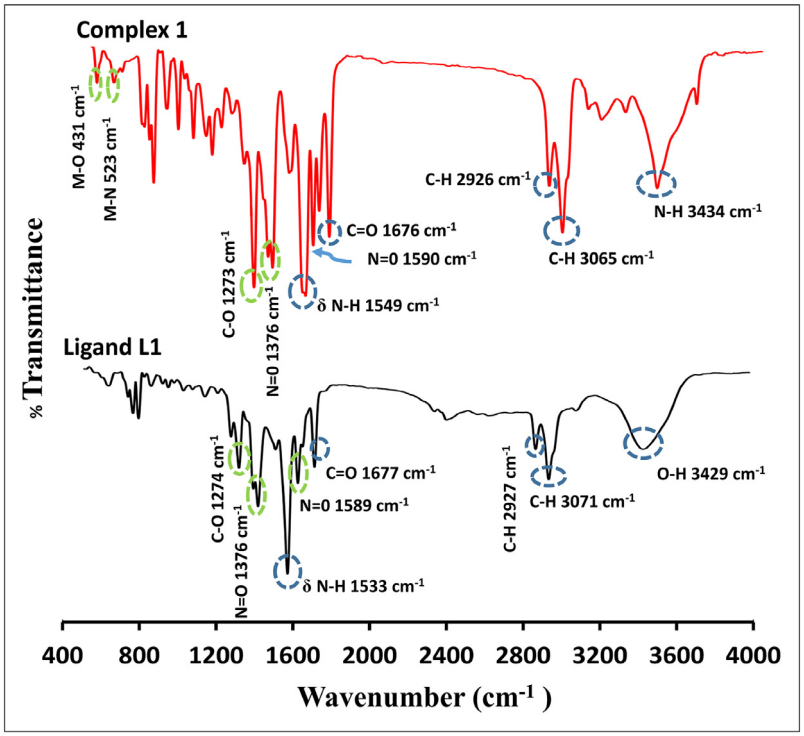

Fig. 2. FT-IR spectra of Complex (1) and Ligand (L1).

1670 cm^{-1}. It does not show shifting in stretching frequency as compared to ligand, which indicates it does not participate in complexation [30]. In the case of ligand L1 and complex 1, the symmetric and asymmetric stretching frequencies for the nitro group were observed at 1593 cm^{-1} and 1349 cm^{-1} respectively (Fig. 2). In the far IR region, medium intensity bands at 500–530 cm^{-1} and 440–410 cm^{-1} were observed and it can be attributed to Cu-N and Cu-O vibrations respectively in all complexes [31,32]. FT-IR overlay of ligand L1 and complex 1 is shown in Fig. 2 while FT-IR spectra of other complexes are provided in the supplementary information (Fig. S2–S6).

In the FT-IR spectra of the complex 6 absorption band at 3472 cm^{-1} assigned to N–H vibration involving coordination through the nitrogen of the secondary amine group, it also shows shifting in N–H bending frequency (Fig. S6). The band at 1634 cm−1can be assigned to υ(C=O) of the carbonyl group, while C=O stretch in the ligand (L4) appears at 1679 cm−1 (Fig. S6). This shift suggests that the oxygen atom of the carbonyl group may be involved in the binding of vanadium in the complex [33]. The V=O stretching frequency of complex 6 was observed at 974 cm^{-1}, which is in the usual range previously reported for the majority of oxovanadium(IV) complexes [25,34].

In addition, post simulation analysis of the DFT calculated IR could provide detailed view of vibration associated with complexes. The calculated values are close to the experimentally observed data. The graphs obtained from theoretical study are provided in supplementary information (Figs. S7–S12), while comparison between experimental and theoretical values are shown in table S2.

3.4. UV-Visible and molar conductance analysis

UV–Vis spectra of ligands and complexes were recorded in chloroform and are shown in Fig. 3. The electronic spectra of all ligands and complexes were recorded in chloroform ($CHCl_3$) while spectra of complexes 5 and 6 were recorded in dimethyl sulfoxide (DMSO). The intense absorption band was observed between 450 to 490 nm for ligands L1-L5. It can be attributed to *n*-Π* transition of the lawsone quinoid ring oxygen atom [35]. These bands showed a blue shift and were observed between 425 to435 nm for all complexes 1–5. An intense band at 436 nm was observed for the complex 6 which can be attributed to ligand-to-metal charge transfer (LMCT) of the naphthoquinone moiety to the metal ion [36,37]. The -d transition band appears at 590 nm and 680 nm for complexes 1–3 and 4–5, respectively (inset Fig. 3a–e). It supports the square planar or distorted octahedral geometry for the Cu(II) complexes in solution [38,39]. The low intensity ᴅ-d absorbance band was observed at 856 nm for complex 6. It can be assigned to a $b_2(dxy) \rightarrow e_{\Pi^*}$ (dxy; dyz) transitions VO^{2+} ion. These bands are typical for distorted octahedral VO^{2+} complex [37,40]. The Π-Π* band was also observed for all ligands (L1-L5) 235–250 nm, which remains unaltered after complexation.

The molar conductance of complexes 1–6 recorded in DMSO (1.0×10^{-3} M) revealed their non-electrolytic nature. The molar conductance values are 6.67, 18.74, 6.26, 17.95 and 15.44 S cm^2 mol^{-1} for complexes 1–5, respectively [31]. The molar conductance of complex 6 was 114 S cm^2 mol^{-1} corresponding to 1:1 electrolyte [41].

3.5. Electrochemical characteristics

The redox behavior of complexes 4 and 6 was evaluated by cyclic voltammetry (CV) at room temperature in DMSO with tetrabutylammonium perchlorate as a supporting electrolyte. The CV of complexes depicted in Fig. 3 was obtained versus ferrocene/ferrocenium. The data obtained for complexes 4 & 6 are depicted in Table 3. The CV of Complex 4 and 6 showed a quasi-reversible process attributed to the quinone group of the ligand. The CV of complex 4 showed one characteristic wave for quinone of ligand (E_p around −1.4 V) confirms the interaction of naphthalene-2-olate oxygen in solution (Fig. S13a) [6,36]. In CV of complex 4 one irreversible peak was observed around −0.65 V,

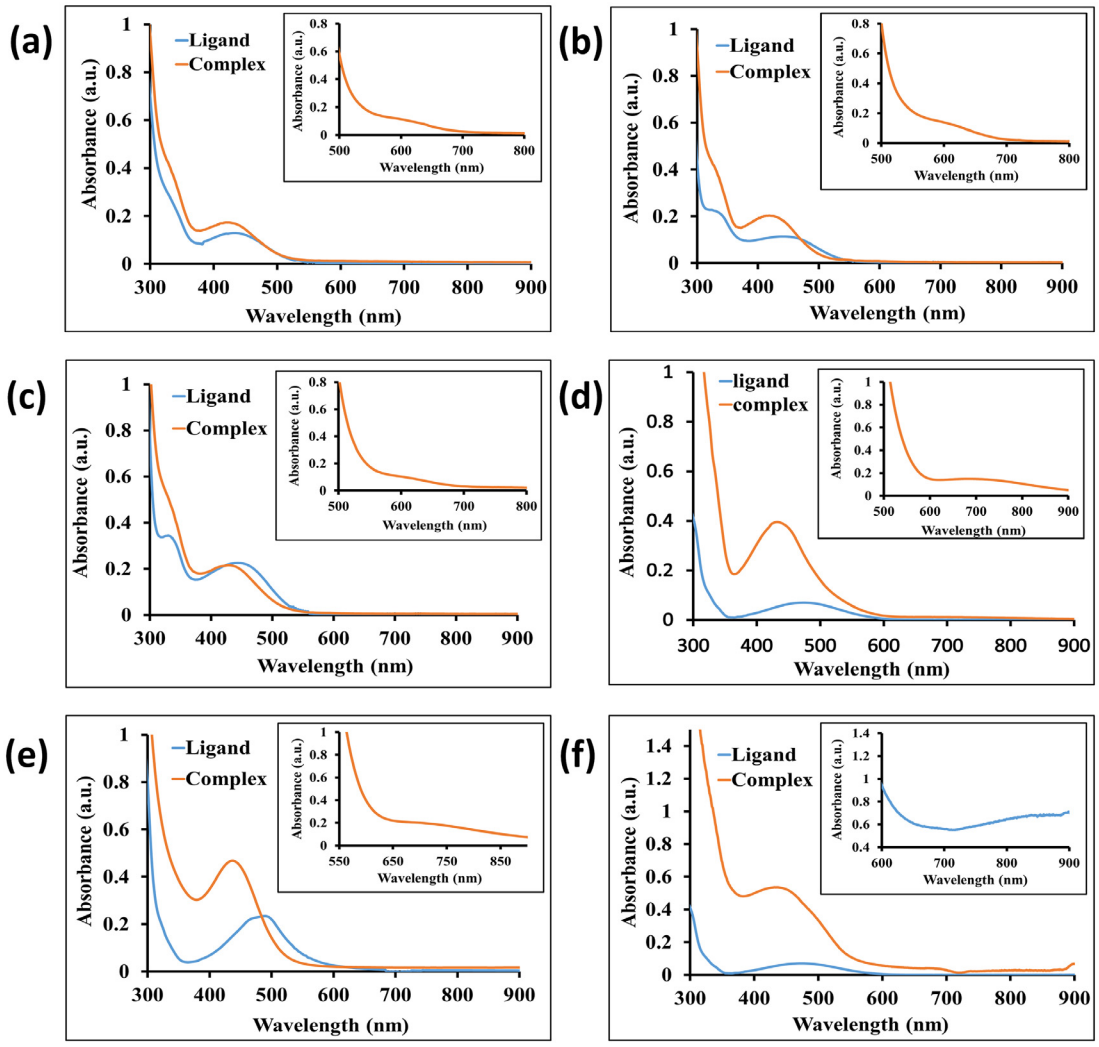

Fig. 3. UV-Visible spectra of complexes (a) 1, (b) 2, (c) 3, (d) 4, (e) 5 and (f) 6 with corresponding ligands (6.6×10^{-5} M solution of ligands and complex, inset 1.0×10^{-3} M for Copper complex and 3.0×10^{-3} M for Vanadium complex).

Table 3
Electrochemical data for complex 4 & 6 determined by CV in DMSO at a glassy carbon electrode; scan rate 0.1 V/s and 0.3 V/s for complex 4 & 6, respectively.

Complex	E_{p1c}(V)	E_{p2c}(V)	$E_{p1/2(3)}$(V)
4	−0.807	−1.343	−1.075
6	−0.773	−1.313	−0.725

which can be assigned to Cu^{II}, $Cu^{II} \rightarrow Cu^{II}$, Cu^{I} process [36]. Similar behavior was also observed in presence of ferrocene/ferrocenium along with its characteristic redox potential peak $E_{p1/2} = 0.404$ V of ferrocene [42].

The CV of complex 6 exhibited two cathodic and two anodic waves (Fig. S13b). Both redox process is quasi reversible with reduction at –0.773 V and −1.376 V. The reduction waves are larger than oxidation waves confirms the chemical change in VO^{2+} complex [43,44]. The electrochemical analysis confirms the formation of complexes.

3.6. Thermogravimetric analysis (TGA)

The synthesized Cu(II) and V(IV) complexes were air stable. The thermogravimetric analysis of complexes 1–6 was carried out under a nitrogen atmosphere at elevated temperature with a heating rate of 10 °C min^{-1}. TGA plots of complexes 1–6 are shown in Fig. S14.

Complexes 1–6 were stable in air. For complexes 1–5, the first degradation occurred up to 160 °C can be attributed to the loss of lattice solvent [45]. The second degradation from 210 °C occurs due to the decomposition of the organic ligand from complexes [46]. In the case of complex 6, the mass loss up to 150 °C occured due removal of lattice solvent and weakly coordinated H_2O. A second degradation stage after 150 °C was obtained due to pyrolysis of imidazole and an organic ligand. Thus, the TGA results indicated that all the complexes have good thermal stability.

3.7. Mass spectral studies

All the complexes have been characterized by ESI-MS in DMSO. The mass spectra of the coplexes were in good agreement with the proposed structures. The mass spectrum of complex 1 prominent peak at *m/z* 936.50 corresponds to molecular ion peak $[C_{50}H_{54}CuN_4O_{10}]^+$(inset Fig. S15). Other fragment peaks for complex 1 were observed at *m/z* 874.56, 438.05 which were assigned to $[C_{50}H_{54}N_4O_{10}]^+$ and $[C_{25}H_{27}N_2O_5]^{2+}$ moieties respectively (Fig. S15).

The mass spectra of complexes 2, 4 and 5 exhibited a prominent peak at *m/z* 936, 848.19, 790 corresponds to molecular ion

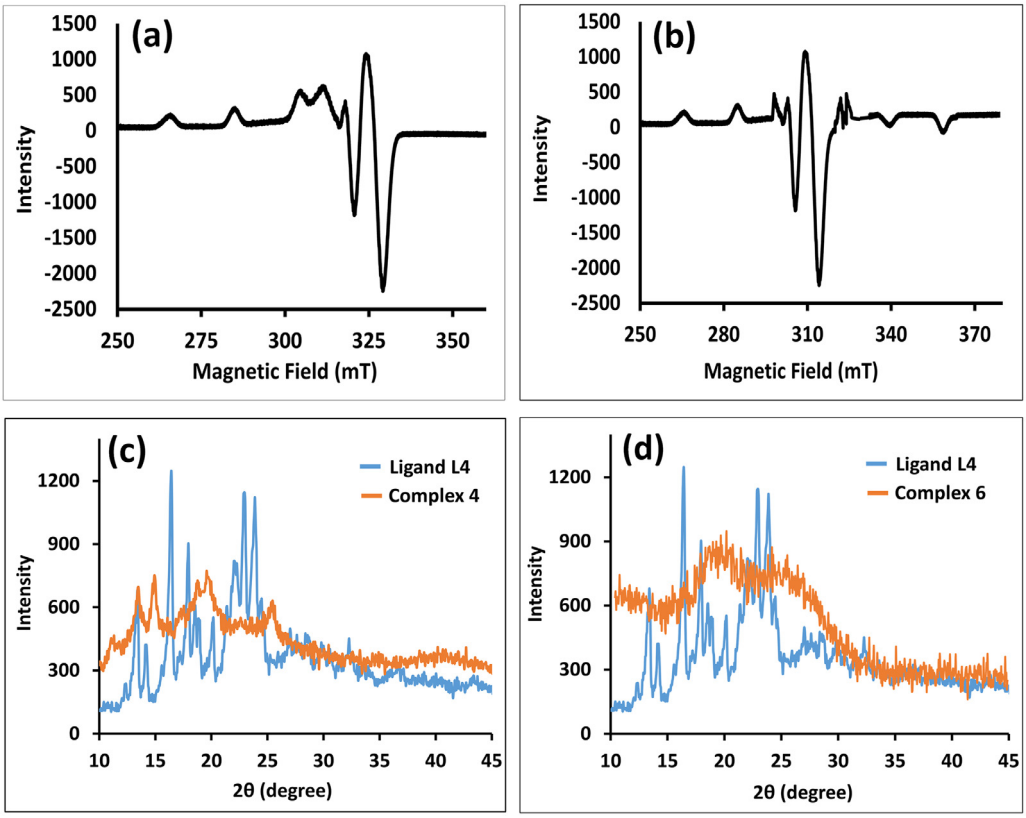

Fig. 4. EPR spectra of (a) complex 1, (b) complex 6 and powder XRD pattern of (c) complex 4 and (d) complex 6 overlayed with Ligand L4.

peak $[C_{52}H_{60}CuN_2O_{10}]^+$, $[C_{48}H_{54}CuN_4O_6]^{2+}$ and $[C_{42}H_{36}CuN_2O_{10}]^{2-}$ respectively (Figs. S16, S18 and S19). Complex 3 showed a peak at *m/z* 1077 corresponding to $[C_{50}H_{54}Cl_2CuN_2O_6{\cdot}DMSO]^+$(Fig. S17). It might have resulted from the replacement of weakly coordinated H_2O molecules by DMSO [45]. Similarly, mass spectra of complex 6 exhibited a peak at *m/z* = 545 corresponds to molecular ion peak $[C_{27}H_{33}VN_4O_5]^+$ which confirms the formation of oxovanadium complex (Fig. S20).

3.8. Electron paramagnetic resonance (EPR) analysis

To further investigate the coordination modes of Cu(II) and oxovanadium complexes EPR measurements were done at 77 K in the solution state.

The EPR spectra of complex 1 and 6 are shown in Fig. 4,b. and anisotropic g and A values obtained for complexes 1–6 are given in Table 2. The spectra of complexes (1, 2, 3, and 5) resolved four hyperfine lines of copper which indicate magnetic anisotropy in these systems and characteristics of monomeric Cu(II) complexes (Fig. S21a, b and d) [46]. The EPR spectra of complex 4 showed single isotropic peak may be due to occupancy of an unpaired electron to degenerate *p* orbitals (Fig. S21c) [47].

The values of $g_{\|}$and $g_{\perp}$were in ranges 2.203–2.252 and 2.017–2.033, respectively. The complexes possess $g_{\|} < 2.3$ suggesting an appreciable metal-ligand covalent bonding [31,46]. The complexes demonstrated $g_{\|} > g_{\perp} > 2$ and $A_{\|} = (206.39–213.35) \times 10^{-4}$ cm^{-1}, which revealed that unpaired electrons were mainly located in d_{x2-y2} orbital [18,31]. The empirical ratio of $g_{\|}$:$A_{\|}$ for all complexes is between 103 and 106 and $g_{0=}$2.06–2.10 suggested square planar geometry. The data was in good agreement with axially symmetrical Cu(II) complexes with square planar geometry [46–49].

In order to ascertain the oxidation state of vanadium, the X band EPR spectrum of complex 6 was recorded at liquid nitrogen temperature in DMSO (Fig. 4b). The spectra exhibit an axially symmetrical hyperfine eight-line pattern that originates from d electron interaction with a nuclear spin $I = 7/2$. Thus spectra display well resolved ^{51}V hyperfine lines and signal parameters for the complex are given in Table 4. The $g_{\|} >> g_{\perp}$ and $A_{\|} >> A_{\perp}$ relationships are characteristics of an axially compressed d_{xy} configuration. Thus, an oxidation state of +4 can be assigned to vanadium similar to other oxovanadium complexes reported earlier [25,33].

Table 4
EPR parameters of complexes 1–6.

Complex	$g_{\|}$	$g_{\perp}$	g_0	$A_{\|}$(× 10^{-4} cm^{-1})	$A_{\perp}$(× 10^{-4} cm^{-1})
1	2.2037	2.0172	2.0794	206.39	21.64
2	2.2069	2.0185	2.0638	213.04	19.61
3	2.2094	2.0179	2.0817	213.35	23.90
4	–	–	2.1035	–	–
5	2.2522	2.0337	2.1065	–	–
6	2.1056	2.0868	2.0930	165	34.4

3.9. Powder X-ray diffraction

The powder X-ray diffraction (XRD) pattern of Cu(II) complex 4 and oxovanadium complex 6 overlayed with ligand L4 are shown in Fig. 4c and 4d, respectively. The diffraction pattern was recorded from 2θ = 10–50° The ligand L4 showed the peak at 2θ= 12.43°, 13.69°, 14.20°, 16.43°, 17.95°, 18.45°, 20.58°, 21.34°, 22.25°, 22.96°, 23.87°, 32.28°, and 36.85° while complex 4 displayed peak at 2θ = 11.52°, 13.49°, 14.96°, 18.86°, 19.62° and 25.64° The peaks at 2θ = 12.43°, 14.20°, 16.43°, 17.95°, 20.58°, 21.34°, 22.25°, 22.96°, 23.87°, 32.28°and 36.85° of the ligand L4 disappeared in the complex 4 and new peaks appeared at 2θ = 11.52°, 14.96°, 19.62° and 25.64°(Fig. 4c). This diffraction pattern confirms the formation of

Table 5
Calculated frontier molecular orbital energies of complexes 1–6.

Complex	LUMO	HOMO	ΔE (eV)
1	−3.34	−6.45	3.10
2	−3.22	−5.45	2.23
3	−3.25	−6.64	3.39
4	−3.03	−5.23	2.19
5	−3.67	−5.56	1.89
6	−2.54	−3.69	1.19

Table 6
Metal ligand bond length and bond angle of complex 5 and 6 under study obtained from geometry optimization.

Complex 5			
Bond length (Å)	R(1,2)	Cu1- O2	1.9354
	R(1,40)	Cu1- O2	1.9464
	R(1,43)	Cu1-N43	2.0578
	R(1,5)	Cu1-N5	2.0472
Bond angle (°)	A(2,1,5)	O2-Cu1-N5	91.3379
	A(2,1,43)	O2-Cu1-N43	88.0869
	A(40,1,5)	O40-Cu1-N5	89.6101
	A(40,1,43)	O40-Cu1-N43	91.537
	A(2,1,40)	O2-Cu1-O40	179.6239
	A(5,1,43)	N5-Cu1-N43	181.1417
Complex 6			
Bond length (Å)	R(13,57)	O13-V57	1.9992
	R(59,57)	O59-V57	1.6101
	R(69,57)	N69-V57	2.1317
	R(15,57)	N15-V57	2.2015
Bond angle (°)	A(13,57,69)	O13-V57-N69	79.0648
	A(59,57,69)	O59-V57-N69	83.0692
	A(15,57,59)	N15-V57-O59	94.9665
	A(13,57,15)	O13-V57-N15	87.8228

Cu(II) complex [13]. Similarly, in complex 6 new peaks were observed at 2θ = 10.49°, 19.92°, 25.34°, 26.25°, 35.01°, 38.91°, 42.8° and 44.73° which are in good agreement with previously reported oxovanadium V(IV) complexes (Fig. 4d) [50,51]. The X-ray diffraction patterns for ligand and complexes were different, which confirms the formation of complex 4 and 6.

3.10. DFT based theoretical study

Molecular orbitals of highest occupied and lowest unoccupied (MOs) are collectively referred to as frontier orbitals (FMOs). FMOs were calculated theoretically as they are important parameters for describing chemical behavior. The lowest unoccupied molecular orbitals (LUMO) are primarily electron acceptors and the highest unoccupied molecular orbitals (HOMO) are electron donors. The energy gap between the HOMO and LUMO correlates with the chemical stability of the molecules. Literature reports suggested that the compounds with a small energy gap possess higher chemical reactivity, low kinetic stability, and soft in nature, vice versa for compounds that possess the high energy gap [52–54]. Details of frontier molecular orbitals along with the HOMO-LUMO energy gap are summarized in Table 5, respectively. The energies of the Frontier molecular orbitals (FMOs) for complexes 1–6 had negative values, indicated that the complexes were stable [55].

The metal-ligand bond lengths and bond angles are tabulated in Table 6 for complexes 5 and 6. The metal-ligand bond lengths and bond angles of the remaining complexes are provided in supplementary information (Table S1).

The patterns of the HOMO and LUMO of complexes 1–6 are displayed in Fig. 5. It was observed that the HOMO electron density is delocalized over the oxygen atom of the quinonoid ring of lawsone moiety in all the complexes and the LUMO electron density is localized on both benzenoid and quinonoid rings. In all cases, 1–6 the HOMOs, as well as LUMOs, are not delocalized over the alkyl chains. The HOMO–LUMO gap for complex 5 was observed to be 1.89 eV, which indicated complex 5 is the most chemically reactive among all other copper complexes. It was also observed that the chemical reactivity of the vanadium complex is more than that of all copper complexes as the HOMO-LUMO gap for the vanadium complex was found to be 1.19 eV. The optimized structures of complexes are shown in Fig. S22.

Molecular electrostatic potential (MEP) is widely used as a reactivity map. MEP can display electrophilic sites (positive regions) and nucleophilic sites (negative regions) based on electrostatic potentials, which are represented by red and blue colors respectively [23,56]. The MEP diagram and electrostatic potentials of complexes 1–6 are represented in Fig. S23. The red region can be observed near the O atoms of naphthoquinone ring of complexes 1–6 and near the N atom of the pyridyl ring in complexes 4 and 6 which symbolizes the acceptor site. The blue region near O atom of OH symbolizes the donor sites in complexes 2, 5, and 6. The blue region near the metal atom corresponding to the positive potential indicates it is a good candidate for attack by a nucleophile. These results confirm the formation of copper and vanadium complexes.

3.11. DNA binding studies

3.11.1. UV absorption studies

UV absorption spectroscopy is one of the most common technique to determine the binding strength and its modes of metal complexes toward DNA. The UV spectra of all the complexes (10^{-6} M prepared in DMSO) was recorded in the absence and presence of varying CT-DNA concentration (at the ratio of 0 to 1.8) within. The appearance of hypochromism in absorption bands (Fig. 6a and b) is due to partial occupation of Π* orbitals of the ligands in the complexes which result in a decrease in transition probabilities i.e. intercalation mode and red-shift is the evidence of stabilization of double-helical DNA [57].

To quantitatively compare the binding affinity of complexes, the DNA binding constant (K_b) was calculated by a change in absorption spectra. A plot of [DNA]/(ε_A-ε_f) vs. [DNA] gave a slope 1/(ε_b-ε_f) and an intercept (1/K_b)(ε_b-ε_f), K_b is the ratio of the slope to intercept (Fig. 6c and d). The binding constant (K_b) of complexes is calculated from Wolf –Shimer equation given below (Eq. (1)) [58].

$$\frac{[DNA]}{(\varepsilon A - \varepsilon f)} = \frac{[DNA]}{(\varepsilon b - \varepsilon f)} + \frac{1}{Kb(\varepsilon b - \varepsilon f)} \quad (1)$$

Where [DNA] is the concentration of DNA base pairs, ε_f, and ε_b are the extinction coefficient for the unbounded and free bounded form and $\varepsilon_A = A_{obsd}/[compounds]$.

Fig. 6a illustrates the intensity of free CT-DNA at λ_{max} = 268 nm decreases with an increased amount of complex 1 and exhibits hypochromism with a small redshift (~8 nm). These prominent features indicate complex 1 interact with CT-DNA via intercalative mode. Similar behavior was observed for complexes 2, 3 (Figs. S24,S25), and 6 (Fig. 6b). While complexes 4 and 5 showed hyperchromism (Figs. S26,S27). It can be due to groove binding of CT-DNA with complexes [59]. The binding constant K_b of complexes ranges from 10^5 to 10^6 M^{-1} (Table 7) reveals the strong binding of complexes with DNA. The effect of size, shape, hydrophobicity and electrolytic behavior of the metal complexes play significant roles in the binding of the complexes to DNA. It was observed that complexes 4 and 5 showed high binding affinity due to strong lone pair-Π interaction that has been suggested to stabilize DNA and protein structure, which contributes to the excellent binding affinity towards DNA via intercalative and groove binding mode [59,60]. Complex 6 showed good binding affinity due to positive charge (+2) which may result

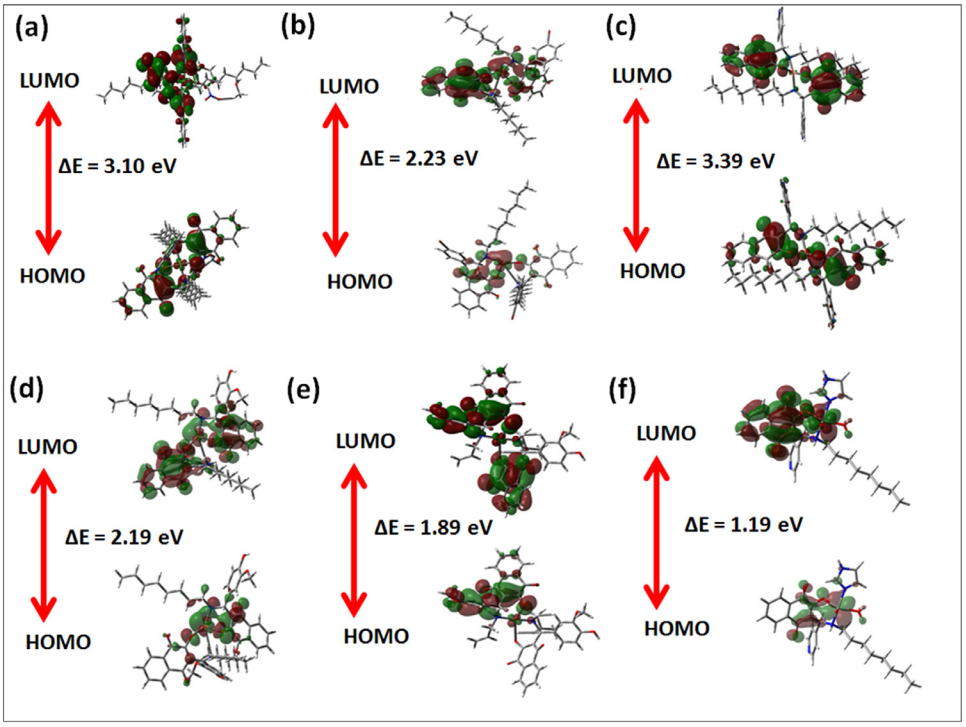

Fig. 5. plots of the frontier molecular orbitals depicting the HOMO and LUMO structure with the energy level diagram of complex (a) 1 (b) 2 (c) 3 (d) 4 (e) 5 and (f) 6.

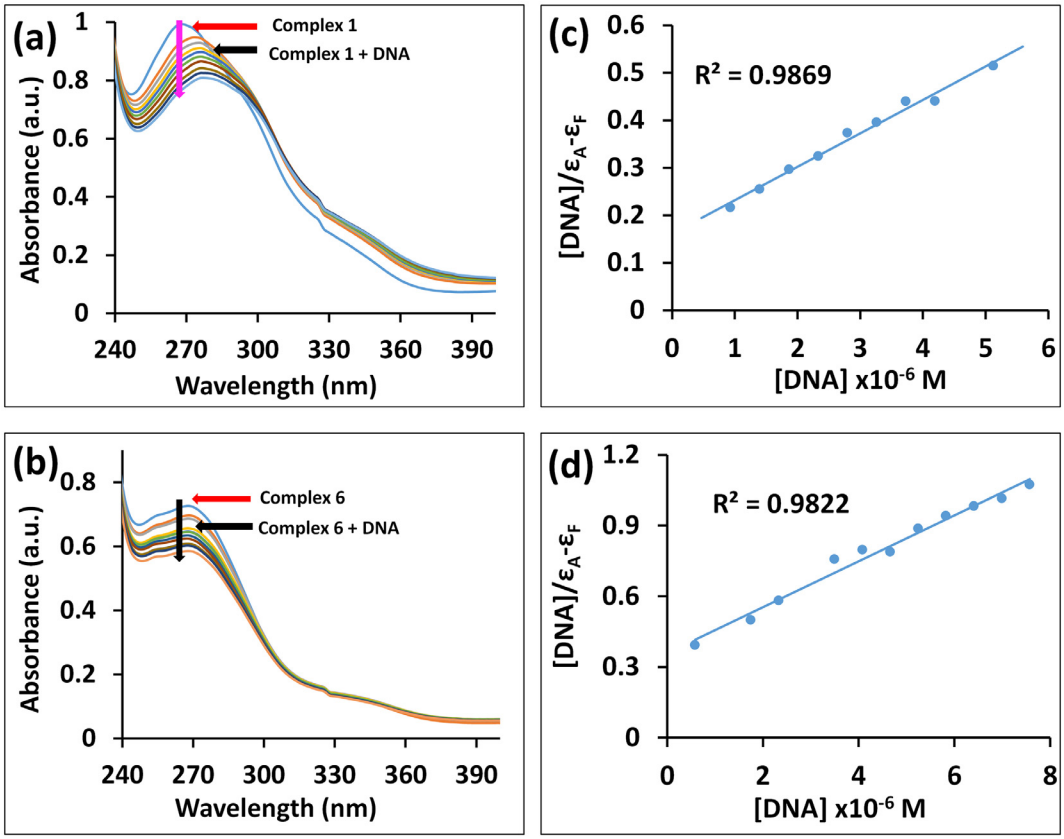

Fig. 6. UV absorption spectra of (a) complex 1 and (b) complex 6 at increasing concentration of CT-DNA, the arrow shows a decrease in intensity upon the increasing concentration of the complexes. Plots of [DNA]/(ε_A-ε_f) vs. [DNA] of (c) complex 1 and (d) complex 6.

Table 7
K_b and Ksv values of complexes 1–6.

Complex	K_b (M^{-1})	Ksv (M^{-1})	ΔG°(KJ mol^{-1})	λ shift (nm)
1	4.36×10^5	6.6×10^3	−32.175	8
2	5.38×10^5	5.0×10^3	−32.695	8
3	1.72×10^5	6.3×10^3	−29.874	7
4	3.57×10^6	8.3×10^3	−37.382	2
5	1.75×10^6	1.02×10^4	−35.621	2
6	2.70×10^5	2.37×10^4	−30.984	–

Table 8
K_a and Ksv values of complexes 1–6.

Complex	K_a (M^{-1})	Ksv (M^{-1})	*n*
1	3.103×10^5	2.828×10^5	1.01
2	2.4677×10^5	2.102×10^5	1.019
3	1.43×10^5	1.539×10^5	0.9962
4	5.0384×10^6	3.426×10^5	1.2463
5	15.790×10^7	3.497×10^5	1.5743
6	1.37×10^6	1.562×10^5	1.19

in electrostatic interactions between positively charged complex unit with the negatively charged phosphate backbone of CT-DNA double helix [61]. The high binding affinity of Complex 5 and 6 to DNA can be attributed to their higher chemical reactivity. They have a low energy difference between HOMO-LUMO. Another important factor which was considered to investigate the nature of complexes towards DNA i.e. spontaneity/non-spontaneity. Gibb's free energy (ΔG) was calculated according to Eq. (2)

$$\Delta G^{\circ} = -RTlnKb \tag{2}$$

Where R = 8.314 $JK^{-1}mol^{-1}$ and T = 298 K. The observed negative values of ΔG (Table 7) suggested that the binding process of complexes towards DNA was energetically favorable and spontaneous [62].

3.11.2. Competitive binding studies with ethidium bromide using fluorescence spectroscopy

To further elucidate the exact binding mode of the complexes with CT DNA, a competitive binding study was carried out by quenching experiment by the use of fluorescence spectroscopy tool. The emission spectra of DNA-EB (λ_{ex} = 546 nm, λ_{em} = 612 nm) in the absence and presence of the increasing amount of complexes (at ratios of 0–2.0) were recorded. With increasing concentration of complexes considerable decrease in intensity of DNA-EB emission band at 612 nm was observed as shown in Fig. 7. The emission band exhibits a significant hypochromism effect that may be attributed to the Π -Π* stacking interaction and stabilization of double-helical DNA. This observation implies that all complexes 1–6 have a great tendency to displace EB from the DNA-EB conjugate and strongly binds with DNA via intercalative or groove binding mode [63]. The displacement of bound EB and quenching of fluorescence proves complexes interact with DNA more strongly via intercalation. It might be due to the planar structure of complexes as proven by single crystal XRD and DFT study [64]. The quenching ability of DNA-EB conjugates by complexes were analyzed according to Stern Volmer Eq. (3).

$$\frac{I0}{I} = 1 + Ksv[Q] \tag{3}$$

Where I_0 and I represent the emission intensities of DNA-EB conjugates in the absence and presence of quencher [Q] (i.e. complexes 1–6) respectively. K_{sv} is Stern Volmer quenching constant and it is obtained by the slope of linear plots between I_0/I versus [Q] (Fig. S28). The Stern-Volmer quenching constant K_{sv} values are given in Table 7 and following the order 6 > 5 > 4 > 1 > 3 > 2. This order suggests that oxovanadium complex 6 and Cu(II) complex 5 exhibits the best results. This might be due to the low HOMO-LUMO gap as shown in DFT study (Fig. 5, Table 5) and presence of a higher positive charge (+2) in oxovanadium complex 6 and allylic group in complex 5 [59,60]. The magnitude of the binding constant value indicated medium to strong binding strength of complexes with CT-DNA [63]. The titration plot of the remaining complexes are provided in supplementary data (Fig. S29a–d).

3.12. BSA binding studies

Albumin is the most abundant protein in vertebrates. Studies on the binding affinity and mechanism of interaction of small molecules with serum albumin is crucial. BSA was selected as a target protein in our case due to its structural similarity with human serum albumin, easy availability and low cost [65]. The addition of increasing concentration of complex 1 (a ratio of 0–5.0) to a solution of BSA leads to a decrease in fluorescence emission at 346 nm as shown in Fig. 7c indicating the formation of a complex-BSA system. A similar trend was also observed for complexes 2–5 (Fig. S30–d).

The fluorescence quenching could be occurred by dynamic quenching and static quenching. The former is a collisional process (the fluorophore and the quencher interact in the excited state), while the latter is related to the formation of a non-fluorescent complex by fluorophore and quencher. This quenching effect was also analyzed by the Stern-Volmer Eq. (3). For static quenching interaction, the apparent binding constant K_a and the number of binding sites n could be obtained from the Scatchard equation: $\log((I_0\text{-}I)/I) = \log Ka + n\log[Q]$ [66,67]. The plot of $\log[I_0\text{-}I/I]$ versus log[Q] for all the complexes 1–6 is linear as shown in figure S31. The binding constant (K_a) and the number of binding sites per albumin (n) have been obtained from the intercept and slope respectively (Table 8). The values of n are approximately ranges between 1 and 1.5, which indicated that there was only one class of independent binding sites for complexes 1–5. Complexes 5, 4 and 6 showed the highest level of BSA binding among all complexes (Table 8). The higher binding affinity of complexes 5, 4 and 6 towards BSA could be explained in terms of the planarity of ligands coordinated to the metal centers. The oxovanadium complex 6 showed higher binding to BSA compared to copper complexes 1–3 may be due to the static and dynamic quenching mechanism [68].

The values of the Stern Volmer quenching constant K_{sv} obtained from the plot of $[I_0/I]$ versus [Q] for the complexes interacting with BSA are in order of 1.56 to 3.49 (x 10^5 M^{-1}). The Stern–Volmer plot for the quenching of BSA fluorescence by complexes 1–6 is shown in Fig. S32. The n value suggests that there is one binding site available on the protein. In addition, the linear nature of the double logarithm plot indicates that only one of the tryptophan residue on the protein is interacting with the complexes.

All spectroscopic method clearly proved that the overall order of interaction is 5 > 4 > 6 > 1 > 3 > 2. Complex 5 exhibits the strongest binding with both DNA and BSA. This phenomenon may be related to the presence of allylic group, which provides planarity to the metal center of the complex and also act as an electron donor group. It may assist the respective interaction between complex and either DNA or protein. A similar phenomenon was also observed in other complexes [63,65].

3.13. Cytotoxicity

Complexes 3, 4, 5 and 6 were selected for *in vitro* cytotoxicity study on HepG2 cell lines (Human liver cancer cells) based on re-

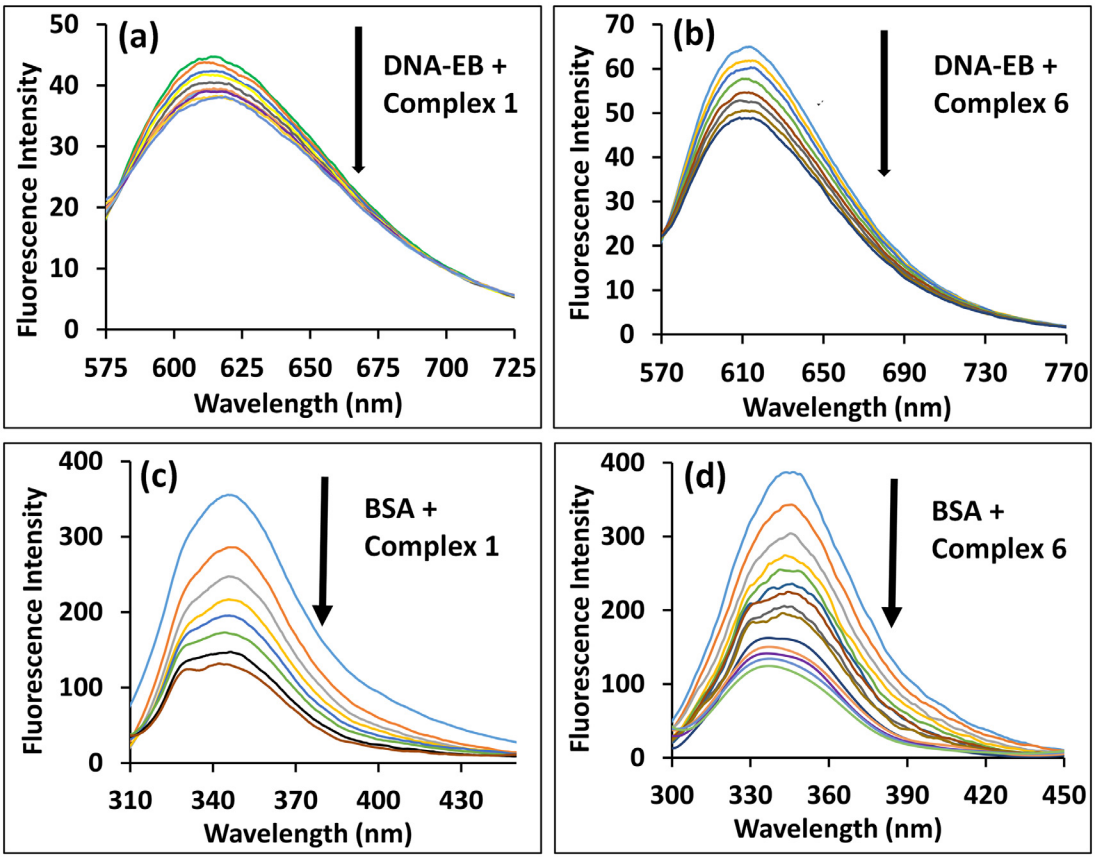

Fig. 7. Plot of fluorescence emission intensity I versus wavelength λ of CT-DNA-EB and BSA at increasing concentration of complex 1 (a, c), and complex 6 (b, d), respectively.

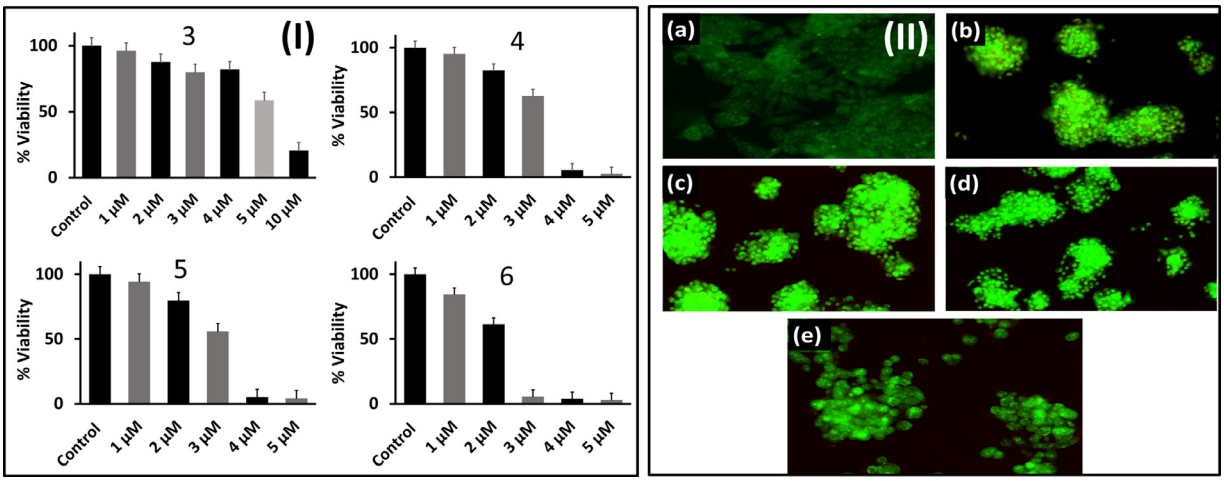

Fig. 8. (I) The plot of% viability vs. concentration of compound obtained from MTT assay of complexes and (II) AO/EB staining for the complexes (a) Control (b) 3 (c) 4 (d) 5 and (e) 6 at their IC_{50} values for 48 h.

sults obtained from DFT and DNA/BSA binding study. All the compounds were screened (at 1, 2, 3, 4, 5, and 10 μM concentrations) for 48 h for cell viability (by MTT) assay and IC_{50} values were obtained [7]. The plot of% viability vs concentration of compound obtained is shown in Fig. 8(I). Complex 3 recorded a moderate (about 8%) cytotoxicity at 5 μM dose. In contrast, Complex 6 had recorded a sharp decline in cell viability at 3 μM of concentration. Complexes 4 and 5 had accounted for approximately 50% decrement in cell viability at 3 μM concentration. The cytotoxicity of complexes in descending order are 6 > 5 > 4 > 3 whereas; their IC_{50} values are shown in Table 9.

Table 9
IC_{50} values of Complexes.

Complex	3	4	5	6
IC_{50} (μM)	5.46 (37.19)	3.325 (4.56)	3.32 (389.54)	2.71 (4.56)

Herein, it is interesting to note that the obtained cytotoxic values are effective than their precursor ligands (mentioned in parenthesis) [7]. And is comparable with IC_{50} value of cisplatin (15.9 μM on HepG2 cells) [69].

3.14. Acridine orange ethidium bromide (AO/EB) staining

The early apoptosis induced by complexes were confirmed by AO/EB staining. It is well known that early apoptosis is close to a physiological phenomenon, such as progressive contraction in cell volume while tumor cell necrosis could induce rupture into membranes, leakage of cellular space into extracellular space, and results in inflammation in normal cells. Green stained unfragmented nuclei were observed in control cells, indicating non-apoptotic cellular status. Whereas, the treated cells were observed with green fragmented nuclei. EB stains the cells with spoor membrane integrity. Cells in complex 3 observed higher red fluoresce, as compared to others, witnessing necrotic cell death. However, the cells in complexes 4 and 5 showed higher nuclear condensation implying towards apoptotic cell death. Cells dosed with complex 6 showed higher nuclear condensation and a lower amount of orange fluorescence implying towards necrotic cell death. AO/EB staining for complexes 3–6 is shown in Fig. 8(II).

4. Conclusion

In conclusion, some copper and vanadium complexes were synthesized from bioactive lawsone based ligands and tested for anticancer activity. Single crystal X-ray diffraction analysis revealed that complex containing copper atom (complex 1), is in slightly distorted square planar geometry. The geometrical parameters of complex 1 obtained by XRD correlated with theoretical DFT studies. Some important parameters such as bond length, bond angle, HUMO and LUMO energy gap (ΔE) were also determined using theoretical DFT study. The CT-DNA and BSA binding of complexes were studied by employing UV-visible and fluorescence spectroscopy. The spectroscopic data have confirmed that all complexes efficiently bind with CT-DNA via intercalative or groove binding mode. Copper (II) complex 4 exhibits the highest binding affinity with binding constant $K_b = 3.57 \times 10^6\ M^{-1}$ for CT-DNA. The results of BSA binding study revealed that quenching of proteins occurs in a static mode. It is noteworthy that complex 5 exhibited higher protein binding affinity than other complexes ($K_a = 15.790 \times 10^7\ M^{-1}$), whereas vanadium complex 6 also has higher protein binding affinity compared to copper complexes 1–3 ($K_a = 1.37 \times 10^6\ M^{-1}$). A theoretical investigation using DFT allows rationalization of experimental findings. A significant cytotoxic potential of complexes 3–6 was recorded against HepG2 cell line (by MTT assay) wherein; the findings are in agreement with experimental results and comparable to known anticancer drug cisplatin. A prominent green fluorescence following AO/EB staining in treated HepG2 cells implies to trigger of an apoptotic cascade that also corroborates with the observed cytotoxicity. The biological studies imply that these new compounds could serve as a non-platinum anticancer compound with remarkable cytotoxic effectiveness.

Declaration of Competing Interest

There are no conflicts to declare.

CRediT authorship contribution statement

Pratik Nariya: Investigation, Formal analysis, Methodology, Writing – original draft. **Falguni Shukla:** Validation, Resources. **Hitarthi Vyas:** Formal analysis, Investigation. **Ranjitsinh Devkar:** Writing – review & editing. **Sonal Thakore:** Conceptualization, Supervision, Project administration, Writing – review & editing, Funding acquisition.

Acknowledgments

The authors acknowledge DST-FIST for ^1H and ^{13}C NMR facility, DST-PURSE for single crystal X-Ray analysis, The Maharaja Sayajirao University of Baroda, SAIF IIT Bombay for ESR analysis, CSIR-CECRI karaikudi for CV analysis. The authors also thankful to KRADLE facility, CHARUSAT for powder XRD analysis. PN is thankful to SHODH fellowship, KCG-Gandhinagar for providing financial assistance. FS is thankful to AACD Sudeep pharma fellowship and HV is thankful to Lady Tata junior research fellowship for financial assistance.

Supplementary materials

Supplementary material associated with this article can be found, in the online version, at doi:10.1016/j.molstruc.2021.131508. CCDC 2092471 contains the supplementary crystallographic data. This data can be obtained free of charge via http://www.ccdc.cam.ac.uk/conts/retrieving.html, or from the Cambridge Crystallographic Data center, 12 Union Road, Cambridge CB2 1EZ, UK; fax: (+ 44) 1223-336-033; or e-mail: deposit@ccdc.cam.ac.uk.

References

[1] T.V. Baiju, R.G. Almeida, S.T. Sivanandan, C.A. de Simone, L.M. Brito, B.C. Cavalcanti, C. Pessoa, I.N.N. Namboothiri, E.N. da Silva Júnior, Quinonoid compounds via reactions of lawsone and 2-aminonaphthoquinone with α-bromonitroalkenes and nitroallylic acetates: structural diversity by C-ring modification and cytotoxic evaluation against cancer cells, Eur. J. Med. Chem. 151 (2018) 686–704, doi:10.1016/j.ejmech.2018.03.079.
[2] T. Sreelatha, S. Kandhasamy, R. Dinesh, S. Shruthy, S. Shweta, D. Mukesh, D. Karunagaran, R. Balaji, N. Mathivanan, P.T. Perumal, Synthesis and SAR study of novel anticancer and antimicrobial naphthoquinone amide derivatives, Bioorg. Med. Chem. Lett. 24 (2014) 3647–3651, doi:10.1016/j.bmcl.2014.04.080.
[3] L. Anaissi-Afonso, S. Oramas-Royo, J. Ayra-Plasencia, P. Martín-Rodríguez, J. García-Luis, I. Lorenzo-Castrillejo, L. Fernández-Pérez, A. Estévez-Braun, F. Machín, Lawsone, juglone, and β-lapachone derivatives with enhanced mitochondrial-based toxicity, ACS Chem. Biol. 13 (2018) 1950–1957, doi:10.1021/acschembio.8b00306.
[4] A.K. Jordão, M.D. Vargas, A.C. Pinto, F.D.C. Da Silva, V.F. Ferreira, Lawsone in organic synthesis, RSC Adv. 5 (2015) 67909–67943, doi:10.1039/c5ra12785h.
[5] V.K. Tandon, D.B. Yadav, A.K. Chaturvedi, P.K. Shukla, Synthesis of (1,4)-naphthoquinono-[3,2-c]-1H-pyrazoles and their (1,4)-naphthohydroquinone derivatives as antifungal, antibacterial, and anticancer agents, Bioorganic Med. Chem. Lett. 15 (2005) 3288–3291, doi:10.1016/j.bmcl.2005.04.066.
[6] G.B. da Silva, A.P. Neves, M.D. Vargas, J.D.B. Marinho-Filho, L.V. Costa-Lotufo, New insights into 3-(aminomethyl)naphthoquinones: evaluation of cytotoxicity, electrochemical behavior and search for structure–activity correlation, Bioorganic Med. Chem. Lett. 26 (2016) 3537–3542, doi:10.1016/j.bmcl.2016.06.027.
[7] P. Nariya, F. Shukla, H. Vyas, R. Devkar, S. Thakore, Synthesis and characterization of Mannich bases of lawsone and their anticancer activity, Synth. Commun. 50 (2020) 1724–1735, doi:10.1080/00397911.2020.1755440.
[8] A.P. Neves, M.X.G. Pereira, E.J. Peterson, R. Kipping, M.D. Vargas, F.P. Silva-Jr, J.W.M. Carneiro, N.P. Farrell, Exploring the DNA binding/cleavage, cellular accumulation and topoisomerase inhibition of 2-hydroxy-3-(aminomethyl)-1,4-naphthoquinone Mannich bases and their platinum(II) complexes, J. Inorg. Biochem. 119 (2013) 54–64, doi:10.1016/j.jinorgbio.2012.10.007.
[9] K.M. Oliveira, L.D. Liany, R.S. Corrêa, V.M. Deflon, M.R. Cominetti, A.A. Batista, Selective Ru(II)/lawsone complexes inhibiting tumor cell growth by apoptosis, J. Inorg. Biochem. 176 (2017) 66–76, doi:10.1016/j.jinorgbio.2017.08.019.
[10] M. Kubanik, W. Kandioller, K. Kim, R.F. Anderson, E. Klapproth, M.A. Jakupec, A. Roller, T. Söhnel, B.K. Keppler, C.G. Hartinger, Towards targeting anticancer drugs: ruthenium(II)-arene complexes with biologically active naphthoquinone-derived ligand systems, Dalton Trans. 45 (2016) 13091–13103, doi:10.1039/c6dt01110a.
[11] A. Ahmad, K. Mahal, S. Padhye, F.H. Sarkar, R. Schobert, B. Biersack, New ferrocene modified lawsone Mannich bases with anti-proliferative activity against tumor cells, J. Saudi Chem. Soc. 21 (2017) 105–110, doi:10.1016/j.jscs.2016.03.005.
[12] L. Xu, H. Wang, Z. Chu, L. Cai, H. Shi, C. Zhu, D. Pan, J. Pan, X. Fei, Y. Lei, Temperature-responsive multilayer films of micelle-based composites for controlled release of a third-generation EGFR inhibitor, ACS Appl. Polym. Mater. 2 (2020) 741–750, doi:10.1021/acsapm.9b01051.
[13] Y. Guo, X. Hu, X. Zhang, X. Pu, Y. Wang, The synthesis of a Cu(II) Schiff base complex using a bidentate N_2O_2 donor ligand: crystal structure, photophysical properties, and antibacterial activities, RSC Adv. 9 (2019) 41737–41744, doi:10.1039/c9ra07298e.

[14] K. Dankhoff, M. Gold, L. Kober, F. Schmitt, L. Pfeifer, A. Dürrmann, H. Kostrhunova, M. Rothemund, V. Brabec, R. Schobert, B. Weber, Copper(II) complexes with tridentate Schiff base-like ligands: solid state and solution structures and anticancer activity, Dalton Trans. 48 (2019) 15220–15230, doi:10.1039/c9dt02571e.
[15] I. Goldwaser, D. Gefel, E. Gershonov, M. Fridkin, Y. Shechter, Insulin-like effects of vanadium: basic and clinical implications, J. Inorg. Biochem. 80 (2000) 21–25, doi:10.1016/S0162-0134(00)00035-0.
[16] A. Banerjee, M. Mohanty, S. Lima, R. Samanta, E. Garribba, T. Sasamori, R. Dinda, Synthesis, structure and characterization of new dithiocarbazate-based mixed ligand oxidovanadium(iv) complexes: DNA/HSA interaction, cytotoxic activity and DFT studies, New J. Chem. 44 (2020) 10946–10963, doi:10.1039/d0nj01246g.
[17] D. Rehder, The medicinal and catalytic potential of model complexes of vanadate-dependent haloperoxidases, Coord. Chem. Rev. 237 (2003) 53–63, doi:10.1016/S0010-8545(02)00300-4.
[18] A.P. Neves, C.C. Barbosa, S.J. Greco, M.D. Vargas, L.C. Visentin, C.B. Pinheiro, A.S. Mangrich, J.P. Barbosa, G.L. da Costa, Novel aminonaphthoquinone Mannich bases derived from lawsone and their copper(II) complexes: synthesis, characterization and antibacterial activity, J. Braz. Chem. Soc. 20 (2009) 712–727, doi:10.1590/S0103-50532009000400015.
[19] O.V. Dolomanov, L.J. Bourhis, R.J. Gildea, J.A.K. Howard, H. Puschmann, OLEX2: a complete structure solution, refinement and analysis program, J. Appl. Crystallogr. 42 (2009) 339–341, doi:10.1107/S0021889808042726.
[20] G.M. Sheldrick, Crystal structure refinement with SHELXL, Acta Crystallogr. Sect. C Struct. Chem. 71 (2015) 3–8, doi:10.1107/S2053229614024218.
[21] K. Hu, F. Li, Z. Zhang, F. Liang, Synthesis of two potential anticancer copper(II) complex drugs: their crystal structure, human serum albumin/DNA binding and anticancer mechanism, New J. Chem. 41 (2017) 2062–2072, doi:10.1039/c6nj02483a.
[22] I.M. Khan, M. Islam, S. Shakya, K. Alam, N. Alam, M. Shahid, Synthesis, characterization, antimicrobial and DNA binding properties of an organic charge transfer complex obtained from pyrazole and chloranilic acid, Bioorg. Chem. 99 (2020) 103779, doi:10.1016/j.bioorg.2020.103779.
[23] I.M. Khan, S. Shakya, R. Akhtar, K. Alam, M. Islam, N. Alam, Exploring interaction dynamics of designed organic cocrystal charge transfer complex of 2-hydroxypyridine and oxalic acid with human serum albumin: single crystal, spectrophotometric, theoretical and antimicrobial studies, Bioorg. Chem. 100 (2020) 103872, doi:10.1016/j.bioorg.2020.103872.
[24] N.M.R. Martins, S. Anbu, K.T. Mahmudov, R. Ravishankaran, M.F.C. Guedes Da Silva, L.M.D.R.S. Martins, A.A. Karande, A.J.L. Pombeiro, DNA and BSA binding and cytotoxic properties of copper(II) and iron(III) complexes with arylhydrazone of ethyl 2-cyanoacetate or formazan ligands, New J. Chem. 41 (2017) 4076–4086, doi:10.1039/c7nj00420f.
[25] H. Han, L. Lu, Q. Wang, M. Zhu, C. Yuan, S. Xing, X. Fu, Synthesis and evaluation of oxovanadium(iv) complexes of Schiff-base condensates from 5-substituted-2-hydroxybenzaldehyde and 2-substituted-benzenamine as selective inhibitors of protein tyrosine phosphatase 1B, Dalt. Trans. 41 (2012) 11116, doi:10.1039/c2dt30198a.
[26] P. Zabierowski, J. Szklarzewicz, K. Kurpiewska, K. Lewiński, W. Nitek, Assemblies of substituted salicylidene-2-ethanolamine copper(II) complexes: from square planar monomeric to octahedral polymeric halogen analogues, Polyhedron 49 (2013) 74–83, doi:10.1016/j.poly.2012.09.029.
[27] V.K. Muppidi, S. Das, P. Raghavaiah, S. Pal, Copper(II) complexes with chiral reduced Schiff bases: helical self-assembly via intermolecular C-H···O interactions, Inorg. Chem. Commun. 10 (2007) 234–238, doi:10.1016/j.inoche.2006.10.011.
[28] V.K. Muppidi, P.S. Zacharias, S. Pal, Metal-organic frameworks from chiral square-pyramidal copper(II) complexes: enantiospecific inclusion and perfectly polar alignment of guest and host molecules, J. Solid State Chem. 180 (2007) 132–137, doi:10.1016/j.jssc.2006.10.002.
[29] H. Thakuria, G. Das, CuO micro plates from a 3D metallo-organic framework (MOF) of a binary copper(II) complex of N,N-bis(2-hydroxyethyl)glycine, Polyhedron 26 (2007) 149–153, doi:10.1016/j.poly.2006.08.012.
[30] P. Yang, D.D. Zhang, Z.Z. Wang, H.Z. Liu, Q.S. Shi, X.B. Xie, Copper(ii) complexes with NNO ligands: synthesis, crystal structures, DNA cleavage, and anticancer activities, Dalt. Trans. 48 (2019) 17925–17935, doi:10.1039/c9dt03746b.
[31] F. Arjmand, Z. Afsan, T. Roisnel, Design, synthesis and characterization of novel chromone based-copper(ii) antitumor agents with N,N-donor ligands: comparative DNA/RNA binding profile and cytotoxicity, RSC Adv. 8 (2018) 37375–37390, doi:10.1039/C8RA06722H.
[32] R. Loganathan, M. Ganeshpandian, N.S.P. Bhuvanesh, M. Palaniandavar, A. Muruganantham, S.K. Ghosh, A. Riyasdeen, M.A. Akbarsha, DNA and protein binding, double-strand DNA cleavage and cytotoxicity of mixed ligand copper(II) complexes of the antibacterial drug nalidixic acid, J. Inorg. Biochem. 174 (2017) 1–13, doi:10.1016/j.jinorgbio.2017.05.001.
[33] C. Yuan, L. Lu, Y. Wu, Z. Liu, M. Guo, S. Xing, X. Fu, M. Zhu, Synthesis, characterization, and protein tyrosine phosphatases inhibition activities of oxovanadium(IV) complexes with Schiff base and polypyridyl derivatives, J. Inorg. Biochem. 104 (2010) 978–986, doi:10.1016/j.jinorgbio.2010.05.003.
[34] L. Lu, S. Wang, M. Zhu, Z. Liu, M. Guo, S. Xing, X. Fu, Inhibition protein tyrosine phosphatases by an oxovanadium glutamate complex, Na2[VO(Glu)2(CH3OH)](Glu = glutamate), BioMetals 23 (2010) 1139–1147, doi:10.1007/s10534-010-9363-8.
[35] S.S. Khadtare, A.P. Ware, S. Salunke-Gawali, S.R. Jadkar, S.S. Pingale, H.M. Pathan, Dye sensitized solar cell with lawsone dye using a ZnO photoanode: experimental and TD-DFT study, RSC Adv. 5 (2015) 17647–17652, doi:10.1039/c4ra14620d.
[36] A.P. Neves, K.C.B. Maia, M.D. Vargas, L.C. Visentin, A. Casellato, M.A. Novak, A.S. Mangrich, Dinuclear copper(II) complexes of a novel 3-(aminomethyl)naphthoquinone Mannich base: synthesis, structural, magnetic and electrochemical studies, Polyhedron 29 (2010) 2884–2891, doi:10.1016/j.poly.2010.07.011.
[37] E. Garribba, G. Micera, A. Panzanelli, D. Sanna, Electronic structure of oxovanadium(IV) complexes of α-hydroxycarboxylic acids, Inorg. Chem. 42 (2003) 3981–3987, doi:10.1021/ic0260567.
[38] A. Hussain, M.F. AlAjmi, M.T. Rehman, S. Amir, F.M. Husain, A. Alsalme, M.A. Siddiqui, A.A. AlKhedhairy, R.A. Khan, Copper(II) complexes as potential anticancer and Nonsteroidal anti-inflammatory agents: *in vitro* and *in vivo* studies, Sci. Rep. 9 (2019) 1–17, doi:10.1038/s41598-019-41063-x.
[39] C. Paquet, T. Lacelle, X. Liu, B. Deore, A.J. Kell, S. Lafrenière, P.R.L. Malenfant, The role of amine ligands in governing film morphology and electrical properties of copper films derived from copper formate-based molecular inks, Nanoscale 10 (2018) 6911–6921, doi:10.1039/c7nr08891d.
[40] J. Dehand, Synthesis, Crystal structure, and electronic properties of (L-Methionylglycinato)copper(II), Inorg. Chem 18 (1979) 1543.
[41] I. Syiemlieh, M. Asthana, S.D. Kurbah, R.A. Lal, Synthesis, crystal structure and reactivity of homobimetallic vanadium(V) complexes derived from oxaloyldihydrazone ligands, Polyhedron 170 (2019) 202–216, doi:10.1016/j.poly.2019.05.047.
[42] N. Frenzel, J. Hartley, G. Frisch, Voltammetric and spectroscopic study of ferrocene and hexacyanoferrate and the suitability of their redox couples as internal standards in ionic liquids, Phys. Chem. Chem. Phys. 19 (2017) 28841–28852, doi:10.1039/c7cp05483a.
[43] R.N. Patel, Y.P. Singh, Synthesis, structural characterization, DFT studies and *in-vitro* antidiabetic activity of new mixed ligand oxovanadium(IV) complex with tridentate Schiff base, J. Mol. Struct. 1153 (2018) 162–169, doi:10.1016/j.molstruc.2017.10.010.
[44] P. Caravan, L. Gelmini, N. Glover, F.G. Herring, J.H. McNeill, S.J. Rettig, I.A. Setyawati, E. Shuter, Y. Sun, V.G. Yuen, C. Orvig, H. Li, A.S. Tracey, Reaction Chemistry of BMOV, Bis(maltolato)oxovanadium(IV)—a potent insulin mimetic agent, J. Am. Chem. Soc. 117 (1995) 12759–12770, doi:10.1021/ja00156a013.
[45] R. Borthakur, A. Kumar, A.K. De, R.A. Lal, Synthesis, characterization and electrochemical properties of copper(II) complexes derived from succinoyldihydrazine Schiff base ligands, Arab. J. Chem. 12 (2019) 2192–2205, doi:10.1016/j.arabjc.2014.12.040.
[46] A. Manimaran, R. Prabhakaran, T. Deepa, K. Natarajan, C. Jayabalakrishnan, Synthesis, spectral characterization, electrochemistry and catalytic activities of Cu(II) complexes of bifunctional tridentate Schiff bases containing O - NO donors, Appl. Organomet. Chem. 22 (2008) 353–358, doi:10.1002/aoc.1400.
[47] C. Elamathi, F.R. Fronczek, A. Madankumar, R. Prabhakaran, Synthesis and spectral characterizations of water soluble Cu(ii) complexes containing N-heterocyclic chelates: cell-proliferation, antioxidant and nucleic acid/serum albumin interactions, New J. Chem. 44 (2020) 4158–4170, doi:10.1039/c9nj04136b.
[48] M. Nasibipour, E. Safaei, G. Wrzeszcz, A. Wojtczak, Tuning of the redox potential and catalytic activity of a new Cu(ii) complex by: o - iminobenzosemiquinone as an electron-reservoir ligand, New J. Chem. 44 (2020) 4426–4439, doi:10.1039/c9nj06396j.
[49] P. Vijayan, P. Viswanathamurthi, K. Velmurugan, R. Nandhakumar, M.D. Balakumaran, P.T. Kalaichelvan, J.G. Malecki, Nickel(ii) and copper(ii) complexes constructed with N2S2 hybrid benzamidine-thiosemicarbazone ligand: synthesis, X-ray crystal structure, DFT, kinetico-catalytic and in vitro biological applications, RSC Adv 5 (2015) 103321–103342, doi:10.1039/c5ra18568h.
[50] Y.P. Chang, L. Furness, W. Levason, G. Reid, W. Zhang, Complexes of vanadium(IV) oxide difluoride with neutral N- and O-donor ligands, J. Fluor. Chem. 191 (2016) 149–160, doi:10.1016/j.jfluchem.2016.09.020.
[51] A. Yaul, G. Pethe, R. Deshmukh, A. Aswar, Vanadium complexes with quadridentate Schiff bases: synthesis, characterization, thermal and catalytic studies, J. Therm. Anal. Calorim. 113 (2013) 745–752, doi:10.1007/s10973-012-2745-0.
[52] S. Murugavel, C. Ravikumar, G. Jaabil, P. Alagusundaram, Synthesis, crystal structure analysis, spectral investigations (NMR, FT-IR, UV), DFT calculations, ADMET studies, molecular docking and anticancer activity of 2-(1-benzyl-5-methyl-1H-1,2,3-triazol-4-yl)-4-(2-chlorophenyl)-6-methoxypyridine – a novel poten, J. Mol. Struct. 1176 (2019) 729–742, doi:10.1016/j.molstruc.2018.09.010.
[53] K.G. Krishnan, C.U. Kumar, W.M. Lim, C.W. Mai, P.V. Thanikachalam, C. Ramalingan, Novel cyanoacetamide integrated phenothiazines: synthesis, characterization, computational studies and *in vitro* antioxidant and anticancer evaluations, J. Mol. Struct. 1199 (2020) 127037, doi:10.1016/j.molstruc.2019.127037.
[54] I.M. Khan, S. Shakya, Exploring colorimetric real-time sensing behavior of a newly designed CT complex toward nitrobenzene and Co^{2+}: spectrophotometric, DFT/TD-DFT, and mechanistic insights, ACS Omega 4 (2019) 9983–9995, doi:10.1021/acsomega.9b01314.
[55] R. Jawaria, M. Hussain, M. Khalid, M.U. Khan, M.N. Tahir, M.M. Naseer, A.A.C. Braga, Z. Shafiq, Synthesis, crystal structure analysis, spectral characterization and nonlinear optical exploration of potent thiosemicarbazones based compounds: a DFT refine experimental study, Inorganica Chim. Acta 486 (2019) 162–171, doi:10.1016/j.ica.2018.10.035.

[56] M. Rocha, M.C. Ruiz, G.A. Echeverría, O.E. Piro, A.L. Di Virgilio, I.E. León, A. Frontera, D.M. Gil, Diethylaminophenyl-based Schiff base Cu(ii) and V(iv) complexes: experimental and theoretical studies and cytotoxicity assays, New J. Chem. 43 (2019) 18832–18842, doi:10.1039/c9nj04975d.
[57] M. Kumar, G. Kumar, D.T. Masram, Copper(ii) complexes containing enoxacin and heterocyclic ligands: synthesis, crystal structures and their biological perspectives, New J. Chem. 44 (2020) 8595–8613, doi:10.1039/d0nj01192d.
[58] M. Zampakou, S. Balala, F. Perdih, S. Kalogiannis, I. Turel, G. Psomas, Structure, antimicrobial activity, albumin- and DNA-binding of manganese(<scp>ii</scp>)–sparfloxacinato complexes, RSC Adv. 5 (2015) 11861–11872, doi:10.1039/C4RA11682H.
[59] A. Draksharapu, A.J. Boersma, M. Leising, A. Meetsma, W.R. Browne, G. Roelfes, Binding of copper(II) polypyridyl complexes to DNA and consequences for DNA-based asymmetric catalysis, Dalton Trans. 44 (2015) 3647–3655, doi:10.1039/C4DT02733G.
[60] J. Novotný, S. Bazzi, R. Marek, J. Kozelka, Lone-pair–π interactions: analysis of the physical origin and biological implications, Phys. Chem. Chem. Phys. 18 (2016) 19472–19481, doi:10.1039/C6CP01524G.
[61] R. Mudavath, B. Ushaiah, C. Kishan Prasad, K. Sudeepa, P. Ravindar, S.N.T. Sunitha, C. Sarala Devi, Molecular docking, QSAR properties and DNA/BSA binding, anti-proliferative studies of 6-methoxy benzothiozole imine base and its metal complexes, J. Biomol. Struct. Dyn. 38 (2020) 2849–2864, doi:10.1080/07391102.2019.1647878.
[62] M. Kumar, G. Kumar, K.M. Dadure, D.T. Masram, Copper(II) complexes based on levofloxacin and 2N-donor ligands: synthesis, crystal structures and *in vitro* biological evaluation, New J. Chem. 43 (2019) 15462–15481, doi:10.1039/C9NJ03178B.
[63] M. Niu, Z. Li, H. Li, X. Li, J. Dou, S. Wang, DNA/protein interaction, cytotoxic activity and magnetic properties of amino-alcohol Schiff base derived Cu(ii)/Ni(ii) metal complexes: influence of the nuclearity and metal ions, RSC Adv. 5 (2015) 37085–37095 C5RA00623F.
[64] C. Santini, M. Pellei, V. Gandin, M. Porchia, F. Tisato, C. Marzano, Advances in copper complexes as anticancer agents, Chem. Rev. 114 (2014) 815–862, doi:10.1021/cr400135x.
[65] P. Sathyadevi, P. Krishnamoorthy, R.R. Butorac, A.H. Cowley, N.S.P. Bhuvanesh, N. Dharmaraj, Effect of substitution and planarity of the ligand on DNA/BSA interaction, free radical scavenging and cytotoxicity of diamagnetic Ni(ii) complexes: a systematic investigation, Dalton Trans. 40 (2011) 9690, doi:10.1039/c1dt10767d.
[66] P. Krishnamoorthy, P. Sathyadevi, R.R. Butorac, A.H. Cowley, N.S.P. Bhuvanesh, N. Dharmaraj, Copper(i) and nickel(ii) complexes with 1 : 1vs. 1 : 2 coordination of ferrocenyl hydrazone ligands: do the geometry and composition of complexes affect DNA binding/cleavage, protein binding, antioxidant and cytotoxic activities? Dalton Trans. 41 (2012) 4423, doi:10.1039/c2dt11938b.
[67] N. Joksimović, D. Baskić, S. Popović, M. Zarić, M. Kosanić, B. Ranković, T. Stanojković, S.B. Novaković, G. Davidović, Z. Bugarčić, N. Janković, Synthesis, characterization, biological activity, DNA and BSA binding study: novel copper(II) complexes with 2-hydroxy-4-aryl-4-oxo-2-butenoate, Dalton Trans. 45 (2016) 15067–15077, doi:10.1039/c6dt02257j.
[68] V. Gomathi Sankareswari, D. Vinod, A. Mahalakshmi, M. Alamelu, G. Kumaresan, R. Ramaraj, S. Rajagopal, Interaction of oxovanadium(iv)–salphen complexes with bovine serum albumin and their cytotoxicity against cancer, Dalton Trans. 43 (2014) 3260–3272, doi:10.1039/C3DT52505H.
[69] F. Pascale, L. Bedouet, M. Baylatry, J. Namur, A. Laurent, Comparative chemosensitivity of VX2 and HCC cell lines to drugs used in TACE, Anticancer Res. 35 (2015) 6497–6504.

Journal of Molecular Structure 1267 (2022) 133601

Contents lists available at ScienceDirect

Journal of Molecular Structure

journal homepage: www.elsevier.com/locate/molstr

Novel substituted isoindolinones derived from lawsone: synthesis, characterization, theoretical, biological activity and docking studies

Pratik Nariya[a], Sunny Kumar[c], Sriram Seshadri[c], Mrugesh Patel[d], Sonal Thakore[a,b,*]

[a] Department of Chemistry, Faculty of Science, The Maharaja Sayajirao University of Baroda, Vadodara 390 002, India
[b] Institute of Interdisciplinary Studies, The Maharaja Sayajirao University of Baroda, Vadodara 390 002, India
[c] Institute of Science, Nirma University, Ahmedabad 382 481, India
[d] K.C.Patel R&D centre, Charotar University of Science and Technology, Changa 388421, India

ARTICLE INFO

Article history:
Received 22 May 2022
Revised 23 June 2022
Accepted 26 June 2022
Available online 27 June 2022

Keywords:
Lawsone
Isoindolinones
Anticancer activity
HepG2 cells
In vivo study
DFT study

ABSTRACT

An efficient Mannich type multicomponent reaction approach was developed for the synthesis of a series of novel substituted isoindolinones derived from Lawsone, 2-formyl benzoic acid, and various primary amines. This protocol features direct construction of C-N and C-C bonds via metal-free method at room temperature using an environment-friendly solvent. The synthesized isoindolinone compounds **4a-4m** were characterized by various spectroscopic techniques such as ^{1}H NMR, ^{13}C NMR, FT-IR, and ESI-MS. Computational studies were carried out by the DFT method using B3LYP/6-31G (d,p) basic set as a tool to analyse the chemical reactivity parameters and comprehend the molecular interaction. The molecular electrostatic potential (MEP), dipole moment, chemical reactivity, and stability features of investigated isoindolinones revealed that **4i, 4j, 4l,** and **4m** could be promising candidates for further biological activity. The cytotoxic activity of selected compounds was evaluated using MTT assay against HepG2 cell lines (Human liver cancer cell line). The data revealed that screened compounds displayed excellent to moderate activity. The docking examination was executed on a promising liver cancer-associated Alpha fetoprotein (AFP). It showed a positive outcome with minimum binding energy and hydrogen bond interaction. Furthermore, In *vivo* studies ascertained that synthesized isoindolinone derivatives can lead to enhanced cancer cell death and prevention of tumor growth by restoring serum SGOT and SGPT levels near to normal. It further restores matrix metallopeptidase (MMP-2 and MMP-9 levels) near to control confirms the effectiveness of the compound.

1. Introduction

Isoindolinone skeleton is ubiquitous in many natural and synthetic products with various biological activities as shown in Fig. 1 [1–3]. These isoindolinone scaffolds tend to possess a broad range of biological activities such as antihypertensive, anti-inflammatory, anesthetic, antiviral, and anticancer [4–9]. Inspired by this fact, the synthesis of isoindolinone derivatives has attracted much attention during the past few decades. The traditional methods to synthesize substituted isoindolinone derivatives are mainly restricted to use of Wittig reaction, Grignard reagents, Heck cyclization, reduction process, Gabriel approach, lithiation process, Dies alder approach, and various enantioselective methods (Scheme 1) [10–16]. These methods are generally associated with several drawbacks such as multistep procedures, high temperature, use of expensive noble metal catalysts, and toxic or inflammable solvents. Therefore, the development of a simple, efficient, and environmentally friendly protocol for the synthesis of isoindolinone is highly desirable [17].

The multicomponent reaction strategy has recently attracted increasing attention for organic synthesis and pharmaceutical industries for the construction of complex molecules [18,19]. A similar one pot three-component reaction of 2-formyl benzoic acid with a variety of nucleophiles and primary amines also provides a direct approach toward the synthesis of isoindolinone derivatives as shown in Scheme 1. However, these methods report the use of high temperatures, expensive catalysts, or microwave heating [16,17,20,21].

Recently we have reported mannich bases derived from biologically important 2-hydroxy-1,4-naphthoquinone (Lawsone), using multicomponent reaction, for potential anticancer activity on HepG2 cell lines (Human liver cancer cell line) [22,23]. Given the importance of the isoindolinone skeleton, it is desirable to establish a practical method to synthesize isoindolinone derived from lawsone employing environment-friendly reaction media and investigating their biological activity.

* Corresponding author.
E-mail address: chemistry2797@yahoo.com (S. Thakore).

https://doi.org/10.1016/j.molstruc.2022.133601
0022-2860/

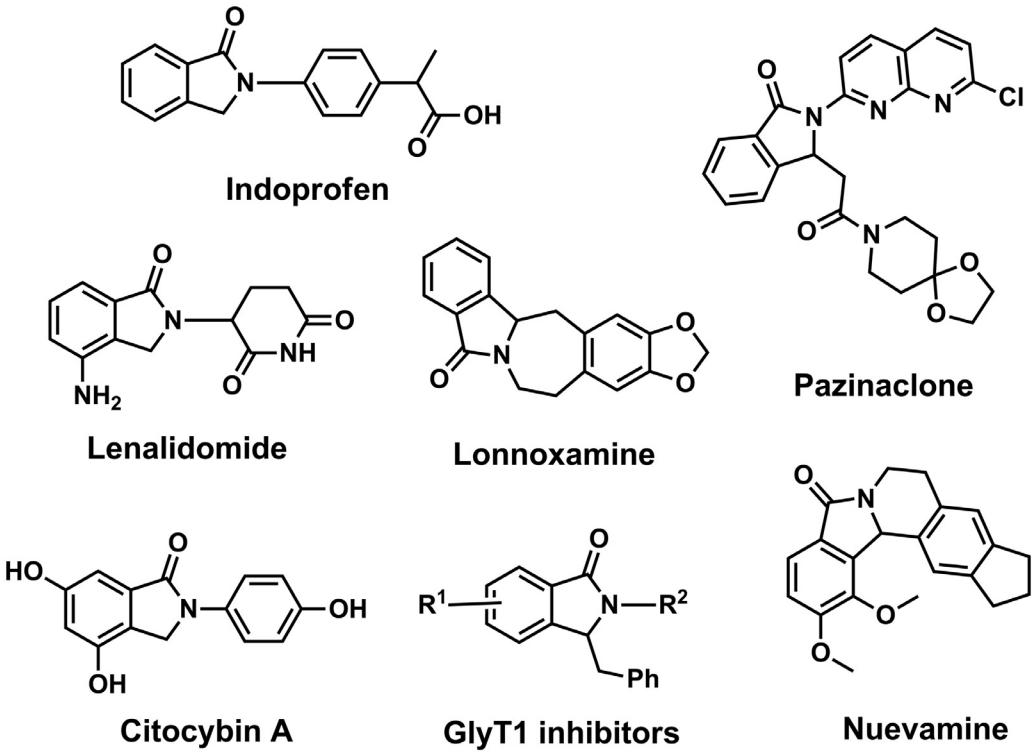

Fig. 1. Examples of natural and synthetic biologically active isoindolinone motifs.

In recent days, computational methods have been promoted as a valid tool for the prediction of pharmacokinetic parameters such as adsorption, distribution, metabolism, and excretion (ADME) when chemical structures are numerous [24]. Density function theory (DFT) is a powerful computing tool for revealing the complete molecular structure, stability, and global reactivity parameters of biomolecules such as dipole moment, electrophilicity (ω), electronegativity (χ), chemical potential (μ), softness (S), hardness (η), and electron affinity (A) [25–27]. The DFT calculations of title compounds have not yet been reported.

Herein we report the synthesis of substituted isoindolinone derivatives via a three-component Mannich-cascade cyclization reaction of lawsone, 2-formyl benzoic acid, and primary amines in presence of acetic acid as a catalyst at room temperature with moderate to high yields. The formation of desired product was confirmed by various analytical techniques such as ^{1}H NMR, ^{13}C NMR, FT-IR, and Mass spectroscopy. In addition, DFT calculations of synthesized compounds were performed to determine molecular structure, dipole moment, Molecular Electrostatic Potential (MEP) maps, and global reactivity parameters. Further, in *vitro* anticancer activity of selected compounds was evaluated against HepG2 (Human liver carcinoma cell lines) employing MTT assay. The compounds with promising activity were further investigated by molecular docking on Alpha fetoprotein (AFP). And finally, by in *vivo* studies.

Table 1
Optimization of reaction conditions[a].

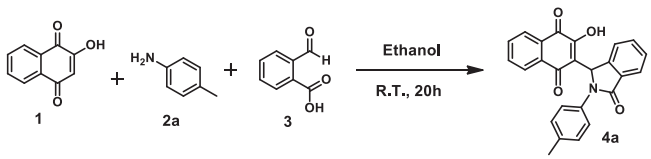

Entry	Solvent	Time (h)	Yield (%)[b]
1	Ethanol	20	81
2	Methanol	20	61
3	Tetrahydrofuran	22	51
4	Dichloromethane	24	72
5	Chloroform	24	70
6	Acetone	21	16
7	Acetonitrile	22	41
8	Water	24	Trace
9	Ethanol[c]	24	56
10	Ethanol[d]	20	92
11	Ethanol[e]	20	79

[a] Reaction conditions: Lawsone (**1**) (1.0 mmol), 4-methyl aniline (**2a**) (1.1 mmol), 2-formyl benzoic acid **(3)** (1.0 mmol), Solvent (5 mL) at room temperature
[b] Yield of isolated product.
[c] Reaction was performed under reflux condition.
[d] Acetic acid (5 mol%) was used as a catalyst.
[e] PTSA (5 mol%) was used as a catalyst.

2. Result and discussion

2.1. Synthesis of isoindolinones

Lawsone **1** (1.0 mmol), 4-methyl aniline **2a** (1.1 mmol), and 2-formyl benzoic acid **3** (1.0 mmol) was used as the model substrates to prepare desired substituted isoindolinone **4a.** As shown in Table 1, the reaction proceeded smoothly at room temperature affording the desired product **4a** in 80% isolated yield without using a catalyst (Table 1, entry 1). Encouraged by this result, we further screened different common organic solvents such as methanol, tetrahydrofuran, dichloromethane, chloroform, acetone, and acetonitrile to find a suitable solvent to promote the model reaction. Lower isolated yields of **4a** were obtained when the reaction was performed in these solvents (Table 1, entry 2-7). When water was used instead of organic solvents to synthesize **4a**, only a trace amount of product was isolated (Table 1, entry 8). When reaction was carried out under reflux conditions, the isolated yield of compound 4a was decreased to 56%, even on extending the reaction time up to 24 h (Table 1, entry 9). Furthermore, it was ob-

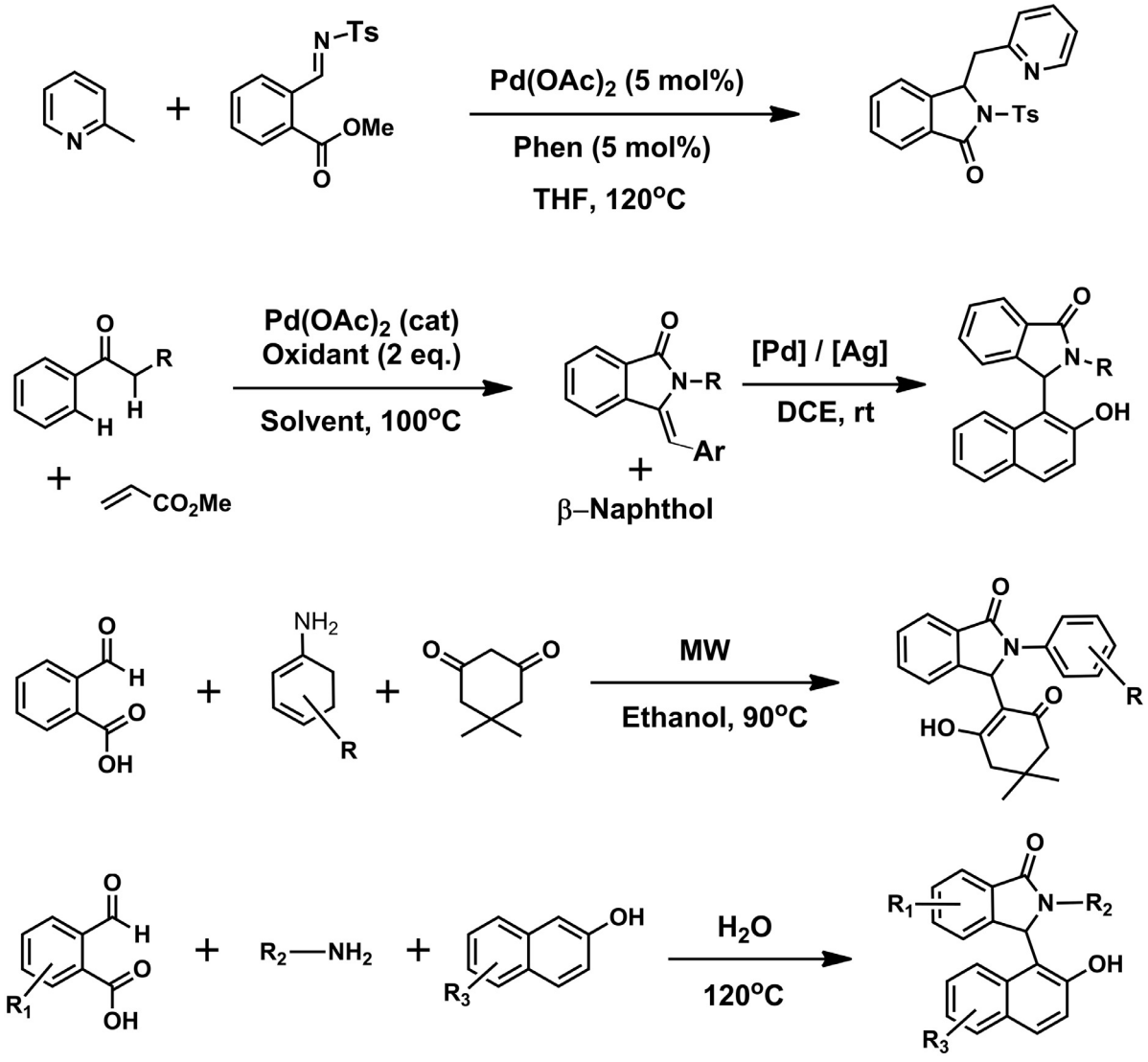

Scheme 1. Synthetic approaches to substituted isoindolinones.

served that when 5 mol% acetic acid was added to the reaction mixture, the yield of corresponding isoindolinone **4a** significantly increases to 92% (Table 1, entry 10). There was no improvement in yield when 5 mol% PTSA was added to the reaction mixture (Table 1, entry 11). Thus optimized reaction conditions are as follows: lawsone **1** (1.0 mmol), 4-methyl aniline **2a** (1.1 mmol), and 2-formyl benzoic acid **3** (1.0 mmol) in ethanol at room temperature for 20 h in presence of 5 mol% acetic acid (Table 1, entry 10).

Isoindolin-1-yl-naphthalene-1,4-dione **4a** was characterized using various spectral studies. The yellow solid showed a molecular ion peak at 396.17 in the ESI-MS spectrum, consistent with molecular formula $C_{25}H_{17}NO_4$. The FT-IR spectrum of **4a** showed bands for hydroxyl and conjugated carbonyl functional groups at 3399 cm^{-1} and 1680 cm^{-1} respectively. While the bands for carbonyl of isoindolinone and naphthoquinone was observed at 1625 cm^{-1} and 1680 cm^{-1} respectively.

^{1}H NMR spectrum indicates one methyl group at δ 2.63 ppm. A singlet was also observed at δ 6.86 ppm due new bond formed between aldehyde, amine, and lawsone. The eight protons of naphthoquinone and aromatic aldehyde appear in δ 7.1-8.3 ppm region as double doublet (dd), and triplet of doublet (td). They were confirmed by their coupling constant values (J) as reported in the literature [23]. The ^{13}C NMR spectra showed three peaks at δ 168.01, 180.48, and 184.01 corresponding to the isoindolinone and naphthoquinone carbonyl group. The methyl group was observed at δ 20.91 ppm, while one aliphatic tertiary carbon near to amide nitrogen was observed at δ 55.58 ppm. All other aromatic carbons were observed in aromatic region δ 118 to 154 ppm. On the spectral evidence, **4a** was confirms to be 2-hydroxy-3-(3-oxo-2-(p-tolyl)isoindolin-1-yl)naphthalene-1,4-dione.

After determining optimized reaction conditions, we next examined a range of primary amines **2a-2m** to test the scope of one pot three-component reaction with Lawsone **(1)** and 2-formyl benzoic acid **(3).** As shown in Table 2, various primary amines including substituted aryl amines, heteroaryl-alkylamines, and alkyl amines were for reaction. Aryl amine substituted with methyl, chloro, bromo, and fluoro groups (Table 2, entry 1-7) provided the corresponding isoindolinone products **4a-4g** in good to excellent yield (79-92%). Apart from aryl amines, benzyl amine, 2-furfuryl amine, tryptamine, and thiophene-2-ethyl amine (Table 2, entry 8-11) also successfully afforded the corresponding isoindolinone **4i-4k** good to high yields (62-78%). We further examined the reaction with common aliphatic amines like n-butyl amine and n-octylamine (Table 2, entry 12 & 13). These amines successfully gave desired product **4l** and **4m** respectively. However, the reaction of n-butyl amine gave corresponding product **4l** in only 45% yield

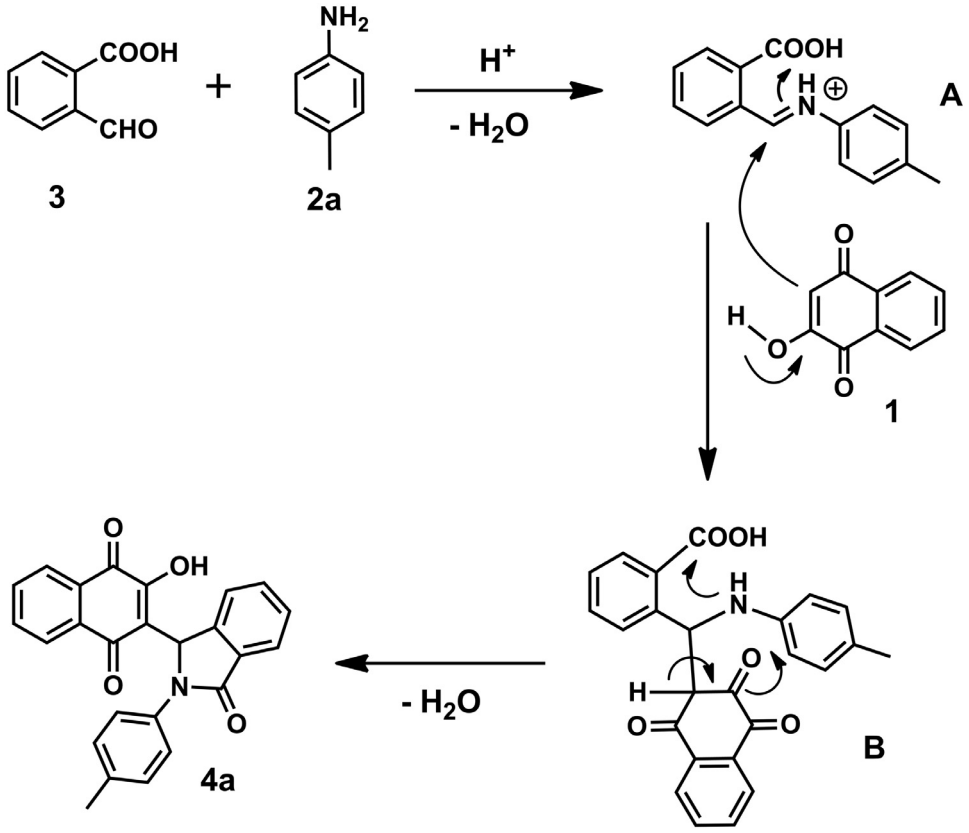

Scheme 2. Proposed plausible reaction pathway for synthesis of isoindolinones.

Table 2
Scope of amines[a].

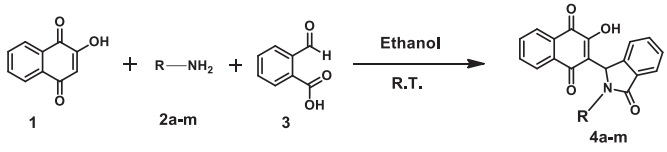

Entry	R	Product	Yield (%)[b,c]
1	4-MeC_6H_5	4a	92 ± 0.60
2	4-MeOC_6H_5	4b	91 ± 0.85
3	C_6H_5	4c	80 ± 1.1
4	4-ClC_6H_5	4d	83 ± 1.2
5	4-BrC_6H_5	4e	79 ± 1.4
6	3-Cl-4F-C_6H_5	4f	83 ± 1.2
7	3,4-$(Me)_2C_6H_5$	4g	81 ± 1.5
8	$C_6H_5CH_2$	4h	78 ± 1.8
9	Furfuryl	4i	62 ± 1.7
10	Tryptamine	4j	65 ± 0.90
11	Thiophene-2-ethyl	4k	68 ± 1.5
12	n-butyl	4l	75 ± 2.1
13	n-octyl	4m	70 ± 1.3
14	2-picolyl [d]	-	0
15	2-pyridinyl [d]	-	0

[a] Reaction conditions: Lawsone (**1**) (1.0 mmol), 4-methylaniline (**2a**) (1.1 mmol), 2-formyl benzoic acid **(3)** (1.0 mmol), Solvent (5 mL), Acetic acid (5 mol%) at room temperature
[b] Yield of isolated product.
[c] n = 3 (experiments were performed in triplicates).
[d] At reflux (80 °C).

(Table 2, entry 12). When 2-picolyl amine and 2-amino pyridine were used as a substrate, the desired product was not observed even on reflux conditions (Table 2, entries 14 & 15).

Based on the literature precedents, a plausible reaction mechanism was proposed and shown in scheme 2. Initially 2-formyl benzoic acid **3** condensed with amine **2a** to generate intermediate **A,** followed by Mannich type reaction of Lawsone with activated iminium intermediate **A,** to give intermediate **B**. It further undergoes subsequent re-aromatization and intramolecular cyclization to form final product **4a.**

2.2. Theoretical studies

The impact of Frontier molecular orbital (FMO) is indispensable in the determination of electronic, optical activity, chemical stability, biological activity, and molecule reactivity. Recently, many reports showed the correlation between FMOs and several biological properties such as antimicrobial, anticancer, antifungal, and cytotoxic activities,[28–35]. There are numerous methods to determine the excitation energies of the molecule (FMO) is the most popular method to determine the gap between the highest occupied molecular orbital (HOMO) and the lowest occupied molecular orbital (LUMO) of a neutral molecule.

The energy gap between HOMO-LUMO can be measured by the excitability of the compound and reports the nature of the molecular system. The higher energy gap between HOMO-LUMO is responsible for low chemical reactivity and high kinetic stability. Since the energy is unfavourable to high lying LUMO to add electron and low lying HOMO to remove an electron, which forms the activated complex of any possible chemical reaction [36–38]. The global reactivity parameters such as dipole moment, electrophilicity (ω), electronegativity (χ), chemical potential (μ), softness (S), hardness (η), and electron affinity (A) provide useful information to understand the pharmacological activity of the compounds in drug modelling by using HOMO-LUMO energies [27,39–42].

The HOMO-LUMO values of compound **4a** are shown in Table 3. The HOMO and LUMO gap of compound **4a** is -2.147 eV. The elec-

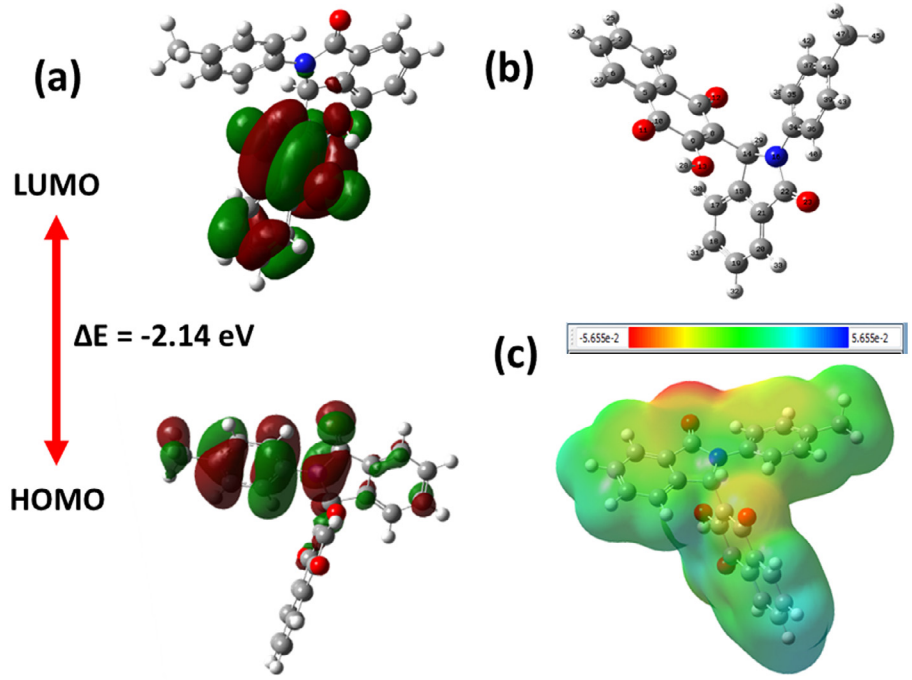

Fig. 2. (a) Surface plot showing the frontier molecular orbitals, (b) optimized structure with atom labeling, and (c) MEP surface diagram of compound 4a.

Table 3
HOMO, LUMO, energy gap, global electronegativity, global hardness and softness, global electrophilicity index, and dipole moment of compound 4a.

Parameters	B3LYP/6-31G (d, p) (eV)
HOMO	-5.549
LUMO	-3.402
ΔE	2.147
Ionization potential (I)	5.549
Electron affinity (A)	3.402
Chemical potential (μ)	-4.475
Hardness (η)	1.073
Electronegativity (χ)	4.475
Softness (σ)	0.536
Electrophilicity index (ω)	9.329
Dipole moment (Debye)	6.195

tron transition alignments for the electron transfer from ground state to the excited state are mainly responsible for electron excitation from HOMO-LUMO. The compositions of atomic orbitals of **4a** derived from FMOs along with optimized structure are shown in Figs. 2a and 2b. The molecular structure optimization and HOMO-LUMO gap of remaining compounds **4b-4m** were calculated using similar basic sets of function (i.e. B3LYP/6-31G (d, p) shown in **table S1**. The compound **4b** showed the lowest (-1.859 eV) while **4l** showed the highest (-2.833 eV) HOMO-LUMO energy gap. The data tabulated in **table S1** indicated that the values of ionization potential are higher that electron affinity, which disclose that all the compounds have better capability to accept electrons. Electrophilicity index (ω) is one of the main quantum chemical descriptors for evaluation of biological activity. Compound **4h, 4i, 4k,** and **4m** possess higher electrophilicity (16.28, 14.39, 16.12, and 16.05) among synthesized compounds. Which denotes that they are stronger electrophiles. As a result, **4i** has lesser energy gap so, making it more polarizable, least kinetic stable and high reactivity making it soft molecule. Furthermore dipole moment of **4i** is low (5.72) and electronegativity (χ = 4.65) is high makes stables and effects biological activity [26,27].

The molecular electrostatic potential (MEP) surface is very important to determine electrophilic and nucleophilic sites based on the electrostatic potential distribution [43]. The MEP surface of compound **4a** was drawn by DFT/B3LYP method and shown in Fig. 2c. The electrostatic values are visualized in terms of color coding. The negative and positive potential regions are shown by red and blue color respectively. While zero and neutral potential regions are shown by green and yellow color respectively. As shown in Fig. 2c the major negative potential appears over O23 atom due to isoindolinone C=O group, while considerably lower negative potential than O23 atom observed near O12 atom of naphthoquinone C=O group. The positive potential is surrounded near phenolic oxygen O13 atom due to nearby hydrogen atoms, which indicates the occurrence of O-H—O interaction [44]. Similar behavior was observed in other compounds **4b-4m** as shown in **figure S53**. In case of compound **4j,** the positive potential was observed near the nitrogen atom of indole ring as shown in **figure S53** due to the presence of the NH group. These data suggest that carbonyl oxygen of isoindolinone and naphthoquinone has a higher electron density and it plays an important role in the biological activity through hydrogen bonding with the target.

The potential of new molecule as new drug can be evaluated by forecasting in silico physicochemical attributes, drug likeness, or adsorption, distribution, metabolism, excretion (ADME) traits. Topological polar surface area (TPSA), an attribute that is explored to forecast the passive molecular transport trait of drugs, was also appraised. The physicochemical properties are shown in **table S2.** The physicochemical properties are in good agreement with the applied criteria. It is expected to have good bioavailability score as all the compounds have TPSA $\leq$ 110 Å. Theoretical data of in silico pharmacokinetic/ADME evaluations are presented in **table S3.** The following predictions can be made based on this. All the compounds showed high gastrointestinal absorptions (GI). All the compounds are P-gp (p- glycoprotein) non inhibitors except **4m,** while half of compounds have no BBB (blood brain barrier) permeability. All the synthesized compounds were tested for inhibition of the Cytochrome P450 isomers, that is, CYP1A2, CYP2C19, CYP2C9, CYP2D6, and CYP3A4. It was found that all compounds are in-

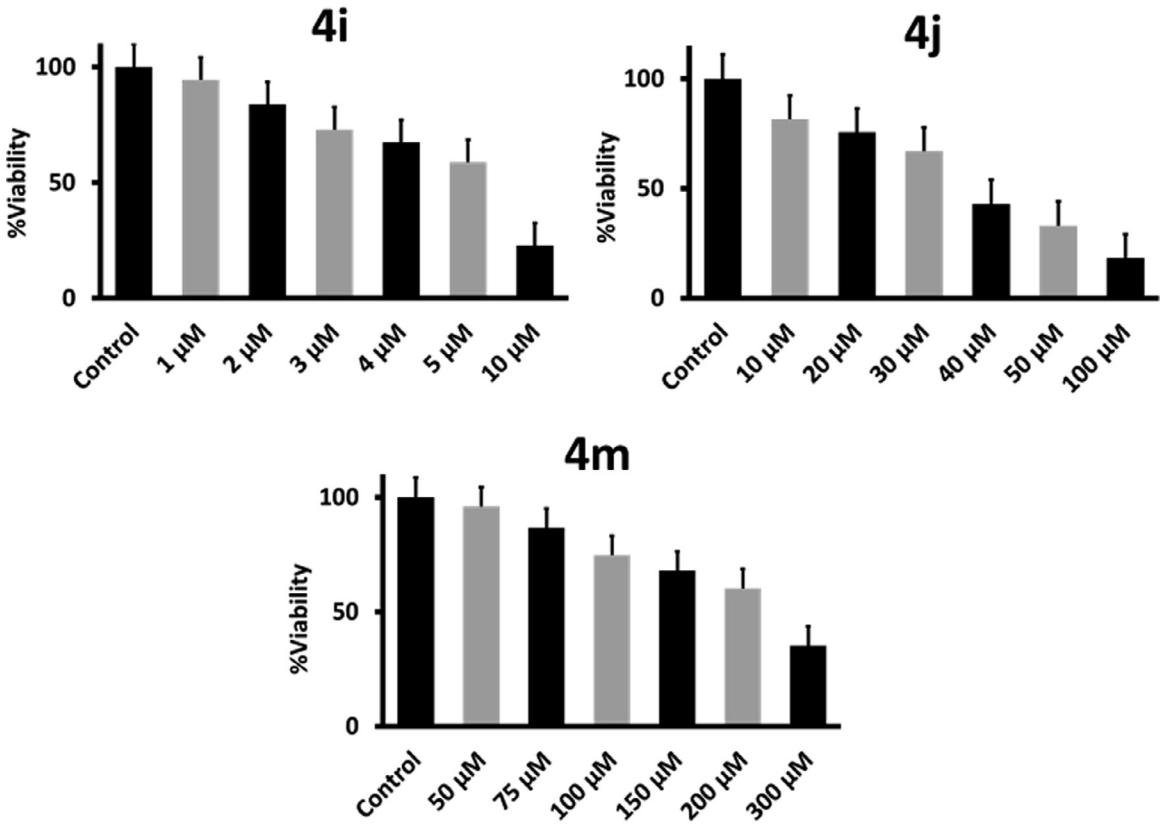

Fig. 3. Graph of %viability against concentration for MTT assay of compound 4i, 4j, and 4m.

hibitor of CYP2C9, CYP3A4 and non-inhibitor of CYP2D6. Most of the compounds are CYP1A2 inhibitors except **4b, 4g** and **4m**. All the tested compounds are inhibitors of CYP2C19 with the exception of compound **4b** and **4i.** The predictions show that they satisfy the Lipinski rule of five [45], Veber rule [46] as well as Egan rule [47] suggesting good bioavailability.

2.3. Cytotoxicity

To investigate the cytotoxic potential of isoindolinone derivatives, some compounds were considered for in vitro cytotoxicity studies on Human liver cancer cells (HepG2 cell lines) based on information obtained from DFT and ADME predictions. The compounds were screened at 1 to 10 µM concentrations for 48h for cell viability assay (by MTT) and their IC_{50} values were obtained.

The compounds **4j** and **4m** were screened at higher concentrations to determine their IC_{50} values as they showed low cytotoxicity at lower concentrations. The plot of % viability *vs* concentration of compound obtained is shown in Fig. 3. The IC_{50} values of compounds **4i, 4j,** and **4m** were also calculated and are 5.29, 39.35, 265.25 µM, respectively. Among all, **c**ompound **4i** showed the lowest IC_{50} value which was also in comparable range with standard drug Dox (IC_{50} 1.30 µM) [48]. While compound **4m** showed high IC_{50} value. Overall the isoindolinone skeleton derived from lawsone with heterocyclic aromatic ring showed high cytotoxicity (i.e. **4i and 4j**) while the compound with long chain showed low cytotoxicity against HepG2 cell lines.

2.4. Molecular docking

The molecular docking of active compounds (**4i**, and **4j**) with the target protein Alpha fetoprotein (PDB ID: 2DA2) a liver cancer-associated protein. As alpha Fetoproteins (APF) is most widely used and accepted serum marker for Hepatocellular carcinoma (HCC) [49–51]. The molecular docking study disclosed that compounds are promising candidates for further studies, which is justified by low binding energy -7.6 and -7.1 kcal/mol for **4i** and **4j** respectively with AFP.

Docking and 2D diagrams illustrating protein ligand interaction are shown in Fig. 4A and 4B. The different interactions were shown by compounds at molecular level such as, hydrogen bond, covalent bond, pi-sigma bond, pi-pi stacked bond. Compound **4i** displayed various binding interactions including hydrogen bonding with residue TRP A54 and ARG A8. It also displayed pi-alkyl bonding with residue VAL A53 and LYS A61. Compounds 4j was involved in binding interactions involves pi-alkyl with PHE A55, PHE A26, and ALA A58. Thus, the minimum binding energies and hydrogen bond interactions of compound **4i** with AFP might be one of the justifications for good in vitro activity.

2.5. In vivo studies

Hepatocellular carcinoma (HCC) is the most common form of liver cancer and causes prominent cancer death worldwide [52]. The anticancer potential of one of the synthesized compounds was assessed for the treatment of liver cancer on nude mice model. The tumor regression observed in the animals dosed with **4i** was compared with the animal treated with a well-known anticancer drug doxorubicin. The changes in body weight and weight of liver in animals revealed that reduction of tumor after treatment with compound **4i.** The tumor induced group showed the most significant decline in body weight (**figure S54 A**). While, no change in body weight was observed after treatment with compound **4i**. As per the **figure S54 B** the increase in weight of the liver suggest tumor growth, which got reversed following treatment.

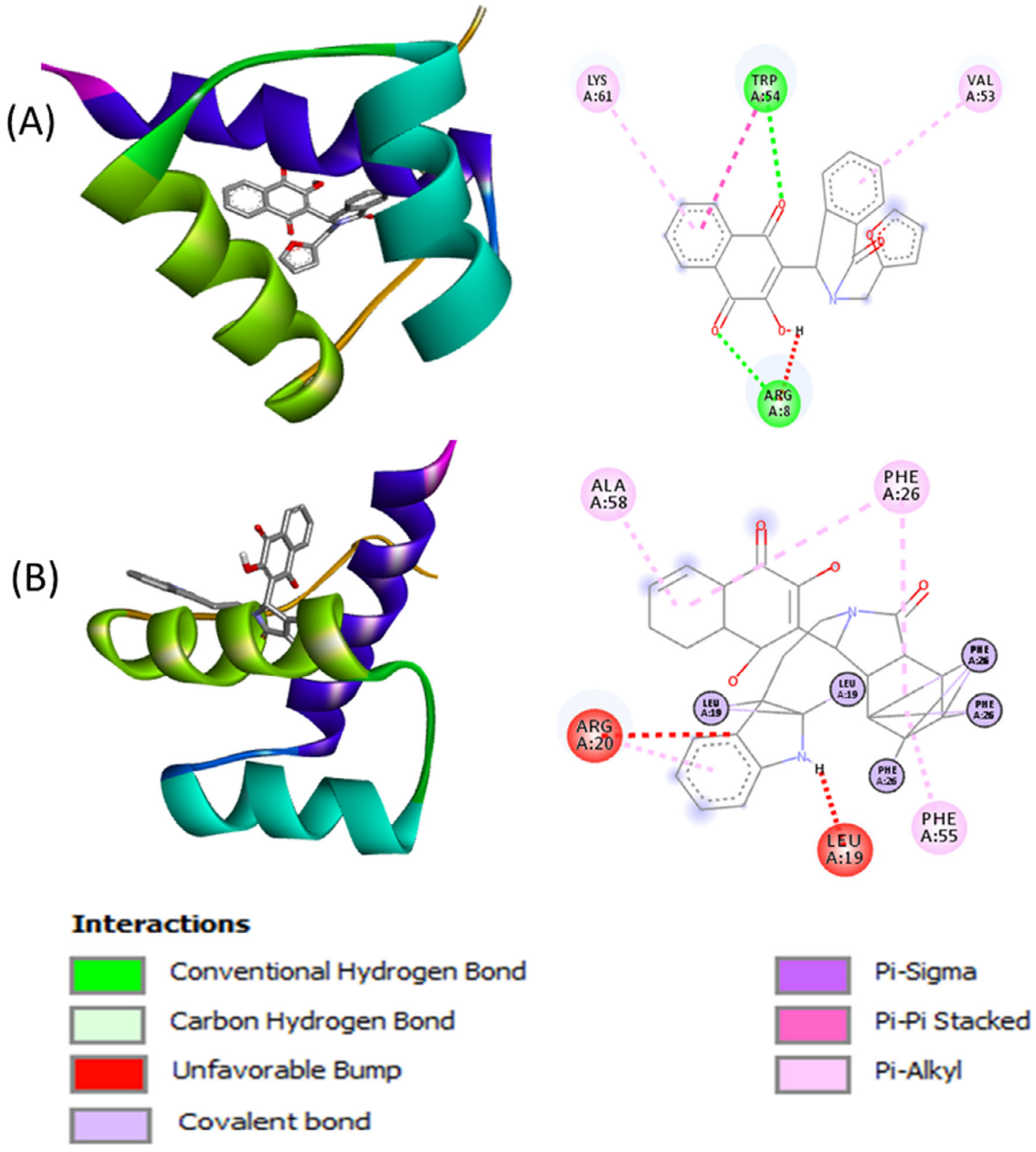

Fig. 4. In silico docking model of AFP protein with (a) 4i, and (b) 4j. 3D and 2D images generated with Biovia Discovery Studio Visualizer.

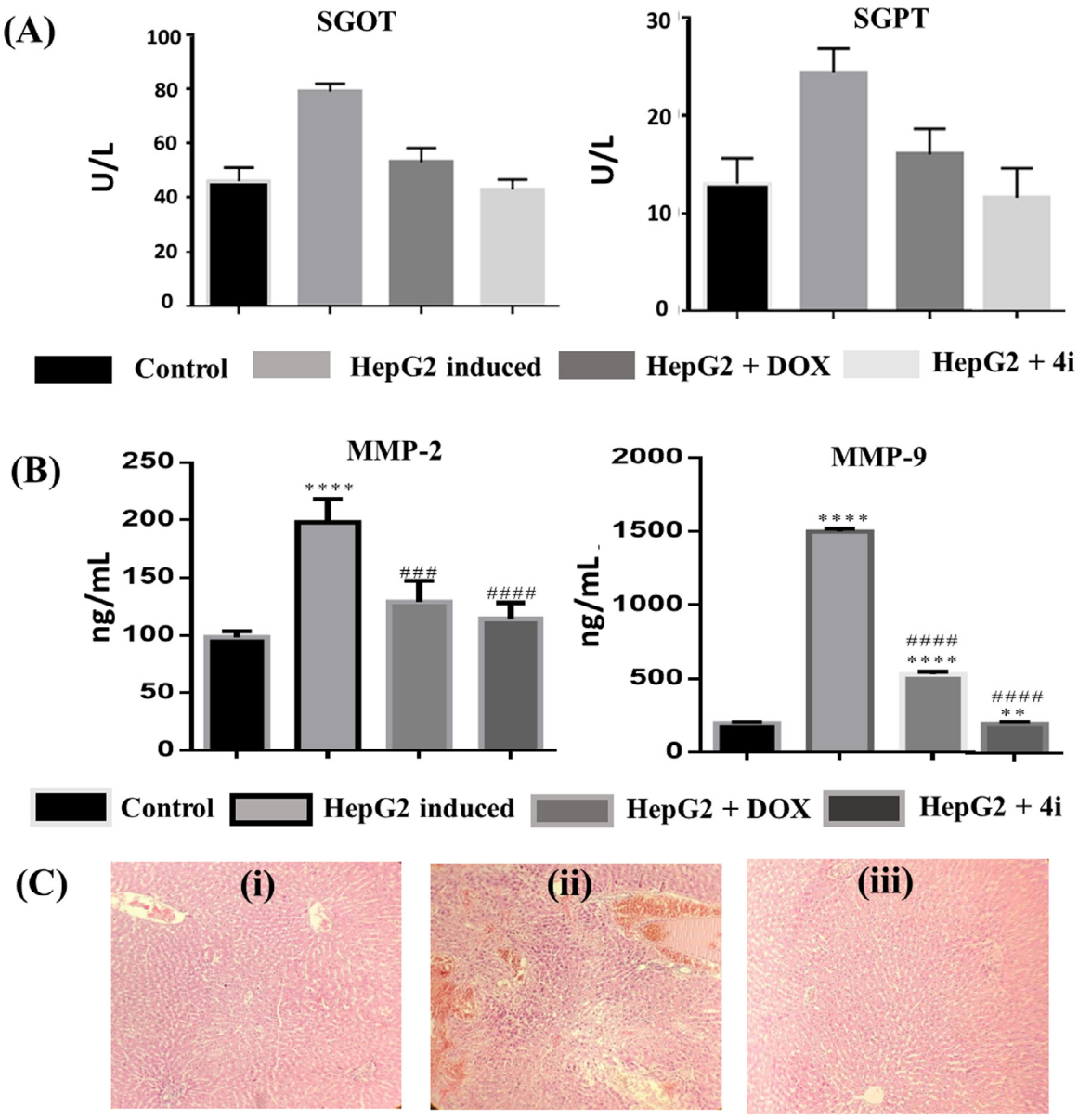

Fig. 5. (A) Serum SGOT and SGPT profile, (B) MMP-2 and MMP-9 profile, (C) histoarchitecture of (i) Control and animals dosed with (ii) HepG2 and (iii) HepG2 + 4i.

The liver functioning was analyzed by testing the serum SGOT and SGPT levels. Both SGOT and SGPT levels were found to be increased in the HCC induced untreated group as shown in Fig. 5A. Upon treatment with DOX and **4i** the levels were observed to attain normal state with **4i** showing anticancer potential comparable to DOX (Fig. 5A). The circulating levels of Alpha Fetoproteins (APF) is an important biomarker accessed to monitor presence and progress of HCC. The AFP level was found to be significantly elevated in HCC induced group **(figure S54 C)**. It is interesting to note that compound **4i** showed lower AFP value than standard drug doxorubicin validates efficacy of isoindolinone derivatives.

The tumor progression and angiogenesis was monitored by analyzing the levels of cancer specific biomarkers, matrix metallopeptidase (MMP) 2 and 9 [53,54]. The results showed an increment in the levels of MMP-2 and 9 in the plasma that marks the beginning of hepatic tumor development (Fig. 5B). The group of animals treated with **4i** showed decrement the levels of both these biomarkers. The results were comparable to the animals treated with DOX. The liver tissues were examined post H&E staining, the untreated group demonstrated severe distortions in the liver lobes and a de-arrangement of hepatic code as well as canaliculi (Fig. 5C (i)) [55]. However, after treatment with compound **4i** the distorted histoarchitecture was restored and showed a morphology that is similar to the animals of control group (Fig. 5C (iii)). Overall, in vivo studies provided valuable insight on the efficiency of substituted isoindolinone derived from Lawsone **(compound 4i)** for the prevention of tumor progression.

3. Conclusion

To summarize, we have developed an efficient method towards the synthesis of biologically active substituted isoindolinone via multi-component Mannich reaction using naturally occurring Lawsone, 2-formyl benzoic acid, and various primary amines. This approach offers the advantage such as the use of environmentally benign solvent, acetic acid as catalyst, column chromatography free workup procedure. The HOMO-LUMO energy gap (ΔE) and MEP surface diagram were also determined using a theoretical

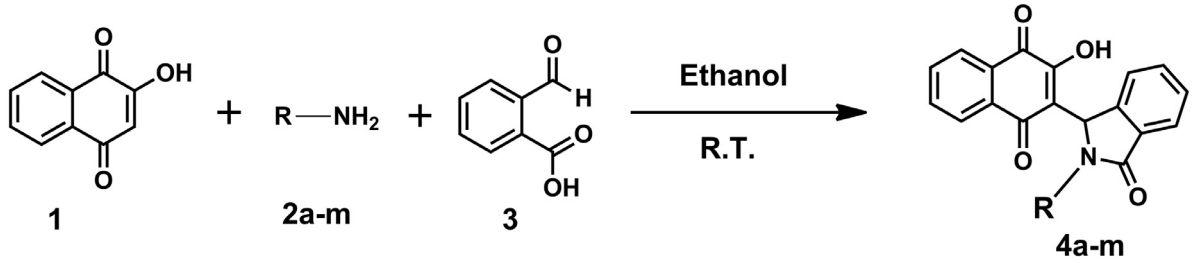

Scheme 3. General schematic for synthesis of substituted isoindolinones.

DFT study. The compound **4b** with 4-methoxybenzene substitution showed the lowest (-1.859 eV) while compound **4l** with n-butyl substitution showed the highest (-2.833 eV) HOMO-LUMO energy gap. The electrostatic potential data derived from MEP surface diagram revealed that carbonyl oxygen of isoindolinone and naphthoquinone has a higher electron density and it plays an important role in the biological activity through hydrogen bonding with the target and was supported by a description of global reactivity parameters. The ADME parameters revealed that compounds have good bioavailability. The IC_{50} value for cytotoxic activity of compound **4i** was found to be 5.29 µM on the HepG2 cell line, which is comparable with the standard drug. Furthermore, molecular docking studies on Alpha fetoprotein (AFP), confirm the minimum binding energy with protein and interaction via hydrogen bonding. In addition, in vivo studies corroborate with in-vitro data. The cancer-induced Balb mice demonstrated noteworthy decrement in levels of biomarkers MMP-2 and MMP-9 indicating significant tumor regression when compound **4i** was injected into animals. It was also evident in the histoarchitecture of the liver. Thus isoindolinone derived from lawsone can be effective as an anticancer drug

4. Experimental

4.1. Material and methods

Lawsone and 2-formyl benzoic acid was purchased from Sigma Aldrich, India. All other reagents Amines were purchased from Sigma-Aldrich, Spectrochem, and SRL chemicals, Mumbai, India. All the reagents were used without further purification. The reaction progress was monitored by TLC in ultraviolet light. Merck TLC plates were used to monitor the reaction progress. All melting points were recorded by the scientific open capillary method and are uncorrected. FT-IR spectra were recorded on Bruker Alpha FT-IR Spectrometer by using KBr pellets. Elemental analysis were recorded on Thermo Finnigan Flash 11-12 series. ^{1}H & ^{13}C NMR spectra were recorded on Bruker Avance (400 MHz) spectrometer in $CDCL_3$ or DMSO-d_6 solvent. Chemical shift are reported in parts per million (ppm) downfield from TMS and coupling constants (J) is reported in Hertz (Hz). Proton count multiplicities are reported as singlet (s), doublet (d), triplet (t), multiplet (m), doublet of doublet (dd), and triplet of doublet (td). Mass spectra were determined by water acquity ultra-performance LC with SQ detector.

4.2. General procedure for synthesis of substituted isoindolinones (4a-4m)

The compounds from **4a-4m** were synthesized following the optimized reaction conditions. Briefly, a mixture of 2-formyl benzoic acid (1 mmol) in ethanol (5 mL), respective amine (1.1 mmol), and Lawsone (1 mmol) were mixed in 25 mL round bottom flask at room temperature in presence of 5 mol% of acetic acid until the reaction was completed. The progress of reaction was monitored by TLC. After completion of the reaction, the obtained solid was filtered and washed by ethanol. Isolated crude product was recrystallized in acetic acid and dried under vacuum. General schematic for synthesis is shown in Scheme 3.

4.3. Details of the compounds synthesized

4.3.1. 2-hydroxy-3-(3-oxo-2-(p-tolyl)isoindolin-1-yl)naphthalene-1,4-dione (4a)

Yellow solid; Yield: 92%; M.P: 210 °C -212 °C

^{1}H NMR ($CDCL_3$, 400 MHz) δ (ppm): 2.63 (s, 1H), 6.86 (s, 1H), 7.12 (d, 2H, J=8.4 Hz), 7.36 (dd, 1H, J=8.4 Hz), 7.54 (m, 4H), 7.72 (td, 1H, J=7.6 Hz, J=1.2 Hz), 7.84 (td, 1H, J=8.2 Hz, J=1.2 Hz), 7.95 (dd, 1H, J=7.6 Hz, J=1.2 Hz), 8.03 (dd, 1H, J=8.8 Hz, J=1.2 Hz), 8.24 (dd, 1H, J=8.8 Hz, J=1.2 Hz). **^{13}C NMR** ($CDCL_3$, 100 MHz) δ (ppm): 20.91, 55.58, 118.16, 121.86, 122.23, 122.32, 123.76, 126.58, 127.12, 128.54, 129.43, 132.17, 133.02, 133.46, 134.79, 134.86, 135.30, 135.40, 142.82, 154.52, 168.01, 180.48, 184.01. **IR (KBr) cm^{-1}**: 3399 (O-H), 3073 (=C-H), 2913 (C-H), 1680 (C=O), 1625 (C=O, amide), 1592 (C=C), 1272 (C-N), 1048 (C-O). **ESI/MS** 396.17 $[M+1]^+$ calculated for $C_{25}H_{17}NO_4$. Anal. Calculated for: C, 75.94; H, 4.33; N, 3.54; O, 16.19; Found C, 75.90; H, 4.35; N, 3.52.

4.3.2. 2-hydroxy-3-(2-(4-methoxyphenyl)-3-oxoisoindolin-1-yl)naphthalene-1,4-dione (4b)

Orange solid; Yield: 91%; M.P: 200 °C

^{1}H NMR ($CDCL_3$, 400 MHz) δ (ppm): 3.75 (s, 1H), 6.82 (d, 1H), 6.85 (d, 2H, J=4 Hz), 7.37 (d, 1H, J=7.2 Hz), 7.54 (m, 4H), 7.72 (td, 1H, J=8.2 Hz, J=1.2 Hz), 7.83 (td, 1H, J=8.2 Hz, J=1.2 Hz), 7.94 (d, 1H, J=6.8), 8.04 (dd, 1H, J=6.4 Hz, J=4.4 Hz), 8.25 (dd, 1H, J=7.2 Hz, J=4.4 Hz). **^{13}C NMR** ($CDCL_3$, 100 MHz) δ (ppm): 55.36, 55.80, 114.19, 118.12, 122.31, 123.74, 123.80, 126.64, 127.19, 128.57, 128.68, 129.31, 130.38, 132.09, 132.20, 133.01, 133.12, 133.51, 135.56, 142.74, 154.13, 156.96, 167.89, 180.47, 183.93. **IR (KBr) cm^{-1}**: 3237 (O-H), 3024 (=C-H), 2962 (C-H), 1671 (C=O), 1639 (C=O, amide), 1586 (C=C), 1273 (C-N), 1049 (C-O). **ESI/MS** 396.17 $[M+1]^+$ calculated for $C_{25}H_{17}NO_4$. Anal. Calculated for: C, 72.99; H, 4.16; N, 3.40; O, 19.14; Found C, 72.95; H, 4.18; N, 3.42.

4.3.3. 2-hydroxy-3-(3-oxo-2-phenylisoindolin-1-yl)naphthalene-1,4-dione (4c)

Yellow solid; Yield: 80%; M.P: 208-210 °C

^{1}H NMR ($CDCL_3$, 400 MHz) δ (ppm): 6.90 (s, 1H), 7.11 (q, 1H, J=8.0 Hz), 7.33 (t, 2H, J=9 Hz), 7.37 (d, 1H, J=6.8 Hz), 7.55 (m, 2H), 7.68 (dd, 2H, J=4.8 Hz), 7.72 (td, 1H, J=8.2 Hz, J=1.2 Hz), 7.84 (td, 1H, J=8.2 Hz, J=1.2 Hz), 7.96 (dd, 1H, J=8.0), 8.03 (dd, 1H, Hz, J=4.4 Hz), 8.27 (dd, 1H, J=4.2). **^{13}C NMR** ($CDCL_3$, 100 MHz) δ (ppm): 20.75, 55.41, 118.16, 121.70, 122.07, 122.34, 123.92, 125.03, 126.66, 127.223, 128.67, 128.99, 129.26, 132.17, 132.37, 132.87, 133.56, 135.48, 137.48, 142.66, 154.03, 168.03, 176.68, 180.45, 183.95. **IR (KBr) cm^{-1}**: 3384 (O-H), 3017 (=C-H), 1706, 1678 (C=O), 1641 (C=O, amide), 1594 (C=C), 1275 (C-N), 1047 (C-O). **ESI/MS** 382.16 $[M+1]^+$ calculated for $C_{24}H_{15}NO_4$. Anal. Calculated for: C, 78.58; H, 3.96; N, 3.58; O, 16.78; Found C, 78.60; H, 3.95; N, 3.56.

4.3.4. 2-(2-(4-chlorophenyl)-3-oxoisoindolin-1-yl)-3-hydroxynaphthalene-1,4-dione (4d)

Yellow solid; Yield: 83%; M.P: 212-214 °C

^{1}H NMR ($CDCl_3$, 400 MHz) δ (ppm): 6.85 (s, 1H), 7.26 (d, 1H, *J*=2.0 Hz), 7.38 (dd, 1H, *J*=7.6 Hz), 7.56 (td, 2H, *J*=8.8 Hz), 7.62 (d, 1H), 7.64 (d, 1H), 7.74 (td, 1H, *J*=16.4 Hz), 7.86 (td, 1H, *J*=16.4 Hz), 7.94 (d, 1H), 8.04 (dd, 1H, Hz, *J*=4.2 Hz), 8.26 (dd, 1H, *J*=4.2). **^{13}C NMR** ($CDCl_3$, 100 MHz) δ (ppm):55.43, 117.73, 122.40, 122.86, 123.12, 123.92, 126.74, 127.24, 128.75, 129.07, 129.31, 130.22, 132.08, 132.57, 133.66, 135.52, 136.06, 142.59, 154.29, 168.07, 180.34, 183.97. **IR (KBr) cm^{-1}**: 3404 (O-H), 3061 (=C-H), 2914 (C-H), 1692, 1667 (C=O), 1650 (C=O, amide), 1590 (C=C), 1277 (C-N), 1038 (C-O). **ESI/MS** 416.70 $[M+1]^+$ calculated for $C_{24}H_{14}ClNO_4$. Anal. Calculated for: C, 69.32; H, 3.39; N, 3.37; O, 15.39; Cl, 8.53; Found C, 69.34; H, 3.42; N, 3.36.

4.3.5. 2-(2-(4-bromophenyl)-3-oxoisoindolin-1-yl)-3-hydroxynaphthalene-1,4-dione (4e)

Yellow solid; Yield: 80%; M.P: 232-236 °C

^{1}H NMR ($CDCl_3$, 400 MHz) δ (ppm): 6.85 (s, 1H), 7.42 (m, 3H), 7.56 (m, 4H), 7.75 (td, 2H, *J*=8.2 Hz, *J*=1.2 Hz), 7.46 (d, 1H), 8.04 (dd, 1H, Hz, *J*=4.4 Hz, *J*=1.2 Hz), 8.28 (dd, 1H, *J*=4.2 Hz, *J*=1.2 Hz). **^{13}C NMR** ($CDCl_3$, 100 MHz) δ (ppm):30.98, 55.33, 117.73, 118.02, 122.41, 123.10, 123.38, 123.93, 126.75, 127.25, 128.76, 129.30, 132.09, 132.35, 132.56, 132.59, 133.67, 135.53, 136.60, 142.55, 154.26, 168.02, 180.33, 183.97. **IR (KBr) cm^{-1}**: 3403 (O-H), 3061 (=C-H), 1691 1667 (C=O), 1650 (C=O, amide), 1584 (C=C), 1277 (C-N), 1037 (C-O). **ESI/MS** 462.83 $[M+1]^+$ calculated for $C_{24}H_{14}BrNO_4$. Anal. Calculated for: C, 62.63; H, 3.07; N, 3.04; O, 13.90; Br, 17.36; Found C, 62.60; H, 3.05; N, 3.06.

4.3.6. 2-(2-(3-chloro-4-fluorophenyl)-3-oxoisoindolin-1-yl)-3-hydroxynaphthalene-1,4-dione (4f)

Yellow solid; Yield: 83%; M.P: 174-178 °C

^{1}H NMR ($CDCl_3$, 400 MHz) δ (ppm): 6.88 (s, 1H), 7.07 (t, 1H, *J*=8.6 Hz), 7.36 (dd, 1H, *J*=7.6 Hz), 7.56 (dd, 1H, *J*=5.8 Hz), 7.59 (td, 1H, *J*=8.0 Hz, *J*=1.2 Hz), 7.75 (td, 1H, *J*=8.2 Hz, *J*=1.2 Hz), 7.78 (dd, 1H, *J*=8.0 Hz, *J*=1.2 Hz), 7.93 (t, 2H, *J*=9.4 Hz), 8.07 (dd, 1H, Hz, *J*=4.2 Hz), 8.23 (dd, 1H, *J*=4.2). **^{13}C NMR** ($CDCl_3$, 100 MHz) δ (ppm): 55.45, 116.53, 117.54, 120.97, 121.89, 122.41, 124.01, 124.12, 126.80, 127.33, 128.87, 129.21, 132.08, 132.30, 134.14, 142.43, 154.07, 167.89, 180.32, 183.92. **19F NMR** (CDCl3, 400 MHz) δ (ppm): -119.48 (s). **IR (KBr) cm^{-1}**: 3389 (O-H), 3088 (=C-H), 2940 (C-H), 1675 (C=O), 1634 (C=O, amide), 1593 (C=C), 1275 (C-N), 1047 (C-O). **ESI/MS** 434.71 $[M+1]^+$ calculated for $C_{24}H_{13}ClFNO_4$. Anal. Calculated for: C, 66.45; H, 3.02; N, 3.23; O, 14.75; Cl, 8.17; F, 4.38; Found C, 66.47; H, 3.04; N, 3.21.

4.3.7. 2-(2-(3,4-dimethylphenyl)-3-oxoisoindolin-1-yl)-3-hydroxynaphthalene-1,4-dione (4g)

Yellow solid; Yield: 81%; M.P: 180-184 °C

^{1}H NMR ($CDCl_3$, 400 MHz) δ (ppm): 2.17 (s, 3H), 2.23 (s, 3H), 6.86 (s, 1H), 7.05 (d, 1H, *J*=8.0 Hz), 7.29 (dd, 1H, *J*=5.2 Hz), 7.36 (d, 1H, *J*=7.2 Hz), 7.52-7.55 (m, 3H), 7.72 (td, 1H, *J*=8.0 Hz, *J*=1.2 Hz), 7.84 (td, 1H, *J*=8.2 Hz, *J*=1.2 Hz), 7.94 (dd, 1H, *J*=4.2 Hz), 8.03 (dd, 1H, Hz, *J*=4.4 Hz), 8.26 (dd, 1H, *J*=4.2). **^{13}C NMR** ($CDCl_3$, 100 MHz) δ (ppm):20.05, 19.26, 55.66, 118.25, 119.39, 121.75, 123.49, 123.77, 124.22, 126.57, 127.12, 128.55, 129.43, 129.94, 132.11, 132.23, 133.09, 133.44, 135.31, 137.16, 142.85, 154.48, 168.08, 180.50, 183.97. **IR (KBr) cm^{-1}**: 3340 (O-H), 3036 (=C-H), 2913 (C-H), 1679 (C=O), 1641 (C=O, amide), 1593 (C=C), 1271 (C-N), 1044 (C-O). **ESI/MS** 410.77 $[M+1]^+$ calculated for $C_{26}H_{19}NO_4$. Anal. Calculated for: C, 76.27; H, 4.68; N, 3.42; O, 15.63; Found C, 76.30; H, 4.66; N, 3.44.

4.3.8. 2-(2-benzyl-3-oxoisoindolin-1-yl)-3-hydroxynaphthalene-1,4-dione (4h)

Light yellow solid; Yield: 78%; M.P: 174-178 °C

^{1}H NMR ($CDCl_3$, 400 MHz) δ (ppm): 4.52 (d, 1H, *J*=14.8 Hz), 4.89 (d, 1H, *J*=14.8 Hz), 6.10 (s, 1H), 7.11 (m, 3H), 7.23 (m, 4H), 7.47 (m, 2H), 7.47 (m, 2H), 7.75 (td, 1H, *J*=8.2 Hz, *J*=1.2 Hz), 7.86 (m, 2H), 8.06 (dd, 1H, *J*=4.4 Hz), 8.23 (dd, 1H, *J*=4.2). **^{13}C NMR** ($CDCl_3$, 100 MHz) δ (ppm):45.27, 54.52, 117.29, 122.27, 123.63, 126.63, 126.47, 127.08, 127.60, 128.26, 128.34, 128.40, 128.54, 128.60, 129.28, 131.68, 132.556, 133.44, 135.35, 135.46, 136.78, 143.83, 154.07, 169.17, 180.42, 183.87. **IR (KBr) cm^{-1}**: 3465 (O-H), 3034 (=C-H), 2917 (C-H), 1664 (C=O), 1652 (C=O, amide), 1592 (C=C), 1272 (C-N), 1037 (C-O). **ESI/MS** 396.20 $[M+1]^+$ calculated for $C_{25}H_{17}NO_4$. Anal. Calculated for: C, 75.94; H, 4.33; N, 3.54; O, 16.19; Found C, 75.90; H, 4.35; N, 3.55.

4.3.9. 2-(2-(furan-2-ylmethyl)-3-oxoisoindolin-1-yl)-3-hydroxynaphthalene-1,4-dione (4i)

Light yellow solid; Yield: 65%; M.P: 200-204 °C

^{1}H NMR ($CDCl_3$, 400 MHz) δ (ppm): 4.56 (d, 1H, *J*=15.6 Hz), 4.86 (d, 1H, *J*=15.6 Hz), 6.08 (d, 1H, *J*=3.2 Hz), 6.12 (d, 2H, *J*=14.4 Hz), 7.11 (s, 1H), 7.47 (m, 2H), 7.26 (s, 1H), 7.47 (q, 2H, *J*=15.6 Hz), 7.76 (t, 1H, *J*=15.2 Hz), 8.10 (d, 1H, *J*=7.6 Hz), 8.26 (d, 1H, *J*=8.0 Hz). **^{13}C NMR** ($CDCl_3$, 100 MHz) δ (ppm): 37.62, 54.64, 109.08, 110.55, 117.25, 122.32, 123.62, 126.51, 127.08, 128.27, 129.41, 131.77, 132.38, 133.45, 135.36, 142.36, 143.75, 150.27, 168.85, 180.63, 183.92. **IR (KBr) cm^{-1}**: 3408 (O-H), 3068 (=C-H), 1670 (C=O), 1641 (C=O, amide), 1592 (C=C), 1272 (C-N), 1045 (C-O). **ESI/MS** 386.68 $[M+1]^+$ calculated for $C_{23}H_{15}NO_5$. Anal. Calculated for: C, 71.68; H, 3.92; N, 3.63; O, 20.76; Found C, 71.70; H, 3.94; N, 3.60.

4.3.10. 2-(2-(2-(1H-indol-3-yl)ethyl)-3-oxoisoindolin-1-yl)-3-hydroxynaphthalene-1,4 dione (4j)

Reddish brown solid; Yield: 65%; M.P: 204-206 °C

^{1}H NMR ($CDCl_3$, 400 MHz) δ (ppm): 3.08 (q, 1H, *J*=14.0 Hz), 3.20 (q, 1H, *J*=14.0 Hz), 3.47 (q, 1H, *J*=13.2 Hz, *J*=6.8 Hz), 4.24 (q, 1H, *J*=13.2 Hz, *J*=6.8 Hz), 6.84 (t, 1H, *J*=7.4 Hz), 6.96 (t, 1H, *J*=7.2 Hz), 7.02 (d, 1H), 7.17-7.22 (m, 2H), 7.42-7.46 (m, 3H), 7.74 (td, 1H, *J*=8.0 Hz, *J*=1.2 Hz), 7.82-7.86 (m, 2H), 7.99 (s, 1H broad), 8.04 (dd, 1H, *J*=7.2 Hz, *J*=0.8 Hz), 8.16 (d, 1H, *J*=7.6 Hz). **^{13}C NMR** ($CDCl_3$, 100 MHz) δ (ppm): 24.28, 54.12, 55.23, 111.58, 111.83, 116.22, 116.66, 118.47, 118.59, 121.35, 122.89, 123.01, 123.11, 126.37, 127.45, 128.27, 130.66, 132.28, 135.27, 136.80, 145.02, 145.63, 168.15, 181, 183.19, 184.67. **IR (KBr) cm^{-1}**: 3447 (O-H), 3054 (=C-H), 1679 (C=O), 1650 (C=O, amide), 1594 (C=C), 1277 (C-N), 1039 (C-O). **ESI/MS** 449.86 $[M+1]^+$ calculated for $C_{28}H_{20}N_2O_4$. Anal. Calculated for: C, 74.99; H, 4.50; N, 6.25; O, 14.27; Found C, 74.95; H, 4.55; N, 6.27

4.3.11. 2-hydroxy-3-(3-oxo-2-(2-(thiophen-3-yl)ethyl)isoindolin-1-yl)naphthalene-1,4-dione (4k)

Yellow solid; Yield: 68%; M.P: 182 °C

^{1}H NMR ($CDCl_3$, 400 MHz) δ (ppm): 3.12 (m, 2H), 3.27 (t, 1H, *J*=13.6 Hz), 4.25 (q, 1H, *J*=12.6), 6.12 (s, 1H), 6.81 (q, 2H, *J*=5.2 Hz), 7.03 (dd, 1H, *J*=6 Hz, *J*=1.2 Hz), 7.26 (s, 1H), 7.47 (td, 2H, *J*=7.6 Hz), 7.80 (td, 1H, *J*=7.6), 7.84-7.91 (m, 2H), 8.134 (dd, 1H, *J*=6.8 Hz), 8.28 (dd, 1H, *J*=6.8 Hz). **^{13}C NMR** ($CDCl_3$, 100 MHz) δ (ppm):28.72, 20.59, 42.63, 54.85, 117.04, 122.37, 123.37, 123.93, 125.40, 126.69, 127.05, 127.22, 128.30, 129.37, 131.69, 132.35, 132.57, 133.60, 135.53, 141.06, 143.62, 154.22, 169.41, 180.60, 184.10. **IR (KBr) cm^{-1}**: 3430 (O-H), 2924 (C-H), 1668 (C=O), 1635 (C=O, amide), 1592 (C=C), 1273 (C-N), 1044 (C-O). **ESI/MS** 416.70 $[M+1]^+$ calculated for $C_{24}H_{27}NO_4S$. Anal. Calculated for: C, 69.38; H, 4.12; N, 3.37; O, 15.40; S, 7.72; Found C, 69.35; H, 4.16; N, 3.39.

4.3.12. 2-(2-butyl-3-oxoisoindolin-1-yl)-3-hydroxynaphthalene-1,4-dione (4l)

Yellow solid; Yield: 67%; M.P: 174 °C

^{1}H NMR ($CDCl_3$, 400 MHz) δ (ppm): 0.905 (q, 3H), 1.58 (q, 2H), 1.37 (q, 2H), 2.83 (q, 1H, *J*=13.6 Hz), 3.99 (q, 1H, *J*=15.2 Hz), 7.31 (d, 1H, *J*=8.4 Hz), 7.41 (d, 1H, *J*=7.6 Hz), 7.47 (td, 1H, *J*=8 Hz), 7.73 (d, 1H, *J*=7.6 Hz), 7.79 (td, 1H, *J*=7.6 Hz), 7.88 (td, 1H, *J*=7.6), 8.13 (dd, 1H, *J*=7.6 Hz), 8.29 (dd, 1H, *J*=7.6 Hz). **^{13}C NMR** ($CDCl_3$, 100 MHz) δ (ppm): 13.76, 20.08, 30.26, 40.20, 54.39, 117.14, 122.26, 123.26, 126.71, 127.06, 128.16, 129.65, 131.40, 132.35, 132.90, 133.53, 135.31, 143.86, 155.16, 169.53, 180.68, 184.35. **IR (KBr) cm^{-1}**: 3408 (O-H), 2958 (C-H), 1668 (C=O), 1638 (C=O, amide), 1593 (C=C), 1273 (C-N), 1046 (C-O). **ESI/MS** 362.67 $[M+1]^+$ calculated for $C_{22}H_{19}NO_4$. Anal. Calculated for: C, 73.12; H, 5.30; N, 3.38; O, 17.70; Found C, 73.10; H, 5.32; N, 3.39.

4.3.13. 2-hydroxy-3-(2-octyl-3-oxoisoindolin-1-yl)naphthalene-1,4-dione (4m)

Yellow solid; Yield: 70%; M.P: 152 °C

^{1}H NMR ($CDCl_3$, 400 MHz) δ (ppm): 0.85 (t, 3H), 1.25 (s, 12H, broad), 2.81 (s, 1H, *J*=13.8 Hz), 3.97 (s, 1H, *J*=15 Hz), 7.30 (d, 1H, *J*=7.6 Hz), 7.43 (t, 1H, *J*=7.2 Hz), 7.47 (dd, 1H, *J*=8.4 Hz), 7.78 (td, 2H, *J*=10.4 Hz), 7.88 (td, 1H, *J*=9.2), 8.15 (dd, 1H, *J*=8.4 Hz, *J*=1.2 Hz), 8.29 (dd, 1H, *J*=8.8 Hz). **^{13}C NMR** ($CDCl_3$, 100 MHz) δ (ppm): 14.10, 22.62, 26.88, 28.16, 29.16, 31.77, 40.51, 54.38, 117.17, 122.26, 123.27, 126.44, 126.71, 127.04, 127.10, 128.17, 129.63, 131.39, 132.35, 133.21, 133.53, 135.32, 143.66, 155.08, 169.08, 180.68, 164.33. **IR (KBr) cm^{-1}**: 3432 (O-H), 2925 (C-H), 1668 (C=O), 1639 (C=O, amide), 1592 (C=C), 1273 (C-N), 1045 (C-O). **ESI/MS** 418.4 $[M+1]^+$ calculated for $C_{26}H_{27}NO_4$. Anal. Calculated for: C, 74.80; H, 6.52; N, 3.35; O, 15.33; Found C, 74.82; H, 6.50; N, 3.38.

4.4. Computational studies

The Gaussian 16 software was used to carry out all theoretical calculations. Density functional theory (DFT) calculation was assigned to optimize the geometry of substituted isoindolinones **(4a-4m)** using B3LYP/6-311G (d,p) basis sets [56]. Gauss View 6 visualization program was used to determine frontier molecular orbitals and HOMO-LUMO energy gap of isoindolinones **(4a-4m)**. Molecular electrostatic potential was performed using a similar set of theoretical calculations and designed with GaussView 6 [22]. Various ADME traits were forcasted employing SwissADME online tool [24].

All computation related to docking were performed on AutodockVina software [57]. The structure of ligand was optimized using Gaussian 16 software. The target protein Alpha fetoprotein (AFP) was extracted from protein databank (PDB ID: 2DA2). The PDB file of selected protein was processed by deleting ligands and non proteins using discovery studio visualizer v20.1.0.19295. Further, the protein structure was prepared by removing water molecules and then the addition of Kollman charges and polar hydrogen atoms. Next, the ligands were processed by merging Gastiger charges to their structures [58]. Finally, both ligand and protein structures were converted to pdbqt file using AutoDock Tools 1.5.6. Autodock Vina v1.1.2 carried out docking calculations. The dimension for grid used for protein was kept 40 × 60 × 60 Å and separated by 0.375 Å. The exhaustiveness for the docking run was set to the default value of eight. The ligand's binding energy was calculated using the default Lamarckian genetic algorithm of the AutoDock Vina software package [58]. Biovia Discovery Studio Visuliser v20.1.0.19295 generated the representative 2D and 3D structure showing protein-ligand structures.

4.5. In vitro studies

4.5.1. Cell line and culture

HepG2 Cells (Human Liver cancer cell lines) were procured from National Center for Cell Science (NCCS) Pune. Dubecoos Modified Essential Medium (DMEM), Fetus Bovine Serum (FBS) and antimycotic–antibiotic solution were obtained from HiMedia. Cells were cultured in Dulbecco's Modified Eagle's Medium (DMEM) supplemented with 10% Fetal Bovine Serum (FBS) (Gibco) and 1% antimycotic-antibiotic solution (HiMedia). Cells were maintained at 37°C temperature in incubator with 5% CO_2. Cells were subcultured at about 80% confluency using 0.25% Trypsin Phosphate Versene Glucose (TPVG) Solution (Himedia). Cell lines were utilized to examine the antitumor activity of testing compound at varying concentration.

4.5.2. Cell viability assay

IC_{50} values of the synthesized compounds were determined using MTT assay on HepG2 cell line. HepG2 cells (10^4 cells/well) were seeded in 96 well plate in 10% DMEM media. 0.1% dimethyl sulfoxide was used to dissolve lawsone and its isoindolinone derivatives. Untreated cells were taken as positive control. Dilutions of the compounds were prepared in incomplete DMEM media. Dosing was done at about 70% confluency. After 48h incubation 3-(4, 5-dimethylthiazol-2-yl)-2, 5-diphenyltetrazoliumbromide (MTT; 5 mg/ml) was added for 4h. At the end of incubation MTT was removed from the wells and 150 µL/well of DMSO was added and incubated till formazan crystals dissolved completely. Reading was taken at 570 nm in synergy HTX multimode reader.

5. In vivo studies

In vivo studies were carried out using our previously reported protocol [59]. Laboratory animals (Balbc mice 28–30 g, n = 24, male/female) were procured from Zydus Research Center, Ahmedabad. Ethical clearance for animal experimentation was obtained from Institutional Animal Committee (IAEC) and CPCSEA. Animals were housed under standard conditions of LD 12:12 with food and water ad libitium. The animals were divided in various treatment groups as follows: the experiment consisted of 4 groups of animals with n=6 mice per group. The animals in group 1 were dosed only with double distilled water and it was considered as control group. Various physiological parameters determined in this group were considered as the standard values for tumor free condition. The animals in the remaining groups (2 to 4) were administered intraperitoneal injections of HePG2 cells for the induction of hepatic tumor (HCC). Post successful tumor induction the animals of group 2 were dosed with only PBS and this was considered as untreated group. The treatment groups comprised of group 3 dosed only with DOX.HCl group 4 dosed with compound **4i**.

The experiment continued for 14 days and at the end, body weights were recorded. Blood was collected by retro-orbital sinus puncture and serum was separated in the cold centrifuge (3000 rpm). Hepatic markers for liver function (SGPT and SGOT) were assessed using standard kits (Reckon diagnostics Ltd., Vadodara, India). Markers of matrix modulation (MMP-2 and 9) were assessed by ELISA kits (Krishgen Biosystems, Mumbai, India). Animals were sacrificed under mild ether anesthesia and the liver autopsy was conducted. Pieces of liver tissue obtained from control and experimental groups were stored in RNA later solution. Forward and reverse primers of genes controlling immunity (TLR-2 and 4) were procured from Eurofins Scientific, New Delhi, India. RNA extraction was done by Trizol reagent and cDNA was synthesized using iscript^{TM} cDNA kit (BIORAD, California,USA). Quantitative RT- PCR was performed using SYBR select master mix (Applied Biosystems in Quant Studio 12 K (Life Technologies) real time PCR machine.

Declaration of Competing Interest

The authors declare that there is no conflicts of interest regarding the publication of this paper

CRediT authorship contribution statement

Pratik Nariya: Investigation, Formal analysis, Methodology, Writing – original draft. **Sunny Kumar:** Formal analysis, Investigation. **Sriram Seshadri:** Writing – review & editing. **Mrugesh Patel:** Formal analysis, Investigation. **Sonal Thakore:** Conceptualization, Supervision, Project administration, Writing – review & editing, Funding acquisition.

Data availability

No data was used for the research described in the article.

Acknowledgments

The authors acknowledge DST-FIST for ^{1}H and ^{13}C NMR facilities. O_2H Discovery, Ahmedabad for ESI-MS analysis. The authors acknowledge. PN is thankful to SHODH fellowship, Gandhinagar for providing financial assistance. SK is thankful to ICMR-New Delhi for SRF fellowship.

Supplementary materials

Supplementary material associated with this article can be found, in the online version, at doi:10.1016/j.molstruc.2022.133601.

References

[1] D.L. Boger, J.K. Lee, J. Goldberg, Q. Jin, Two comparisons of the performance of positional scanning and deletion synthesis for the identification of active constituents in mixture combinatorial libraries, J. Org. Chem. 65 (2000) 1467–1474, doi:10.1021/jo9916481.
[2] D.L. Comins, S. Schilling, Y. Zhang, Asymmetric synthesis of 3-substituted isoindolinones: Application to the total synthesis of (+)-lennoxamine, Org. Lett. 7 (2005) 95–98, doi:10.1021/ol047824w.
[3] K. Speck, T. Magauer, The chemistry of isoindole natural products, Beilstein J. Org. Chem. 9 (2013) 2048–2078, doi:10.3762/bjoc.9.243.
[4] D. Augner, D.C. Gerbino, N. Slavov, J.M. Neudörfl, H.G. Schmalz, N-Capping of primary amines with 2-Acylbenzaldehydes to give isoindolinones, Org. Lett. 13 (2011) 5374–5377, doi:10.1021/ol202271k.
[5] D. Augner, O. Krut, N. Slavov, D.C. Gerbino, H.G. Sahl, J. Benting, C.F. Nising, S. Hillebrand, M. Krönke, H.G. Schmalz, On the antibiotic and antifungal activity of pestalone, pestalachloride a, and structurally related compounds, J. Nat. Prod. 76 (2013) 1519–1522, doi:10.1021/np400301d.
[6] N.J. Lawrence, J. Liddle, S.M. Bushell, D.A. Jackson, A three-component coupling process based on vicarious nucleophilic substitution (VNSAR)-alkylation reactions: An approach to indoprofen and derivatives, J. Org. Chem. 67 (2002) 457–464, doi:10.1021/jo0159901.
[7] C. Riedinger, J.A. Endicott, S.J. Kemp, L.A. Smyth, A. Watson, E. Valeur, B.T. Golding, R.J. Griffin, I.R. Hardcastle, M.E. Noble, J.M. McDonnell, Analysis of chemical shift changes reveals the binding modes of isoindolinone inhibitors of the MDM2-p53 interaction, J. Am. Chem. Soc. 130 (2008) 16038–16044, doi:10.1021/ja8062088.
[8] Z. Zhuang, M. Kung, M. Mu, H.F. Kung, Isoindol-1-one Analogues of 4-(2′ -methoxyphenyl) -1- [2′ - [N - (2′′ -pyridyl) - p -iodobenzamido] ethyl] piperazine (p -MPPI) as 5-HT 1A Receptor Ligands 2623 (1998) 157–166.
[9] I. Sovic, S.K. Pavelic, E. Markova-Car, N. Ilic, R. Nhili, S. Depauw, M.H. David-Cordonnier, G. Karminski-Zamola, Novel Phenyl and Pyridyl Substituted Derivatives of Isoindolines: Synthesis, Antitumor Activity and DNA Binding Features, Elsevier Ltd, 2014, doi:10.1016/j.ejmech.2014.09.079.
[10] Y. Tian, Q. Liu, Y. Liu, R. Zhao, G. Li, F. Xu, Catalyst-free Mannich-type reactions in water: Expedient synthesis of naphthol-substituted isoindolinones, Tetrahedron Lett 59 (2018) 1454–1457, doi:10.1016/j.tetlet.2018.02.083.
[11] B. Qian, S. Guo, J. Shao, Q. Zhu, L. Yang, C. Xia, H. Huang, Palladium-catalyzed benzylic addition of 2-methyl azaarenes to N - sulfonyl aldimines via C - H bond activation in furnishing the subsequent nucleophilic addition . 1 Recent studies have alternative method for generating R - M intermediates, which have be, J. Am. Chem. Soc. 132 (2010) 3650–3651.
[12] C. Xia, A.J.P. White, K.K.M. Hii, Synthesis of isoindolinones by Pd-catalyzed coupling between N-methoxybenzamide and styrene derivatives, J. Org. Chem. 81 (2016) 7931–7938, doi:10.1021/acs.joc.6b01696.
[13] J.W. Wrigglesworth, B. Cox, G.C. Lloyd-Jones, K.I. Booker-Milburn, New heteroannulation reactions of N-Alkoxybenzamides by Pd(II) Catalyzed C-H activation, Org. Lett. 13 (2011) 5326–5329, doi:10.1021/ol202187h.
[14] M. Dutta, S.M. Mandal, R. Pegu, S. Pratihar, PdII/AgI-catalyzed room-temperature reaction of γ-hydroxy lactams: mechanism, scope, and anti-staphylococcal activity, J. Org. Chem. 82 (2017) 2193–2198, doi:10.1021/acs.joc.6b02378.
[15] D.D. Li, T.T. Yuan, G.W. Wang, Synthesis of isoindolinones via palladium-catalyzed C-H activation of N-methoxybenzamides, Chem. Commun. 47 (2011) 12789–12791, doi:10.1039/c1cc15897j.
[16] K.V. Sashidhara, L.R. Singh, G.R. Palnati, S.R. Avula, R. Kant, A catalyst-free one-pot protocol for the construction of substituted isoindolinones under sustainable conditions, Synlett 27 (2016) 2384–2390, doi:10.1055/s-0035-1562614.
[17] Y. Tian, J. Sun, K. Zhang, G. Li, F. Xu, Catalyst-Free Synthesis of 3-(2-Quinolinemethylene)-Substituted Isoindolinones in Water, Synth. 50 (2018) 2255–2265. doi:10.1055/s-0037-1609491.
[18] B.H. Rotstein, S. Zaretsky, V. Rai, A.K. Yudin, Small heterocycles in multicomponent reactions, Chem. Rev. 114 (2014) 8323–8359, doi:10.1021/cr400615v.
[19] R.C. Cioc, E. Ruijter, R.V.A. Orru, Multicomponent reactions: Advanced tools for sustainable organic synthesis, Green Chem 16 (2014) 2958–2975, doi:10.1039/c4gc00013g.
[20] Y. Tian, J. Wei, M. Wang, G. Li, F. Xu, Hantzsch ester triggered metal-free cascade approach to isoindolinones, Tetrahedron Lett 59 (2018) 1866–1870, doi:10.1016/j.tetlet.2018.04.009.
[21] T. Chen, C. Cai, An efficient approach to 3-oxoisoindoline-1-difluoroalkyl derivatives via a metal triflate-catalyzed Mannich/lactamization cascade reaction, New J. Chem. 41 (2017) 2519–2522, doi:10.1039/c6nj03813a.
[22] P. Nariya, F. Shukla, H. Vyas, R. Devkar, S. Thakore, Synthesis, characterization, DNA/BSA binding and cytotoxicity studies of mononuclear Cu(II) and V(IV) complexes of Mannich bases derived from Lawsone, J. Mol. Struct. 1248 (2022) 131508, doi:10.1016/j.molstruc.2021.131508.
[23] P. Nariya, F. Shukla, H. Vyas, R. Devkar, S. Thakore, Synthesis and characterization of Mannich bases of lawsone and their anticancer activity, Synth. Commun. 50 (2020) 1724–1735, doi:10.1080/00397911.2020.1755440.
[24] A. Daina, O. Michielin, V. Zoete, SwissADME: A free web tool to evaluate pharmacokinetics, drug-likeness and medicinal chemistry friendliness of small molecules, Sci. Rep. 7 (2017) 1–13, doi:10.1038/srep42717.
[25] A. Al Sheikh Ali, D. Khan, A. Naqvi, F.F. Al-Blewi, N. Rezki, M.R. Aouad, M. Hagar, Synthesis Design, Molecular Modeling, Anticancer studies, and density functional theory calculations of 4-(1,2,4-triazol-3-ylsulfanylmethyl)-1,2,3-triazole derivatives, ACS Omega 6 (2021) 301–316, doi:10.1021/acsomega.0c04595.
[26] Y.T. Hussein, Y.H. Azeez, DFT analysis and in silico exploration of drug-likeness, toxicity prediction, bioactivity score, and chemical reactivity properties of the urolithins, J. Biomol. Struct. Dyn. 0 (2021) 1–10, doi:10.1080/07391102.2021.2017350.
[27] M. Khalid, R. Jawaria, M.U. Khan, A.A.C. Braga, Z. Shafiq, M. Imran, H.M.A. Zafar, A. Irfan, An efficient synthesis, spectroscopic characterization, and optical nonlinearity response of novel salicylaldehyde thiosemicarbazone derivatives, ACS Omega 6 (2021) 16058–16065, doi:10.1021/acsomega.1c01938.
[28] M. Ricardo, J.K. Bastos, M.C.A. Costa, M.M.C. Ferreira, C.S. Mizuno, G.F. Caramori, G.R. Nagurniak, M.R. Simão, A. Raquel, R.C.S. Veneziani, S.R. Ambrósio, R.L.T. Parreira, N. De Pesquisa, U. De Franca, Phytochemistry In vitro cytotoxicity and structure-activity relationship approaches of ent - kaurenoic acid derivatives against human breast carcinoma cell line, Phytochemistry 156 (2018) 214–223, doi:10.1016/j.phytochem.2018.10.005.
[29] K. Rachedi, T. Ouk, R. Bahadi, A. Bouzina, S. Djouad, K. Bechlem, R. Zerrouki, T. Ben Hadda, F. Almalki, M. Berredjem, Synthesis, DFT and POM analyses of cytotoxicity activity of α-amidophosphonates derivatives: Identification of potential antiviral O,O-pharmacophore site, J. Mol. Struct. (2019), doi:10.1016/j.molstruc.2019.07.053.
[30] M.S. Ali, M.A. Farah, H.A. Al-lohedan, K.M. Al-anazi, Activities of procaine and its binding with calf modelling study†, (2018) 9083–9093. doi:10.1039/c7ra13647a.
[31] R. Joshi, N. Pandey, S.K. Yadav, R. Tilak, H. Mishra, S. Pokharia, Synthesis, spectroscopic characterization, DFT studies and antifungal activity of (E)-4-amino-5-[N'-(2-nitro-benzylidene)-hydrazino]-2,4-dihydro-[1,2,4]triazole-3-thione, J. Mol. Struct. (2018), doi:10.1016/j.molstruc.2018.03.081.
[32] M. Hagar, H.A. Ahmed, R. Alnoman, Mesophase behavior and DFT conformational analysis of new symmetrical diester chalcone liquid crystals, J. Mol. Liq. (2019), doi:10.1016/j.molliq.2019.04.083.
[33] S.S. Kumar, S. Athimoolam, B. Sridhar, Structural, spectral, theoretical and anticancer studies on new co-crystal of the drug 5- Fluorouracil, J. Mol. Struct. (2018), doi:10.1016/j.molstruc.2018.07.079.
[34] A.I. Khodair, M.K. Awad, J. Gesson, Y.A.M.M. Elshaier, New N -ribosides and N -mannosides of rhodanine derivatives with anticancer activity on leukemia cell line : Design, synthesis, DFT and molecular modelling studies, Carbohydr. Res. 487 (2020) 107894, doi:10.1016/j.carres.2019.107894.
[35] M. Grover, B. Singh, M. Bakshi, S. Singh, Quantitative structure – property relationships in pharmaceutical research – Part 1, 3 (2000).
[36] L.H. Abdel-Rahman, B.S. Al–Farhan, N.O. Al Zamil, M.A. Noamaan, H. El-Sayed Ahmed, M.S.S. Adam, Synthesis, spectral characterization, DFT calculations, pharmacological studies, CT-DNA binding and molecular docking of potential N, O-multidentate chelating ligand and its VO(II), Zn(II) and ZrO(II) chelates, Bioorg. Chem. 114 (2021) 105106, doi:10.1016/j.bioorg.2021.105106.

[37] A.S. El-Azab, Y. Sheena Mary, C. Yohannan Panicker, A.A.M. Abdel-Aziz, M.A. El-Sherbeny, C. Van Alsenoy, DFT and experimental (FT-IR and FT-Raman) investigation of vibrational spectroscopy and molecular docking studies of 2-(4-oxo-3-phenethyl-3,4-dihydroquinazolin-2-ylthio)-N-(3,4,5-trimethoxyphenyl) acetamide, J. Mol. Struct. 1113 (2016) 133–145, doi:10.1016/j.molstruc.2016.02.038.
[38] R.V. Solomon, A.P. Bella, S.A. Vedha, P. Venuvanalingam, Designing benzosiloles for better optoelectronic properties using DFT & TDDFT approaches, Phys. Chem. Chem. Phys. 14 (2012) 14229–14237, doi:10.1039/c2cp41554b.
[39] R.G. Parr, L.V. Szentpály, S. Liu, Electrophilicity index, J. Am. Chem. Soc. 121 (1999) 1922–1924, doi:10.1021/ja983494x.
[40] K.S. Devi, P. Subramani, N. Sundaraganesan, M. Jeeva, S.J. Pradeepa, B. Karthikeyan, Synthesis, spectra, electronic structure, molecular docking and cytotoxicity investigation on 2-(piperidin-1-ylmethyl)-isoindoline-1,3-dione – A Mannich base system, J. Mol. Struct. (2021) 1224, doi:10.1016/j.molstruc.2020.129151.
[41] M. Khalid, A. Ali, R. Jawaria, M.A. Asghar, S. Asim, M.U. Khan, R. Hussain, M. Fayyaz, C.J. Ennis, M.S. Akram, First principles study of electronic and nonlinear optical properties of A–D–p–A and D–A–D–p–A configured compounds containing novel quinoline–carbazole derivatives, RSC Adv 10 (2020) 22273–22283, doi:10.1039/D0RA02857F.
[42] M. Khalid, M.N. Arshad, M.N. Tahir, A.M. Asiri, M.M. Naseer, M. Ishaq, M.U. Khan, Z. Shafiq, An efficient synthesis, structural (SC-XRD) and spectroscopic (FTIR, 1HNMR, MS spectroscopic) characterization of novel benzofuran-based hydrazones: An experimental and theoretical studies, J. Mol. Struct. 1216 (2020) 1–12, doi:10.1016/j.molstruc.2020.128318.
[43] A.M. Deghady, Density functional theory and molecular docking investigations of the chemical and antibacterial activities for 1-(4-hydroxyphenyl)-3-phenylprop-2-en-1-one, Molecules 26 (2021), doi:10.3390/molecules26123631.
[44] S. Murugavel, C. Ravikumar, G. Jaabil, P. Alagusundaram, Synthesis, crystal structure analysis, spectral investigations (NMR, FT-IR, UV), DFT calculations, ADMET studies, molecular docking and anticancer activity of 2-(1-benzyl-5-methyl-1H-1,2,3-triazol-4-yl)-4-(2-chlorophenyl)-6-methoxypyridine – A novel poten, J. Mol. Struct. 1176 (2019) 729–742, doi:10.1016/j.molstruc.2018.09.010.
[45] C.A. Lipinski, F. Lombardo, B.W. Dominy, P.J. Feeney, Experimental and computational approaches to estimate solubility and permeability in drug discovery and development settings, Adv. Drug Deliv. Rev. 64 (2012) 4–17, doi:10.1016/j.addr.2012.09.019.
[46] D.F. Veber, S.R. Johnson, H.Y. Cheng, B.R. Smith, K.W. Ward, K.D. Kopple, Molecular properties that influence the oral bioavailability of drug candidates, J. Med. Chem. 45 (2002) 2615–2623, doi:10.1021/jm020017n.
[47] W.J. Egan, K.M. Merz, J.J. Baldwin, Prediction of drug absorption using multivariate statistics, J. Med. Chem. 43 (2000) 3867–3877, doi:10.1021/jm000292e.
[48] F. Pascale, L. Bedouet, M. Baylatry, J. Namur, A. Laurent, Comparative chemosensitivity of VX2 and HCC cell lines to drugs used in TACE, Anticancer Res 35 (2015) 6497–6504.
[49] P.R. Galle, F. Foerster, M. Kudo, S.L. Chan, J.M. Llovet, S. Qin, W.R. Schelman, S. Chintharlapalli, P.B. Abada, M. Sherman, A.X. Zhu, Biology and significance of alpha-fetoprotein in hepatocellular carcinoma, Liver Int 39 (2019) 2214–2229, doi:10.1111/liv.14223.
[50] X. Wang, Q. Wang, Alpha-Fetoprotein and Hepatocellular Carcinoma Immunity, Can. J. Gastroenterol. Hepatol. 2018 (2018) 1–8, doi:10.1155/2018/9049252.
[51] A. Gupta, P. Singh, B. Kamble, A. Kulkarni, M. Joghee Nanjan Chandrasekar, Synthesis, docking and biological evaluation of some novel 5-bromo-2- (5-aryl-1,3,4-thiadiazol-2-yl)isoindoline-1,3-dione derivatives targeting ATP-binding site of topoisomerase II, Lett. Drug Des. Discov. 9 (2012) 668–675, doi:10.2174/157018012801319463.
[52] J.M. Llovet, R.K. Kelley, A. Villanueva, A.G. Singal, E. Pikarsky, S. Roayaie, R. Lencioni, K. Koike, J. Zucman-Rossi, R.S. Finn, Hepatocellular carcinoma, Nat. Rev. Dis. Prim. 7 (2021), doi:10.1038/s41572-020-00240-3.
[53] M. Morini, M. Mottolese, N. Ferrari, F. Ghiorzo, S. Buglioni, R. Mortarini, D.M. Noonan, P.G. Natali, A. Albini, The $\alpha 3\beta 1$ integrin is associated with mammary carcinoma cell metastasis, invasion, and gelatinase B (MMP-9) activity, Int. J. Cancer. 87 (2000) 336–342, doi:10.1002/1097-0215(20000801)87:3⟨336::AID-IJC5⟩3.0.CO;2-3.
[54] R. Klopfleisch, Macrophage reaction against biomaterials in the mouse model – Phenotypes, functions and markers, Acta Biomater 43 (2016) 3–13, doi:10.1016/j.actbio.2016.07.003.
[55] A.G.A. El-Helby, H. Sakr, R.R. Ayyad, H.A. Mahdy, M.M. Khalifa, A. Belal, M. Rashed, A. El-Sharkawy, A.M. Metwaly, M.A. Elhendawy, M.M. Radwan, M.A. ElSohly, I.H. Eissa, Design, synthesis, molecular modeling, in vivo studies and anticancer activity evaluation of new phthalazine derivatives as potential DNA intercalators and topoisomerase II inhibitors, Bioorg. Chem. 103 (2020) 104233, doi:10.1016/j.bioorg.2020.104233.
[56] A. Kumar, V. Narayan, O. Prasad, L. Sinha, Monomeric and dimeric structures, electronic properties and vibrational spectra of azelaic acid by HF and B3LYP methods, J. Mol. Struct. 1022 (2012) 81–88, doi:10.1016/j.molstruc.2012.04.089.
[57] O. Trott, A.J. Olson, AutoDock Vina: Improving the speed and accuracy of docking with a new scoring function, efficient optimization, and multithreading, J. Comput. Chem. (2010) 455–461, doi:10.1002/jcc.21334.
[58] M. Patel, N. Pandey, J. Timaniya, P. Parikh, A. Chauhan, N. Jain, K. Patel, Coumarin-carbazole based functionalized pyrazolines: synthesis, characterization, anticancer investigation and molecular docking, RSC Adv. 11 (2021) 27627–27644, doi:10.1039/d1ra03970a.
[59] M. Das, P. Nariya, A. Joshi, A. Vohra, R. Devkar, S. Seshadri, S. Thakore, Carbon nanotube embedded cyclodextrin polymer derived injectable nanocarrier: A multiple faceted platform for stimulation of multi-drug resistance reversal, Carbohydr. Polym. 247 (2020) 116751, doi:10.1016/j.carbpol.2020.116751.